Universität Bremen*

The importance of the western Weddell Sea to Weddell Sea Deep Water formation

Dissertation zur Erlangung des Doktorgrades der Naturwissenschaften Dr. rer. nat.

dem Fachbereich Physik/Elektrotechnik der Universität Bremen

vorgelegt von

MATHIAS VAN CASPEL

May 12, 2016

ALFRED-WEGENER-INSTITUT
HELMHOLTZ-ZENTRUM FÜR POLAR-
UND MEERESFORSCHUNG

Universität Bremen
Fachbereich 1
Dr.- rer. - nat.

E r k l ä r u n g

Hiermit versichere ich, dass ich

1. die Arbeit ohne fremde
Hilfe angefertigt habe,

2. keine anderen als die von mir an-
gegeben Quellen und Hilfsmittel
benutzt habe

und

3. die den benutzten Werken wörtlich
oder inhaltlich entnommenen Stellen
als solche kenntlich gemacht habe.

_____ ,den _____

_____
(Unterschrift)

Declaration of Authorship

I, Mathias van CASPEL, declare that this thesis titled, "The importance of the western Weddell Sea to Weddell Sea Deep Water formation" and the work presented in it are my own. I confirm that:

- This work was done wholly or mainly while in candidature for a research degree at this University.

- Where any part of this thesis has previously been submitted for a degree or any other qualification at this University or any other institution, this has been clearly stated.

- Where I have consulted the published work of others, this is always clearly attributed.

- Where I have quoted from the work of others, the source is always given. With the exception of such quotations, this thesis is entirely my own work.

- I have acknowledged all main sources of help.

- Where the thesis is based on work done by myself jointly with others, I have made clear exactly what was done by others and what I have contributed myself.

Signed:

_____

Date:

_____

Abstract

The importance of the western Weddell Sea to Weddell Sea Deep Water formation
by Mathias van CASPEL

The dense water flowing out from the Weddell Sea (WS), the Weddell Sea Deep Water (WSDW), significantly contributes to Antarctic Bottom Water (AABW) and plays an important role in the Meridional Overturning Circulation. However, the relative importance of the western Weddell Sea as a major source region remains unclear. Several studies hypothesized that the continental shelf off Larsen Ice Shelf (LIS) is important for deep and bottom water production, but the role of the Larsen Ice Shelf remains speculative. In this work the importance of the western WS including the LIS to the production of WSDW is investigated using *in situ* observations and results from numerical simulations.

Measurements made during the Polarstern cruise ANT XXIX-3 (2013) in the northwestern WS add evidence to the importance of the western WS as a dense water source. An Optimum Multiparameter Analysis shows that the dense water found near the shelf break in front of the former Larsen A and B ice shelves, together with a very dense water observed off Larsen C Ice Shelf, increases the thickness and changes the θ/S characteristics of WSDW that leaves the WS through gaps in the South Scotia Ridge to form AABW. A numerical experiment performed with the Finite Element Sea-ice Ocean Model (FESOM) was used to verify the hypothesis that the continental shelf of the western WS is important for dense water formation.

The model results show the changes in the thermohaline properties of the WSDW flowing along the continental slope of the western WS, as well as an increase in the transport downstream. The variability along the continental slope can be explained by fluctuations of the large-scale circulation, namely the Weddell Gyre. In addition, there is no indication that dense waters are formed in the continental shelf of the western WS, and the exchanges between continental shelf and continental slope are small. These results suggest that the area is not important for WSDW formation as previously inferred from the sparse observations mainly along the continental slope. Instead, the western WS seems to be a region where the characteristics of WSDW are determined due to mixing of waters formed upstream. Two sensitivity experiments were designed to investigate whether LIS plays an indirect role in the dense water production: (1) Larsen B Ice Shelf was added to the grid, (2) Larsen C Ice Shelf was completely removed from the grid. The experiments show that LIS plays an important role for the waters on the continental shelf but has only minor importance for the WSDW.

Given the disagreement between the hypothesis derived from the observations and the model results, more *in situ* data are needed to determine whether the western Weddell Sea is a region where dense water is formed or whether it only serves as a conduit for dense waters formed further upstream, which interact in the western WS before reaching the final WSDW characteristics.

Acknowledgements

My deepest gratitude goes to Dr. Hartmut Hellmmer for the guidance and patience during my PhD. The support started by suggesting a topic and assistance with the proposal writing, continued with interesting scientific discussions during the whole period, and culminated with constructive suggestions that improved the quality of this manuscript. Hartmut also introduced me to Dr. Michael Schröder and Dr. Ralph Timmermann, essential persons for the conclusion and quality of this thesis. I am thankful to Dr. Michael Schröder, who oriented me during the data analysis and was/is aways open for discussions about the circulation, his nice ideas for figures often made it easier to explain the facts without words. I also want to express my gratitude to Dr. Ralph Timmermann for presenting me to FESOM and providing all I needed to start my own simulations, and when the model crashed with no obvious reason he could always find some time to solve the mystery.

I would like to acknowledge Prof. Dr. Peter Lemke who accepted me as student and provided valuable advices during the beginning of my PhD. I thank Prof. Dr. Torsten Kanzow who accompanied me during the last year and was always willing to help me to make good science, usually, by asking the right questions. I also show my appreciation to Prof. Dr. Monika Rhein for accepting to review my thesis.

Dr. Yoshihiro Nakayama taught me how to use FESOM and was always willing to help with the beginners mistakes or the unexpected bugs, and therefore I am grateful. Thanks to Andreas Wisotzki for calibrating the oceanographic data and provide insightful observations about them. Dr. Oliver Huhn shared the noble gas measurements and helped with the interpretation of the OMP results.

I thank the Council for Research and Scientific Development of Brazil (CNPq) for the grant 290034/2011-6, which allowed me to conduct my studies in Germany.

This study is a contribution to the Earth System Science Research School (ESSReS) and I would like to thank the amazing team, specially Dr. Klaus Grosfeld, Stefanie Klebe, Dr. Helge Meggers, and Dr. Ludvig Löwemark. It is also a contribution the Brazilian High Latitudes Oceanography Group (GOAL; www.goal.furg.br). Thanks to the GOAL member, Prof. Dr. Mauricio Mata, for showing me Antarctica and guiding me to AWI.

To all my friends, close by or far way, that made life nicer and enjoyable, thank you.

My most sincere gratitude to my family, for all the support and nurture that made who I am. Thanks to my second family for all the nice moments and for raising such a great person as Camila Campos. Thank you Camila for joining me in Bremerhaven, thanks for all the push and effort to make me break the inertia, but most of all thank you for sharing happiness with me.

Contents

List of Figures

List of Tables

List of Abbreviations

$*^{SWT}$	used to refer to the Source Water Type representing an water mass ($*$)
γ^n	neutral density (Jackett and McDougall, 1997))
θ	potential temperature
AABW	Antarctic Bottom Water
AASW	Antarctic Surface Water
ACC	Antarctic Circumpolar Current
AP	Antarctic Peninsula
ASF	Antarctic Slope Front
BS	Bransfield Strait
BWγ^n	Neutral Bottom Water; waters within the γ^n range of the WSBW
CC	Antarctic Coastal Current
CDW	Circumpolar Deep Water
CFSR	Climate Forecast System Reanalysis
DWγ^n	Neutral Deep Water; waters within the γ^n range of the WSDW
EXLB	sensitivity experiment including Larsen B Ice Shelf
EXLC	sensitivity experiment removing Larsen C Ice Shelf
FESOM	Finite Element Sea-ice Ocean Model
FRIS	Filchner-Ronne Ice Shelf
GMW	Glacial Melt Water
HSSW	High Salinity Shelf Water
ISPOL	Ice Station Polarstern drift experiment
ISW	Ice Shelf Water
IUP	Institute for Environmental Physics
IW	Intermediate Water
JOEL	section between Joinville Island and Elephant Island
LABW	dense water observed on the shelf in front of Larsen A and B
LCW	dense water observed on the shelf in front of Larsen C
LIS	Larsen Ice Shelf
LIS-A	Larsen A Ice Shelf
LIS-B	Larsen B Ice Shelf
LIS-C	Larsen C Ice Shelf
MOC	Meridional Overturning Circulation
MWDW	Modified Warm Deep Water
OMP	Optimum Multiparameter Analysis
R$_X$	residual difference of property 'x'
SSR	South Scotia Ridge
SST	South Sandwich Trench
SSW	Salty Shelf Water
SWT	Source water type
ULS	upper looking sonar
VWSDW	ventilated type of Weddell Sea Deep Water
VWSBW	ventilated type of Weddell Sea Bottom Water

WDW	Warm Deep Water
WG	Weddel Gyre
WOA	World Ocean Atlas
WS	Weddell Sea
WSBW	Weddell Sea Bottom Water
WSDW	Weddell Sea Deep Water
WW	Winter Water

Chapter 1

Introduction

1.1   Introduction

Antarctic Bottom Water (AABW) is formed around Antarctica and can be found in the deep basins of all oceans. The spreading of this water mass is a key component of the Meridional Overturning Circulation (MOC) (e.g. Talley, 2013; Marson et al., 2015). The Weddell Sea Deep Water (WSDW), which is formed directly along the slope of the western Weddell Sea (WS) or due to mixing with Weddell Sea Bottom Water (WSBW) (e.g. Foster and Carmack, 1976; Foldvik and Gammelsrød, 1988; Caspel et al., 2015a), is the most important source of AABW (e.g. Orsi et al., 1999; Meredith, 2013).

The production of WSDW and WSBW is linked to sea ice formation on the continental shelf and the melting of ice shelves (Fig. 1.1). Once the surface freezing temperature of -1.9^{o}C (depending on salinity) is reached, sea water starts to freeze and most of the salt is expelled forming a salty solution called brine. Brine can be trapped in the ice as brine pockets, or be directly released to the ocean where it sinks, since it is denser then the surrounding waters.

Polynyas observed near the coast or ice shelf margins are particularly important for the changes in sea water density. Persistent offshore winds blow sea ice away from the coast facilitating the heat exchange between ocean and atmosphere. When the atmosphere is cold enough more ice is formed and the process is repeated. The export of fresh water in form of sea ice and the intense brine release due to the constant freezing of water produce the High Salinity Shelf Water (HSSW).

HSSW is dense enough to reach the bottom of the continental shelf. From there it can flow down the continental slope where it mixes with ambient waters to form either WSDW or WSBW. In the presence of an ice shelf, HSSW can flow into the cavity and melt the glacier at its base, where the *in situ* freezing temperature is lower than -1.9^{o}C because of the high pressure. In addition to HSSW, other water masses can enter the ice shelf cavity, and the mixture of these water masses with Glacial Melt Water (GMW) is called Ice Shelf Water (ISW), defined as a water mass with temperature below the surface freezing point (Foldvik and Gammelsrød, 1988).

When ISW leaves the cavity it can mix with ambient water to form the colder and fresher WSBW or end up as WSDW in shallower layers of the water column. If the shelf water causing the melting has low salinity, the resulting mixture with GMW is light and might end up at the ocean surface (Kusahara and Hasumi, 2014). In this case, the water column
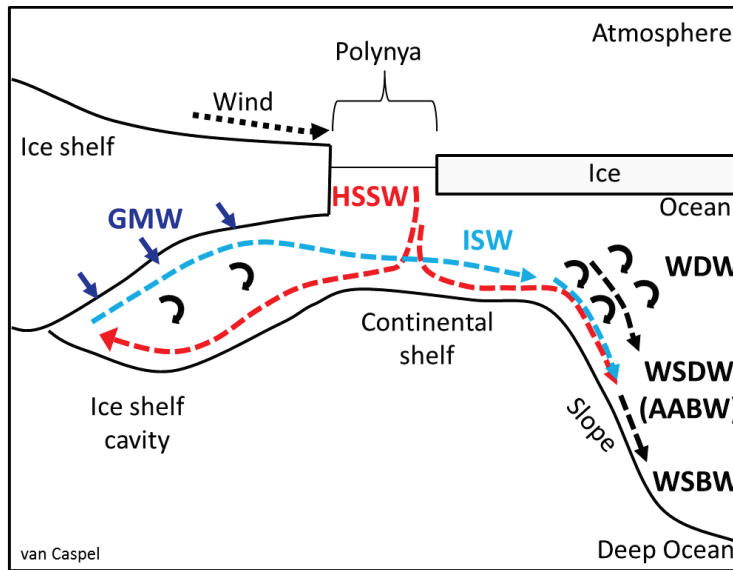
FIGURE 1.1: Schematic representation of Weddell Sea Bottom Water (WSBW) and Weddell Sea Deep Water (WSDW) formation. The paths of High Salinity Shelf Water (HSSW) and Ice Shelf Water are indicated as well as the input of Glacial Melt Water (GMW). ISW and HSSW contribute to the WSBW, mixtures of this water masses with Warm Deep Water (WDW) form WSDW.

becomes stable and less salt is injected in the ocean when the water freezes, leading to a lower production of HSSW (Hellmer, 2004). Similar mechanisms can be observed when sea ice melts; in both cases it can cause a reduction on the AABW formation or changes in its thermohaline characteristics.

This and other processes that modify AABW characteristics can be traced back to the regions where the water masses are formed. In the WS, the most important sources of WSDW are the continental shelf in front of the Filchner-Ronne Ice Shelf (FRIS), located in the southwestern WS (Foldvik and Gammelsrød, 1988; Foldvik et al., 2004; Nicholls et al., 2009), and the continental shelf off Larsen Ice Shelf (LIS) in the northwestern WS (Gordon et al., 1993; Fahrbach et al., 1995; Gordon, 1998; Gordon et al., 2001; Schröder et al., 2002; Nicholls et al., 2004; Absy et al., 2008; Huhn et al., 2008; Jullion et al., 2013).

Until recently, FRIS was considered to be protected from melting caused by the ocean, i.e. from increased basal melting, in a warmer climate because of the need of HSSW to transport heat into the ice shelf cavity (Nicholls, 1997). Nicholls (1997) believed that, with a lower HSSW formation caused by smaller sea ice growth rate, deep convection would be reduced and no other water mass would be able to carry heat into the ice shelf cavity. Hellmer et al. (2012) showed that in the absence or with a reduced volume of dense waters, HSSW or ISW, Warm Deep Water (WDW) can flow over the continental shelf and underneath FRIS via the Filchner Trough. The inflow of this relatively warm water mass would lead to massive ice shelf melting and substantial changes to the properties of WSDW and WSBW.

While the consequences of climate change for FRIS lie in the future, LIS already experienced sizable changes. In the past, Larsen Ice Shelf was formed by Larsen A (LIS-A), Larsen B (LIS-B), and Larsen C (LIS-C), but nowadays only LIS-C and a small portion of LIS-B exist. In January 1995, Larsen A disintegrated in a few days (e.g. Rott et al., 1996), and in February

of 2002 something similar happened to Larsen B (e.g. Rack and Rott, 2004). Despite of this visible changes to the ice shelf configuration, it is unknown if the absence of LIS-A and LIS-B had any consequences for the local hydrography or WSDW formation in the northwestern WS.

So far, LIS-C appears to be stable, but there is evidence of a thinning with time, possibly due to basal melting (e.g. Shepherd et al., 2003). The loss of air contained in glacial firn and consequent densification of the ice shelf could also account for the lowering of the ice shelf surface (Holland et al., 2011). A model study performed by Holland et al. (2009) suggests that marine ice and oceanic freezing can heal rifted meteoric ice, and thus reduce the likelihood of LIS-C collapse. They also state that the warming of waters in the ice shelf cavity would cause greater melting and less-widespread freezing. Modifications in the melting and freezing rates or in LIS-C morphology could cause changes to the WSDW formed in this area.

Although the dense water formation is small in the northwestern WS (Huhn et al., 2008; Caspel et al., 2015a), the contributions from the LIS region are found shallower in the water column than those originating from FRIS, 1000 km upstream (Gordon et al., 2001) and thus are more likely to escape from the WS to form AABW. The passages connecting the WS and the Scotia Sea are less than 3500 m deep (Naveira Garabato et al., 2002; Franco et al., 2007), so the shallower WSDW has a larger contribution to AABW. Schröder et al. (2002) observed a high variability in the properties of the dense waters able to cross the South Scotia Ridge and suggest that the fluctuations are related to an intermittent contribution of water masses from the Larsen region.

Fahrbach et al. (1995) compared a hydrographic section in front of Larsen C and one close to the tip of the Antarctic Peninsula (AP) and observed fresher and warmer deep and bottom water on the slope of the northern section. They argued that the changes along the flow were caused by a mixture of LIS shelf waters with WDW. Gordon et al., 2001 observed a fresher and more ventilated type of WSDW (VWSDW) and WSBW (VWSBW) south of the South Orkney Plateau both formed by the interaction between shelf water from the Antarctic Peninsula and WSDW. The authors suggest that the VWSBW is produced at a site more to the south with a stronger component of WSDW than the VWSDW. [1]

Measurements made in March 2002 on the shelf just north of Larsen C revealed the presence of water colder than the surface freezing point, originating from the interaction with the ice shelf (Nicholls et al., 2004). Hydrographic data from 2004-2005 collected during the Ice Station Polarstern (ISPOL) drift experiment (Hellmer et al., 2008) also showed evidence for dense water production in this region and revealed the presence of lenses of relatively salty and cold waters on the continental slope at a depth of 1600 m (Absy et al., 2008). Optimum Multiparameter Analysis (OMP) using temperature, salinity, and noble gas observations together with chlorofluorocarbons (CFCs) as age tracers supported the hypothesis of a nearby source (Huhn et al., 2008).[1]

In this study, the properties and pathways of dense waters coming from LIS surroundings are investigated using data from Polarstern Cruise ANT XXIX/3 (Gutt et al., 2013) and

---

[1]Paragraph copied from Caspel et al., 2015a

the Finite Element Sea-ice Ocean Model (FESOM). Besides of giving a broader view on the circulation with the present ice shelf configuration, the model will be used to (1) explore the importance LIS-B had to the regional circulation and to (2) evaluate an hypothetical scenario where LIS-C is completely absent.

In the following, a brief description of the hydrography and circulation is given to support the discussion in subsequent sections. In the second chapter, the hydrographic data used is described and the ideas derived from the observations are presented and discussed. In the remaining chapters FESOM and the sensitivity experiments are described, the results are analyzed and discussed in view of previous ideas. Finally, a summary and an outlook are given.

1.2   Hydrography and circulation

The WS circulation is dominated by the Weddel Gyre (WG - Fig. 1.2), a cyclonic gyre forced by the wind and enhanced by the baroclinic circulation caused by density gradients in the ocean. The southern and western boundaries of the WG are delimited by Antarctica and the AP, the northern 'margin' is set by the South Scotia Ridge and the Southwest Indian Ridge. There is no clear physical barrier at the eastern border of the WG making the eastern inflow and recirculation highly dynamic features (e.g. Schröder and Fahrbach, 1999).

The water masses carried by the WG are: Antarctic Surface Water (AASW), Winter Water (WW), WDW, WSDW, and WSBW (Fig. 1.3). AASW characteristics vary seasonally; during austral summer AASW is warmed by the sun and its salinity is reduced by melting of sea ice, in winter it cools down to surface freezing temperatures (-1.9^{o}C) and its salinity is usually higher. The mixed layer is deeper in winter, and the water portion below the surface water that remains cold during summer time is named WW.

WDW originates from Circumpolar Deep Water (CDW) that enters the WS mainly through its eastern margin (e.g. Ryan et al., 2016). CDW is light (lower density) compared to the water masses found at same depth inside the WS and upwells when entering the WG (Fig. 1.4 A). WDW occupies the depth range from 200 to 1500 m (e.g., Fahrbach et al., 2011), has a neutral density (γ^n - Jackett and McDougall, 1997) between 28.0 and 28.27 kg m^{-3}, and a potential temperature (θ) greater than 0°C (Fig. 1.4).

While flowing around the Weddell Basin, WDW is cooled by mixing with the surrounding shelf waters and recirculates as the WDW 'cold regime' (e.g. Ryan et al., 2016). Near the shelf break, WDW may become colder than 0°C, then called Modified Warm Deep Water (MWDW) if it has the same density as WDW. The mixture of MWDW or WDW with dense shelf waters forms WSDW or WSBW.

WSDW is found below the WDW, and WSBW occupies the bottom layer of the deep ocean. The γ^n of 28.4 kg m^{-3} separates the two water masses, the γ^n limits used to define the WSDW (28.4 kg m^{-3} > WSDW > 28.27 kg m^{-3}) and the WSBW (WSBW > 28.4 kg m^{-3}) correspond closely to the 0°C and -0.7^{o}C limits used in earlier studies (Fahrbach et al., 2011). The γ^n of 28.27 kg m^{-3} is also the lower density limit of AABW originating from the Weddell Sea (Orsi et al., 1999).
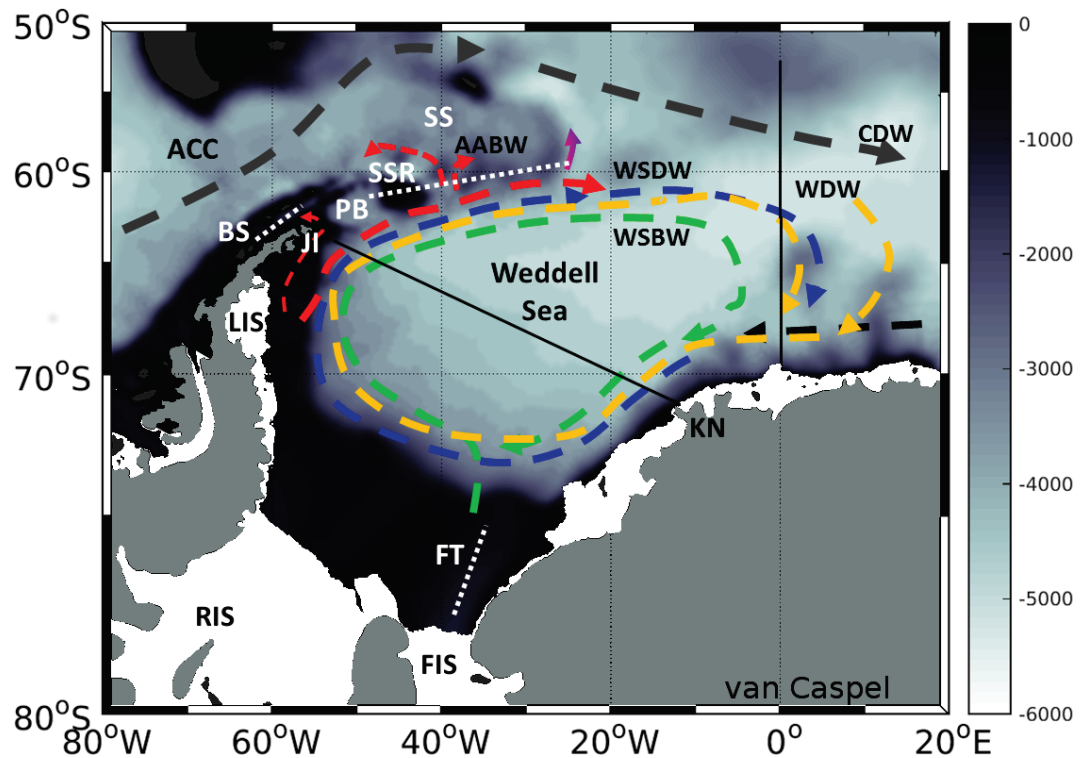
FIGURE 1.2: Schematic representation of the deep circulation in the Weddell Sea and surrounding basins. The black lines show the position of the sections shown in Figure 1.4. The abbreviations stand for Antarctic Bottom Water (AABW), Antarctic Circumpolar Current (ACC), Bransfield Strait (BS), Circumpolar Deep Water (CDW-gray), Filchner Ice Shelf (FIS), Filchner Through (FT-dotted line), Joinville Island (JI), Larsen Ice Shelf (LIS), Ronne Ice Shelf (RIS), Scotia Sea (SS), South Scotia Ridge (SSR-dotted line), Warm Deep Water (WDW-yellow), Weddell Sea Bottom Water (WSBW-green), and deep (blue) and shallow (red) Weddell Sea Deep Water (WSDW).
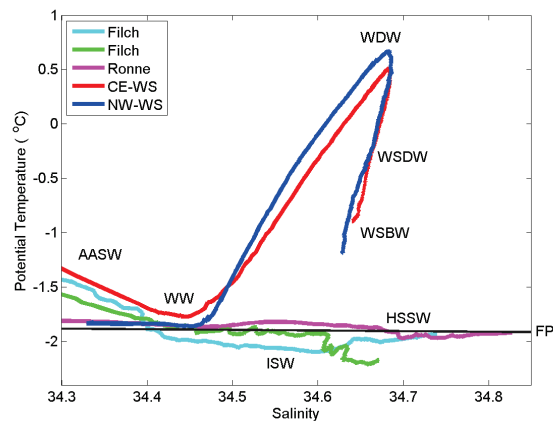
FIGURE 1.3: TS diagram showing the main water masses found in the Weddell Sea (WS). Two casts from the Fichner Through near the ice shelf (Filch), one cast from the western margin of Ronne Ice Shelf (Ronne), one from the northwestern Weddell Sea (NW-WS), and one from central WS (CE-WS), aprox. 35 ^{o}W along the section shown in Figure 1.2. Abbreviations are Antarctic Surface Water (AASW),High Salinity Shelf Water (HSW), Ice Shelf Water (ISW), Warm Deep Water (WDW), Weddell Sea Bottom Water (WSBW), Weddell Sea Deep Water (WSDW), and Winter Water (WW).

Here, two hydrographic sections are used to illustrate the water column structure: one along the Prime Meridian, and a second that runs from the tip of the Antarctic Peninsula to Kapp Norvegia (SR04)(Figs. 1.2 and 1.4). The data shown is from the World Ocean Atlas (WOA) (Locarnini et al., 2013), and these sections were chosen because they were repeated several times (e.g. Huhn et al., 2013). Along the Prime Meridian, the WOA data shows the CDW upwelling into the WS to form the WDW in the northern part of the section and WDW carried by southern branch of the WG near Antarctica. WSDW is found below the WDW and, between Maud Rise and the Southwestern Indian Ridge, where it overlays the WSBW. The WSBW occupies the deeper parts of the WS basin and is trapped there by bathymetric constrains, the total volume of this water mass is balanced by the conversion into WSDW due to mixture and its formation rate; small portions of WSBW can flow northward through the South Sandwich Trench (SST).

Along the upper part of the continental slope, the Antarctic Slope Front (ASF) is embedded in the WG (Fig. 1.4 B) .The ASF is a quasi-circumpolar structure characterized by a 'V'-shaped alignment of the isopycnals where deep water formation occurs, and tilts downward towards the shore in other areas (e.g. Whitworth et al., 1998; Thompson and Heywood, 2008). It is a highly dynamic feature that acts as a barrier between the colder waters found on the continental shelf and offshore waters.

Where the continental shelf break is close to the coast, the ASF is combined with the Antarctic Coastal Current (CC), which flows westward around Antarctica and in the WS contributes to the total transport of the Weddell Gyre. Including the contributions from CC and ASF, Thompson and Heywood (2008) estimated that the transport between Joinville Island and the 4000 m isobath in the northwestern WS was 46 ± 8 Sv ($1Sv = 10^6$ m^3 s^{-1}). The authors claim that this is a good estimate of the WG transport because 90% of it occurs in the western boundary current (Fahrbach et al., 1991). Nevertheless, they also point out the existence of disparate results regarding the WG transport. For example, along the prime meridian section estimates vary between 30 and 100 Sv (Klatt et al., 2005). This section crosses two branches of the WG, and Klatt et al. (2005) computed a westward transport of 56 ± 8 Sv in the southern limb and a eastward transport of 45 Sv ± 7 Sv in the northern. Thus 11 Sv must enter the WG east of Prime Meridian and leave the WS to the north (Klatt et al., 2005).

The inflow to the WG is composed mainly of AASW and CDW (converted to WDW) (Klatt et al., 2005). As previously mentioned, before escaping the WS part of AASW and WDW become denser and sink. Besides of AASW and CDW, AABW enters the gyre from the Indian sector and undergoes a densification before it is exported to the South Atlantic (Jullion et al., 2014). Naveira Garabato et al. (2002) dervided a LADCP-referenced geostrophic transport of WSDW across the South Scotia Ridge (SSR) of 6.7 ± 1.7 Sv, this estimates agree well with the model results presented by Schodlok et al. (2002) which calculated export rates of 6.4 Sv of WSDW through SSR. Using an inverse box model, the outflow of WSDW through the SSR was estimated as 4.7 ± 0.7 Sv, and, assuming that no AABW enters the Weddell Gyre from the Indian Ocean, approximately the same amount is exported further east (Naveira Garabato et al., 2002).
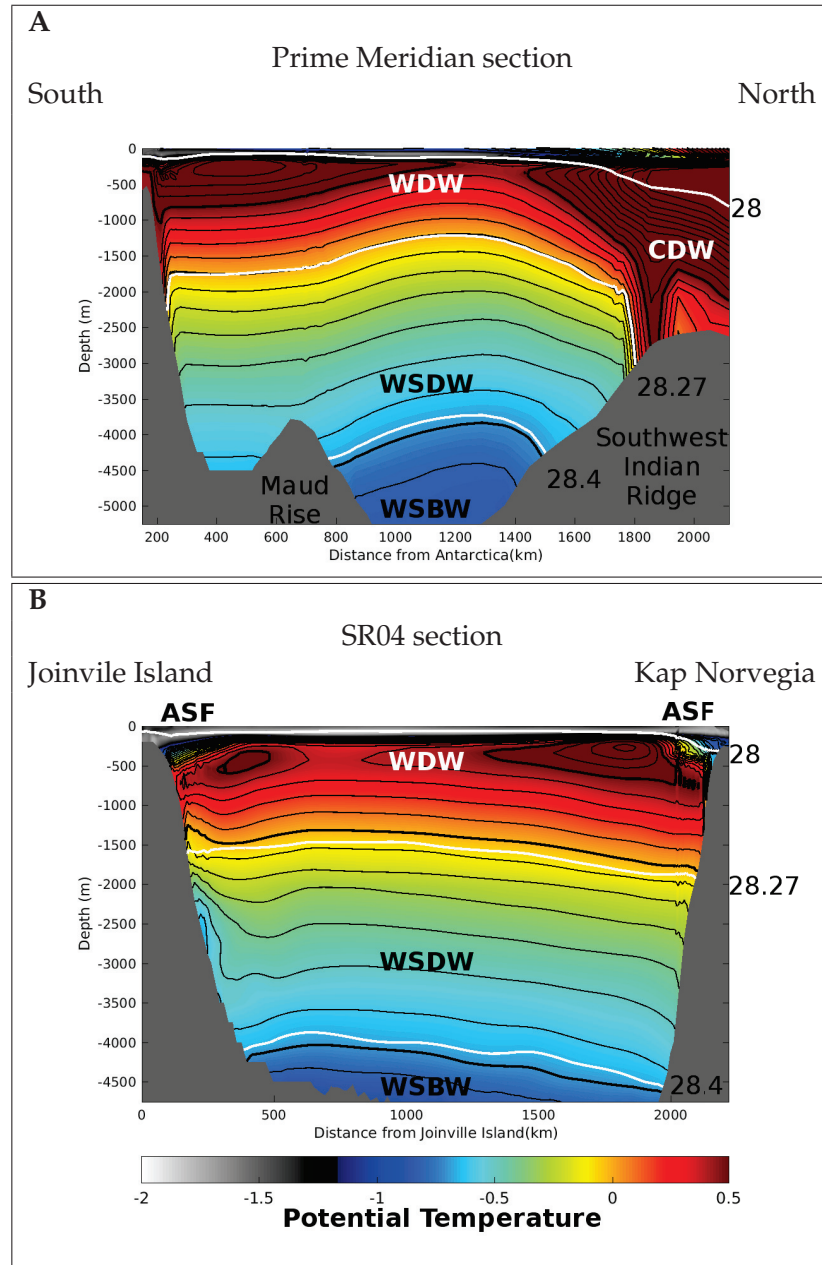
FIGURE 1.4: Potential temperature along the two sections shown in Figure 1.2: from the continental slope to the Southwest Indian Ridge along the prime meridian (A), and from Joinvile Island to Kap Norvegia (B). Contour lines in black every 0.1°C; the 0.5, 0.0, and -0.7 °C are thicker. The white lines are the 28.0, 28.27, and 28.4 kg m^{-3} neutral density contours (γ^n). Values are from World Ocean Atlas 2001 (WOA) and correspond to the initial conditions of the simulations used in this work, see Chapter 3. Abbreviations are: Antarctic Slope Front (ASF), Warm Deep Water (WDW), Weddell Sea Bottom Water (WSBW), and Weddell Sea Deep Water (WSDW).

The share of dense water that does not descend the continental slope flows around the tip of the Antarctica Peninsula and contributes to the deep waters of Bransfield Strait (BS) (e.g. Whitworth et al., 1994; Schodlok et al., 2002; Caspel et al., 2015b). The cyclonic circulation existent in BS carries the dense Weddell waters westward along the southern slope and than eastward on the northern slope (e.g. Gordon et al., 2000).

The WS dense waters escaping to the north become AABW and, thus, are crucial for the MOC while the portion entering BS is important to modulate phytoplankton dynamics within this basin (Gonçalves-Araujo et al., 2015). Therefore understanding the history of WS waters is important to comprehend global changes and the biological production on fringing basins.

Chapter 2

Observations

This chapter was published in the peer reviewed journal 'Deep Sea Research', Caspel et al., 2015a, and citations should refer to this article.

I participated on the hydrogaphic cruise where the data was collected, conducted the significant part of the analysis and interpretation of the data, wrote the text and prepared the figures of the published manuscript. All authors participated in the discussion of the data, interpretation and revision of the source article.

2.1   Polarstern Cruise ANT XXIX/3

The goal of the Polarstern cruise ANT XXIX/3 (January to March 2013) was to perform a multidisciplinary investigation in the area of former LIS-A and LIS-B together with a krill census. In addition, an extensive hydrographic and bathymetric investigation was planned for the continental shelf and slope in front of the LIS-C (Knust, 2012)[1]. Unfortunately, the initial plans had to be changed due to the severe sea-ice conditions (Gutt et al., 2013).

The main oceanographic goal was the investigation of dense water production in the LIS area. Therefore, three hydrographic sections were performed in the northwestern Weddell Sea (WS - Fig. 2.1) almost perpendicular to the continental slope to a depth of 3000 m. Although other casts were performed during the cruise, this work is focused on these three sections.

The data analysis is focused on the dense waters, defined here as all waters with a neutral density (γ^n) greater than 28.27 kg m^{-3}. This value was chosen because it was used in other works to define the interface between WDW and WSDW (e.g., Fahrbach et al., 2011), and also the upper limit of AABW originating from the WS (Orsi et al., 1999). The γ^n of 28.4 kg m^{-3} was used to separate WSDW from WSBW. Nevertheless, the names WSDW and WSBW are misleading when used for waters found in shallow areas, like the continental shelf. To avoid the depth association the terms Neutral Deep Water (DWγ^n) to refer to waters in the γ^n-range from 28.27 to 28.4 kg m^{-3}, and Neutral Bottom Water (BWγ^n) for γ^n higher than 28.4 kg m^{-3} are used. The new terms are especially useful to discuss the mixing processes occuring at the shelf break and on the slope. The terms introduced in this chapther are summarized in Table 2.1.

---

[1]$http://epic.awi.de/31329/7/ANT-XXIX_1-3.pdf$
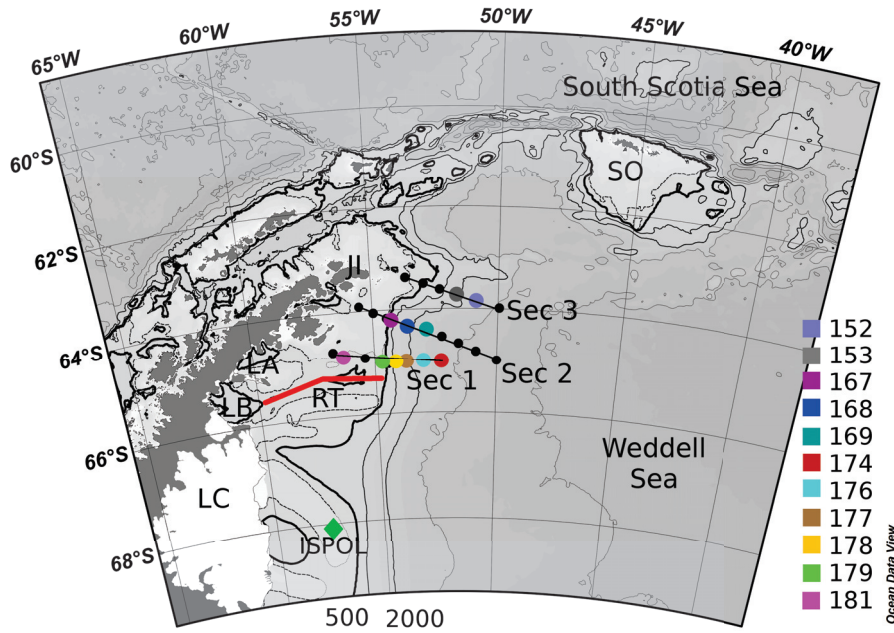
FIGURE 2.1: Regional map of the northwestern Weddell Sea. ANT XXIX/3 stations are marked with circles, stations mentioned in the text are coloured (see label on the lower right corner of the figure). Sections 1 to 3 are labeled (Sec #). The auxilar profile obtained from the ISPOL cruise is marked as a green diamond and labeled. The location of Robertson Trough is shown by the red line. Gray shades represent the bathymetry from Rtopo 1 (Timmermann et al., 2010), the isobaths of 400m (dashed line), 500m (thick line), 1000 and 2000m (thin lines), and 3000m, 4000m, 5000m (very thin lines) are drawn. Abreviations are: Joinville Island (JI), Larsen A, B and C (LA, LB and LC, respectively), Robertson Trough (RT), and South Orkney Island (SO)

2.2   Data quality

The hydrographic measurements during ANT XXIX/3 were made using a SBE 911+ CTD connected to a carrousel with 24 bottles of 12 l. The sensors attached to the system were two conductivity and temperature sensors, a pressure sensor, one oxygen sensor, a transmissometer, a fluorometer, and an altimeter. More details about the sensors are found in Gutt et al. (2013).

The conductivity and temperature sensor calibrations were performed before and after the cruise at Seabird Electronics. The accuracy of the temperature sensors is 2 mK. The readings of the pressure sensor have precision and accuracy better than 1 dbar. The conductivity

TABLE 2.1: New terms

LABW	dense water observed on the continental shelf in front of Larsen A and B
LCW	dense water observed on the continental shelf in front of Larsen C
$DW\gamma^n$	Neutral Deep Water; covers the WSDW and the waters on the continental shelf and slope with γ^n between 28.27 and 28.4 kg m^{-3}
$BW\gamma^n$	Neutral Bottom Water; covers the WSDW and the waters on the continental shelf and slope with γ^n values higher than 28.4 kg m^{-3}
$*^{SWT}$	used to refer to the Source Water Type representing an water mass ($*$)

was corrected using salinity measurements from water samples. IAPSO Standard Seawater from the P-series P154 (K15=0.99990, practical salinity 34.996) was used. A total of 98 water samples were measured using an Optimare Precision Salinometer OPS 006. On the basis of the water sample correction and sensor recalibration, salinity is measured to an accuracy of 0.002 (Schröder et al., 2013a).

The oxygen was corrected from water samples using the Winkler method with a Dissolved Oxygen Analyser (DOA,SIS type). In total, 217 water samples were measured from 25 stations, which were used to correct a small trend observed in the sensor measurements so that the final error was 1.34 μmol kg^{-1} (Schröder et al., 2013b) .

In addition to temperature, salinity, and oxygen, noble gas measurements were used to reinforce the OMP results. Water samples were taken from the CTD bottles using gas-tight copper tubes. They were measured by mass spectrometry at the IUP Bremen[2](Sültenfuß et al., 2009) for helium (He) isotopes and neon (Ne) with an accuracy of 1%.

Data from a cast (station 003-1) performed on December, 2004 during ISPOL was also considered (Absy et al., 2008). This station is located close to the shelf break in front of Larsen C and covers the temperature and salinity range necessary to produce the salty and cold WSBW observed during the cruise. The ISPOL cast was made using a CTD system carried by helicopter. The obtained accuracies were 0.005 (salinity), 0.003 (temperature), and 3 dbar (pressure). A Niskin bottle was used to take a water sample close to the bottom, which was analysed for the He and Ne concentrations (Huhn et al., 2008).

2.3 Classical analysis or First look at the data

The entire region was ocupied by cold ($\theta \simeq$ -1.8^{o}C) and fresh (S $<$ 34.4) surface water (Antarctic Surface Water) underlaid by slightly saltier (S $\simeq$ 34.45) Winter Water (WW). WDW is found below this level at stations deeper than 1000 m. The depth of the maximum temperature decreases with increasing distance from the shelf break and varies between 200 and 500 m. WSDW and WSBW are present beneath the WDW layer (Figs. 2.2, 2.3, and 2.4).

Between the shelf break and the 1000-m isobath, the intermediate and bottom layers are filled with a mixture of shelf and ambient waters, i.e., WDW or WSDW, depending on the depth and position in the water column. The mixing products of this interaction are modified WDW, DWγ^n (gray line in Figs. 2.2, 2.3, and 2.4) , and BWγ^n (black line in Fig. 2.2), which is a derivative from the dense water observed on the continental shelf along this section (Fig. 2.2). In sections 2 and 3, BWγ^n is not present at this shallow depth.

At the southern most section on the shelf, station 181 has the thickest BWγ^n layer. Towards the shelf break (#181 - #179) this layer gets thinner (96.9, 66.3, 49.4 m), warmer (mean θ: -1.841, -1.829, -1.654 ^{o}C) and saltier (mean S: 34.555, 34.555, 34.573) while the oxygen values decline (mean O$_2$: 296.865, 295.650, 288.813 μmol kg^{-1}). Station 182 is located on the northern slope of the Robertson Trough (Fig. 2.1). Thus, it is shallower than the other stations and has a thinner BWγ^n-layer, which is concentrated on the deep portions of the trough; Robertson Trough is a depression on the continental shelf that connects the former

---

[2]Institute for Environmental Physics - University of Bremen

LIS-B cavity with the shelf break, and is also connected to a channel coming from the former LIS-A region (e.g., Evans et al., 2005). The deepest part of the depression is not connected to the shelf break and might serve as a reservoir of dense water.

Waters with similar characteristics were observed in Robertson Through in October, 2006 (Lemke, 2009) and in February, 2009 (ATOS2), but they showed a colder and saltier bottom layer. The differences can be caused by seasonal and interannual variability, changes in the pulses of dense water outflow, and/or the older measurements were made closer to the reservoir. The deep troughs found on the continental shelf formerly covered by LIS-A and B (e.g., Arndt et al., 2013) are possible sources for this pulses since there the dense-water layer is much thicker (Graeve et al., 2013). However, because of the bathymetric restrictions, only by mixing with shallower waters can the dense water leave the basins and spill into the Robertson Trough.

Further north, on Sections 2 and 3, no $BW\gamma^n$ was detected on the continental shelf (black line in Figs. 2.3, and 2.4), providing additional evidence that the dense water is guided to the slope by local bathymetry. Following the shelf break downstream, part of the $BW\gamma^n$ observed at # 179 is converted into $DW\gamma^n$ in Section 2 (#167-3), likely due to further mixing with WDW. The temperature, salinity and oxygen profiles of the $DW\gamma^n$ from #167 at 450 m depth (purple arrow in Fig. 2.5) resembles the thin layer of fresh, cold, and ventilated water, observed offshore in the WSDW layer at 1600 m depth (#168, blue arrow in Fig. 2.5). To the south, in Section 1, a similar feature is observed at a depth of 1000 m (#178, yellow arrow in Fig. 2.5).

The stations with the intrusions (#168 and #178) show the densest bottom water sampled during the cruise. The bottom θ/S-values are almost the same (Fig. 2.5), and the oxygen is the highest observed in offshore deep waters (Figs. 2.2, 2.3, and 2.4). These similarities suggest that both have the same origin and are flowing downslope.

Additional evidence that WSDW and WSBW are produced in the northwestern WS is the increase of the dense layer thickness along the 1800-m isobath (#153, #168, and #177) (Fig. 2.6). From Section 1 to Section 2 the thickness increased from 261 to 325 m, reaching 452 m at Section 3. Comparing the vertical profiles of the three stations, a northward freshening, cooling, and oxygen increase can be observed below 1000 m almost down to the sea floor (Figs. 2.5 and 2.6). High vertical gradients are found close to the bottom between Sections 1 and 2, but this change is followed by a warming and oxygen reduction on the northern section (Figs. 2.5 and 2.6).

The existence of thin layers with different properties (Fig. 2.5), the deepening of the densest water, and the increase of the dense layer thickness point to a nearby source. This will be investigated in the next section using the OMP analysis.

2.4 Optimum Multiparameter Analysis (OMP)

OMP is a method used to determine the mixture fractions (f_i) of predefined source water types (SWT) to produce the characteristics of an observed water particle (X_{obs}) (Tomczak, 1981; Mackas et al., 1987; Tomczak and Large, 1989; Huhn et al., 2008; Frants et al., 2013).
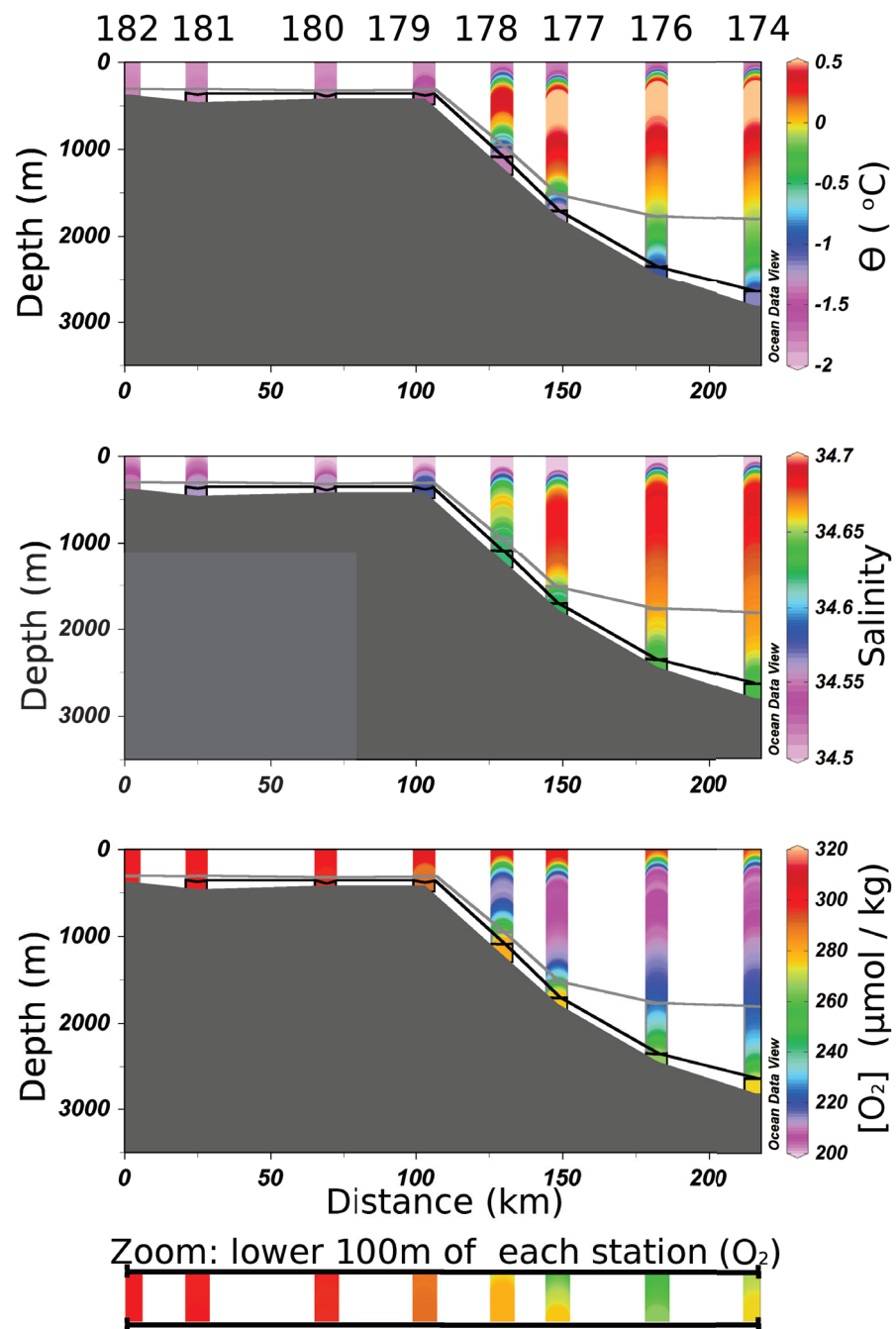
FIGURE 2.2: Section 1 measured values of potential temperature (^{o}C, top) , salinity (middle), and oxygen concentration (μmol kg^{-1}, bottom) as represented by the colours. Station numbers are displayed on top of the first figure. The gray line represents neutral density (γ^n, kg m^{-3}) of 28.27 and the black line of 28.4. The bathymetry corresponds to the bottom depth taken from the casts. The oxygen concentration of the lower 100 m is shown in the lower part of the bottom figure.
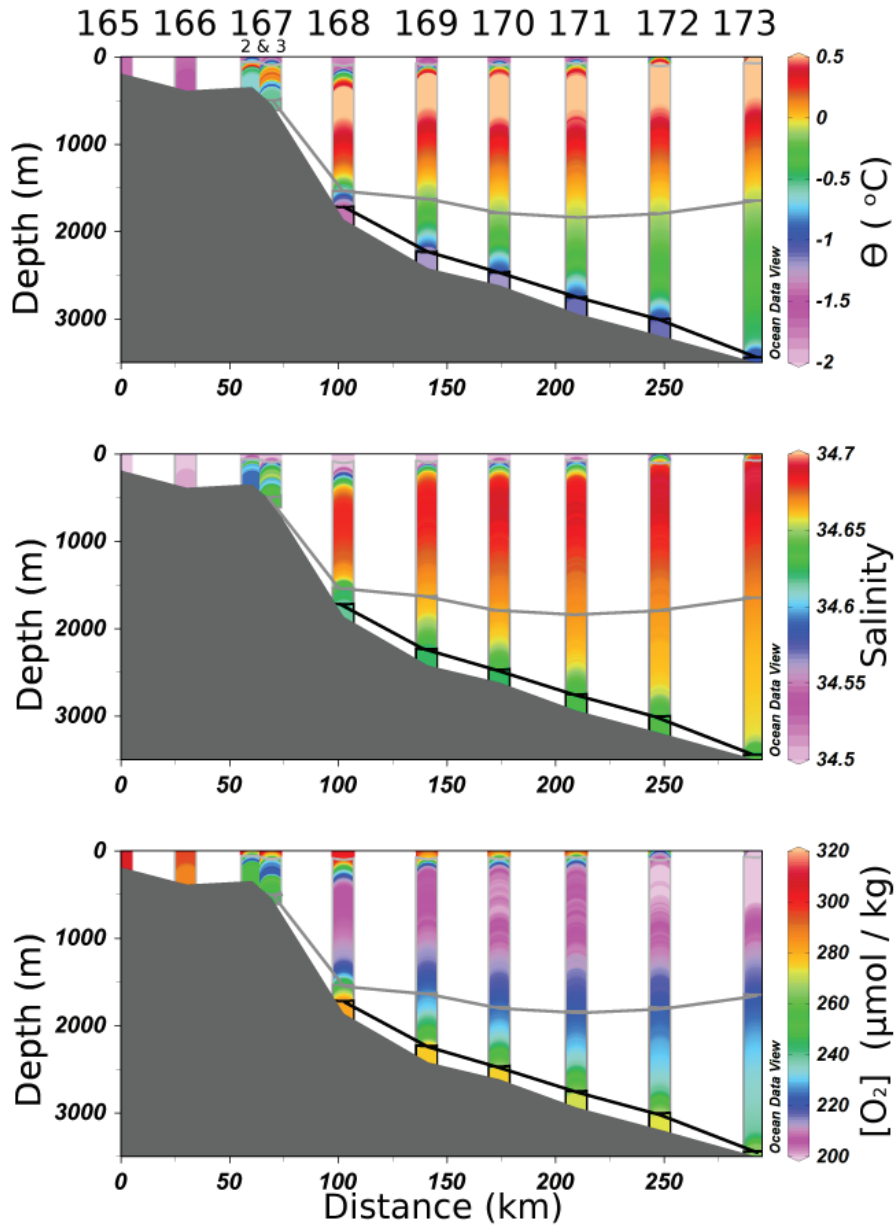
FIGURE 2.3: Section 2 measured values of potential temperature (^oC, top) , salinity (middle), and oxygen concentration (μmol kg^{-1}, bottom) as represented by the colours. Station numbers are displayed on top of the first figure. The gray line represents neutral density (γ^n, kg m^{-3}) of 28.27 and the black line of 28.4. The bathymetry corresponds to the bottom depth taken from the casts.
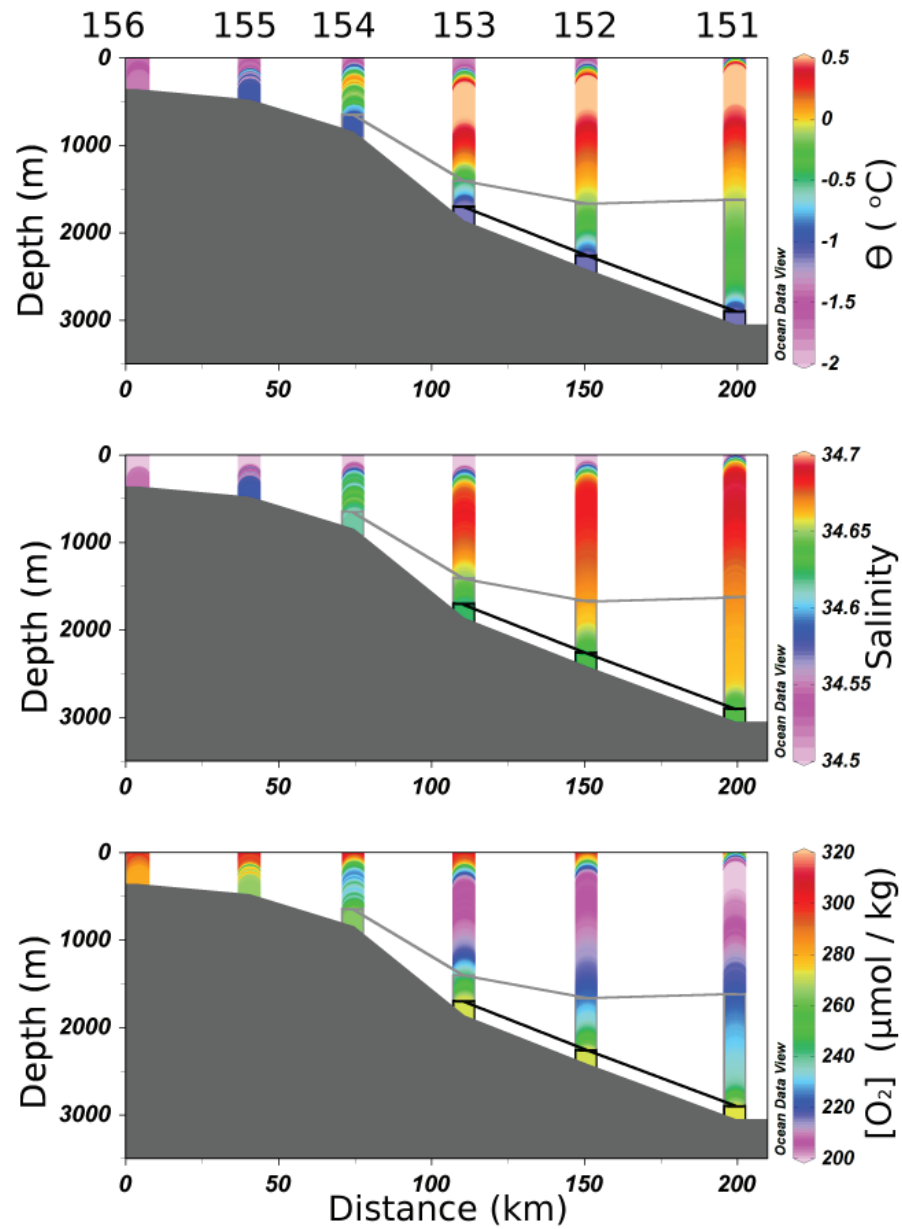
FIGURE 2.4: Section 3 measured values of potential temperature (^{o}C, top) , salinity (middle), and oxygen concentration (μmol kg^{-1}, bottom) as represented by the colours. Station numbers are displayed on top of the first figure. The gray line represents neutral density (γ^n, kg m^{-3}) of 28.27 and the black line of 28.4. The bathymetry corresponds to the bottom depth taken from the casts.
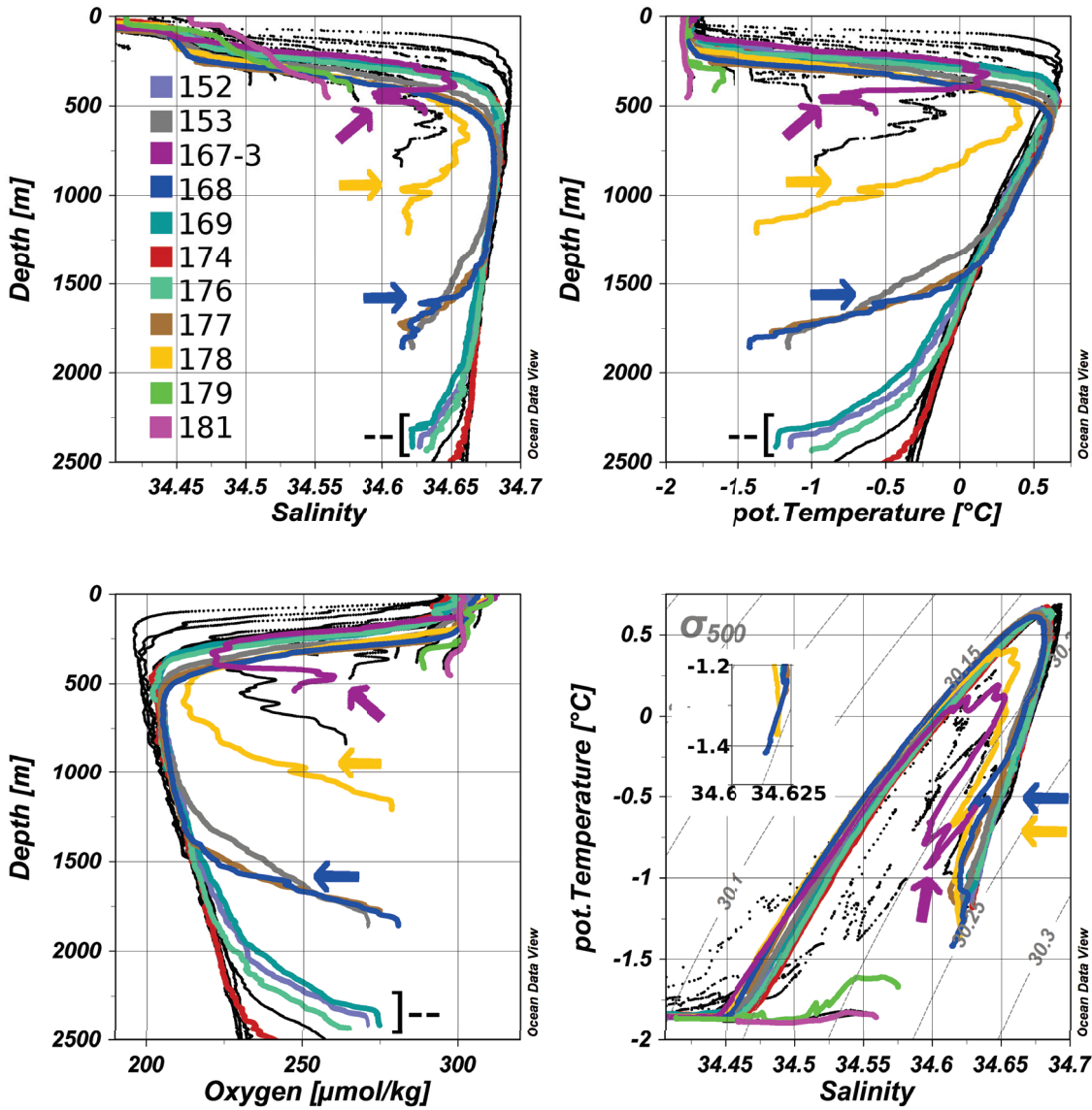
FIGURE 2.5: Vertical profiles of salinity (top left), potential temperature (^{o}C, top right), oxygen concentration (μmol kg^{-1}, bottom left), and a θ/S-diagram (bottom right) with contours of the potential density refered to 500m. The colours are related to different stations as shown in the top left graph, the remaining casts are shown in black. The arrows show the location of the intrusions discussed in the text, and '−−[' is a reference for the three stations along the 2400-m isobath.
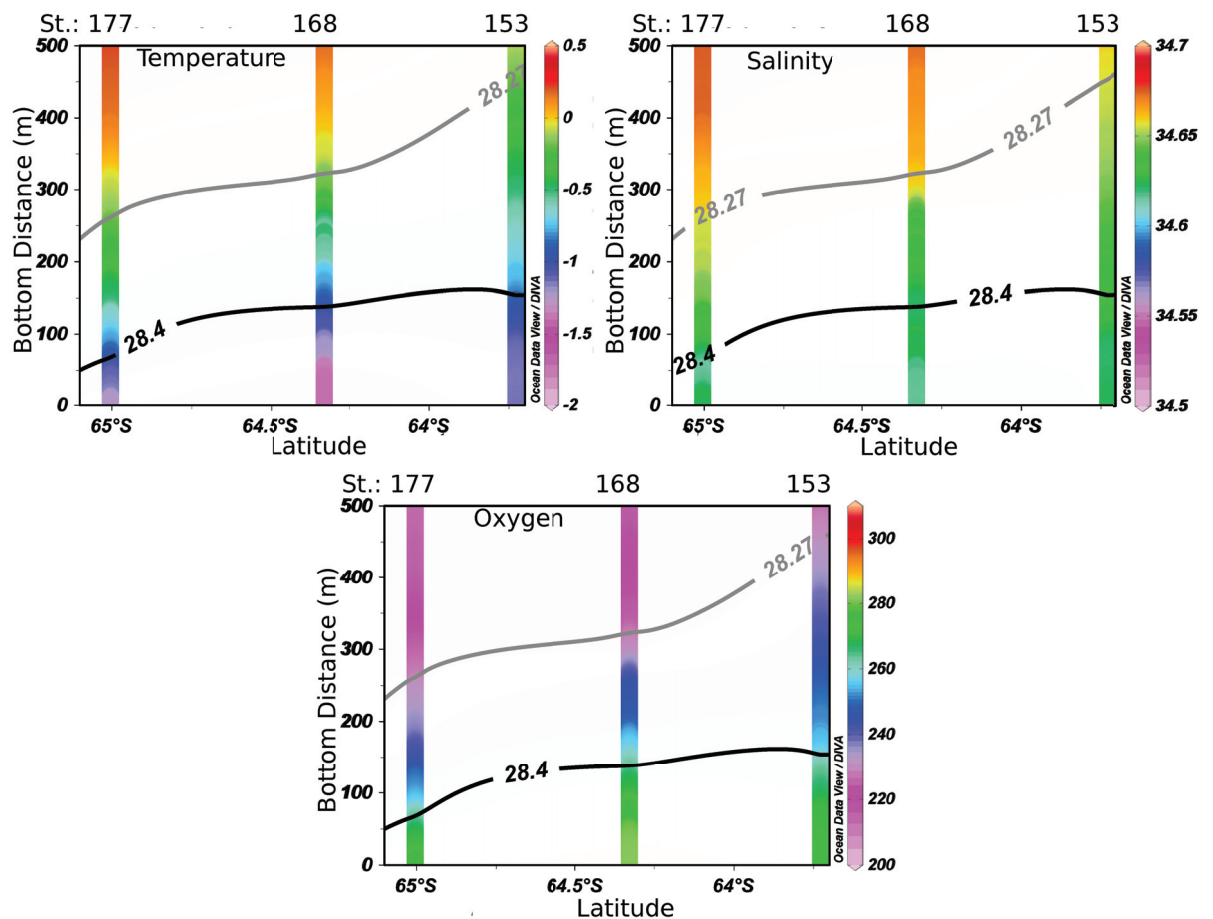
FIGURE 2.6: Transect along the 1800-m isobath. The colours represent potential temperature (^{o}C, top left), salinity (top right), and oxygen concentration (μmol kg^{-1}, bottom). The gray line represents neutral density (γ^{n}, kg m^{-3}) of 28.27 and the black line of 28.4. The abscissa shows latitude and the ordinate distance from the bottom of each cast. The station numbers are on top of each figure.

The method assumes a linear mixing combination of the SWT_i properties (X_i) (Eq. 1) and mass conservation (Eq. 2) under the condition that all f_i should be positive.

$$X_{obs} = \sum f_i X_i \qquad (2.1)$$

$$\sum f_i = 1 \qquad (2.2)$$

The number of SWT that can be considered must be equal or smaller than the number of conservative properties analysed plus one. Inverting this equation system by minimizing the deviations between observed and computed properties (Eq. 2.3) in a least square sense yields the optimum combination of SWT fractions. The equations are normalized by the mean and the standard deviation of each property, and weighted; for more details see Tomczak and Large (1989). The analysis presented here was performed based on the OMP Package for MATLAB Version 2.0 (Karstensen and Tomczak, 1995).

$$R_X = X_{obs} - \sum f_i X_i \qquad (2.3)$$

In an ideal case all measured parameters can be reproduced exactly, but usually there is some residual difference (R_X), which was used to evaluate the quality of the results obtained. In this study potential temperature (θ), salinity, and oxygen were considered as conservative parameters. Changes in oxygen due to biogeochemical processes are expected to be small because the study is confined to a small area and the SWTs are defined from data obtained nearby. Nevertheless, a smaller weight was used for oxygen , 0.3, than for the other parameters, 1.

Since this work is focused on the production of WSDW and WSBW, the OMP analysis was applied only to dense waters, γ^n greater than 28.27, found offshore of the shelf break, i.e., below the gray line and to the right of #179 (Fig. 2.2), #167 (Fig. 2.3), and #154 (Fig. 2.4).

Based on the high oxygen concentrations observed at the bottom of #181, at the northern flank of Robertson Trough, it is assumed that (even) mixing with ambient water will conserve this signal. The gas content gradualy reduces as the dense water flows down the continental slope along the bottom and mixes (lower part of Fig. 2.2), reaching its minimum value at 2400 m depth. It is assumed that the increase in oxygen concentration further downslope, at 2800 m (#174), is associated with WSBW produced in the vicinity of the Filchner-Ronne Ice Shelf (FRIS) and suppose that the portion of this water that remained at shallower depth (Foldvik et al., 2004) is mixed with the overlaying waters (WSDW and WDW) and waters coming from the continental shelf off LIS.

Because of this evidence for a distinction between WSBW from different sources, #174 was chosen to represent the incoming WSBW; here, the bottom value was used to define the WSBW-SWT ($WSBW^{SWT}$) (Table 2.2). Hereafter, the SWT-uppercase is used to distinguish between the water masses, which have property values within a certain range, and the SWT with distinct θ, S, and oxygen values.

For the WDW^{SWT}, the salinity maximum of the same profile (816 m depth of station 174) was selected because it can linearly mix with $WSBW^{SWT}$ to produce the WSDW observed

TABLE 2.2: Source Water Type Parameters. The standard deviation of the layers representing the Larsen waters is also shown

SWT	θ (^{o}C)	S	[O$_2$] (μmol kg^{-1})
WSBW^{SWT}	-1.185	34.629	273
WDW^{SWT}	0.482	34.686	203
LABW^{SWT}	-1.841 $\pm$ 0.005	34.555 $\pm$ 0.003	297 $\pm$ 0.3304
LCW^{SWT}	-1.925 $\pm$ 0.001	34.640 $\pm$ 0.009	300

at the deeper stations (Fig. 2.7). Besides, as shelf water flows downslope the mixtures with water of the salinity maximum are denser than mixtures with water of the temperature maximum, and thus more likely to become WSDW or WSBW.

2.4.1 Larsen area contribution

The OMP analysis was conducted using WDW^{SWT}, WSBW^{SWT} and a third SWT that reflects the dense water observed in the Robertson Trough, named Larsen AB Water (LABW). The LABW^{SWT} parameters were defined as the mean values of the BWγ^n layer at #181 (Table 2); as stated before, #182 suffers less influence of the LABW because it is located on the northern slope of the Robertson Trough. Using the three SWTs, most of the observations can be reproduced with small R$_X$ (R$_\theta$ < 0.01, R$_S$ < 0.005, R$_{O_2}$ < 7, R$_{mass}$ < 0.0005). However, the densest waters observed could not be reproduced (yellow circle in Fig. 2.7), indicating that an additional source water mass is still missing.

As mentioned before, the deepening of this densest water between Sections 1 and 2 suggests a nearby source, but the unsatisfying OMP results indicate that it can not be LABW. The results of previous studies (Absy et al., 2008; Huhn et al., 2008) suggest the production of WSBW in front of Larsen C. Therefore, a fourth SWT representing the Larsen C Water (LCW) was added. A satisfactory reproduction of all dense water characteristics was achieved only when considering this fourth SWT.

LCW^{SWT} characteristics were obtained from the ISPOL station 3-1, with the average of the lower 100 m used to represent temperature and salinity (Table 2, Fig. 2.7). No oxygen sensor was used during the ISPOL cruise, but some water samples collected on the slope, were analyzed with the Winkler method (unpublished data, David Thomas). In the region where the bottom waters were related to the Larsen C Ice Shelf, i.e. at 1500 m depth (Absy et al., 2008), the oxygen values were high (291-294 μmol kg^{-1}). Since the waters on the slope most likely mixed with ambient waters, a value of 300 μmol kg^{-1} was used to represent LCW (Table 2).

With the addition of the Larsen Waters the results in the area between the shelf break and 2000 m depth as well as in the bottom layer (lower 80 m) of #169 and #152 improved in comparison to the tests without them. Although the WSBW^{SWT} temperature and salinity are encompassed by the other SWTs (Fig. 2.7), this water mass is needed to resolve the oxygen observations (not shown). The residual difference (R$_X$) of the BWγ^n-layer is comparable to the accuracy of the measurements and the standard deviation of the values chosen
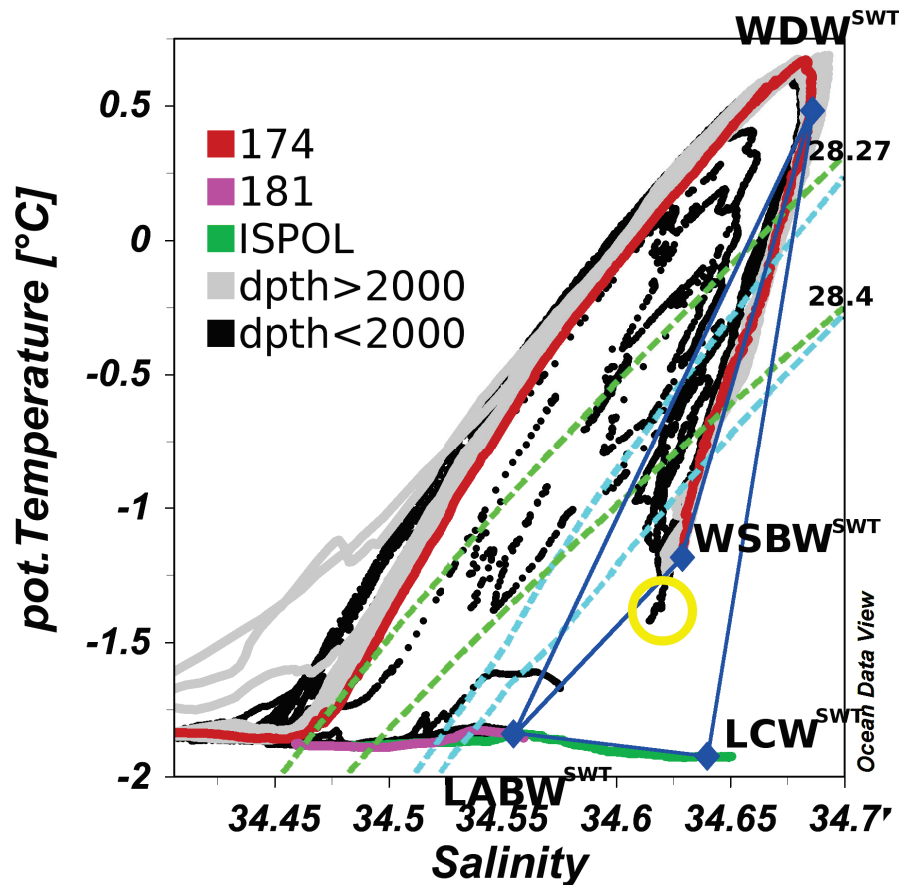
FIGURE 2.7: θ/S-diagram showing the Source Water Types (SWT) used for the Optimum Multi-parameter Analysis (OMP). The values used for OMP are marked as blue diamonds, the stations where they were measured are coloured. Stations in regions deeper than 2000 m are shown in gray and the remaining stations are displayed black. The yellow circle shows water characteristics that cannot be reproduced using only three SWTs, see text for more details. The dashed lines are contours of neutral density refered to 500-m (cian) a 2000-m (light green) depth, 65°S, and 55°W.
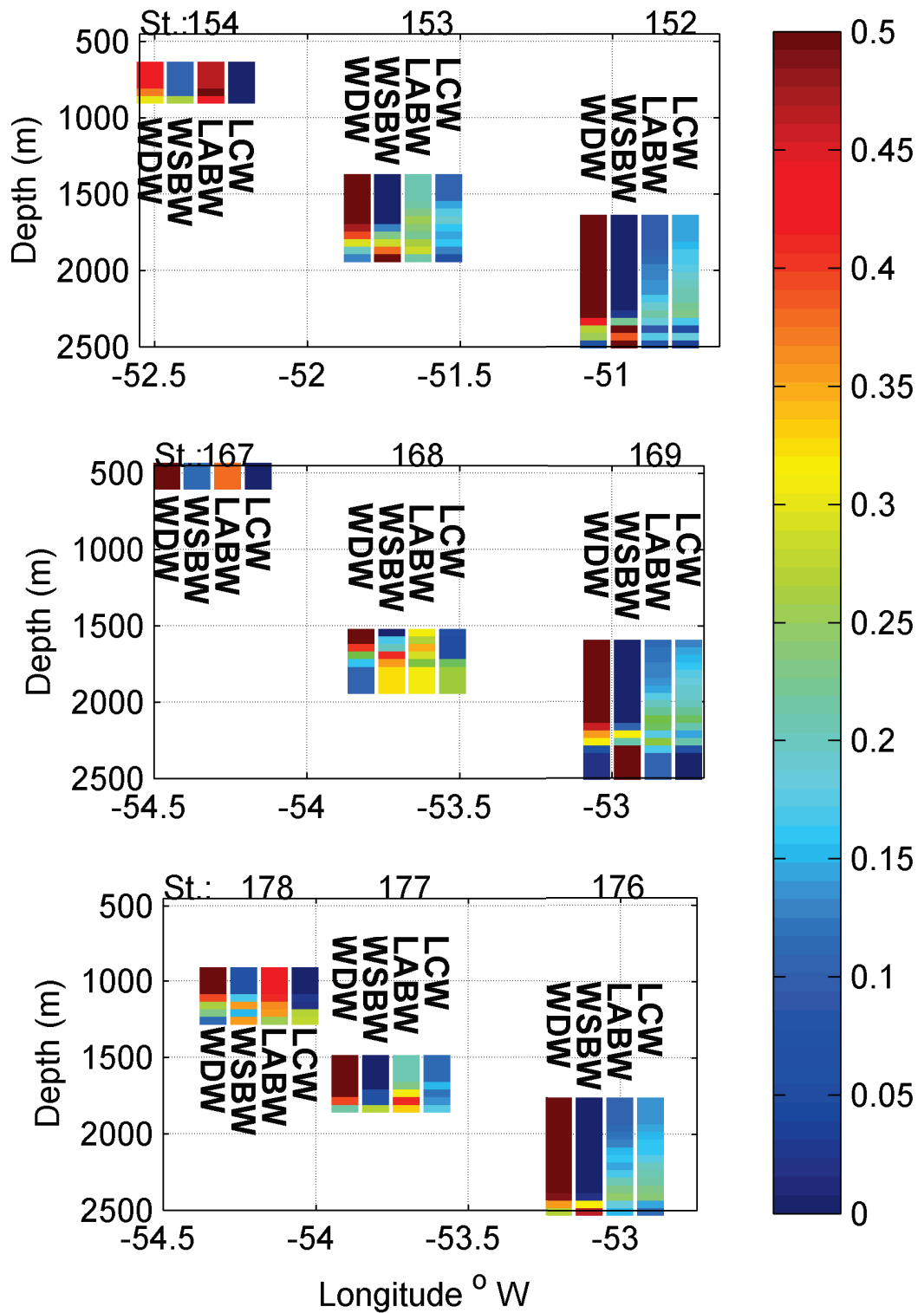
FIGURE 2.8: Source Water Type (SWT) fractions (colour shading) of the dense water layer, $\gamma^n >$ 28.27 kg m^{-3}, along the slope of Section 1 (bottom), Section 2 (middle), and Section 3 (top) . Station numbers are displayed on top of the figures, and the SWT fractions at each station are, from left to right, Warm Deep Water SWT (WDW^{SWT}), Weddell Sea Bottom Water SWT (WSBW^{SWT}), Larsen A and B Water SWT (LABW^{SWT}),and Larsen C Water SWT (LCW^{SWT}). The contributions are averaged every 50 m from the bottom up. The ordinate shows the depth in m, and the abscissa is a reference of longitude; the station is positioned where the LABW^{SWT} contribution is plotted.
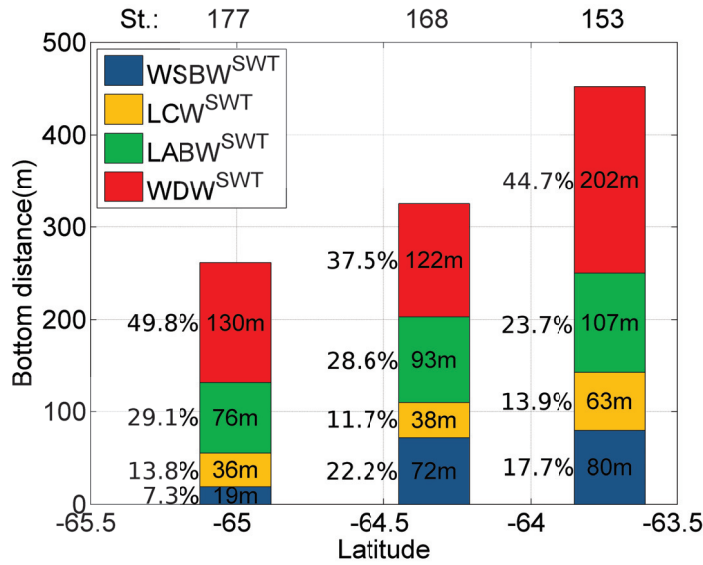
FIGURE 2.9: Composition of the dense water layer, $\gamma^n > 28.27$ kg m^{-3}, along the 1800-m isobath. The contribution of each Source Water Types (SWT) is vertically integrated and represented by the height of the coloured rectangles, Warm Deep Water SWT (WDW^{SWT}, red), Larsen A and B Water SWT (LABW^{SWT}, green), Larsen C Water SWT (LCW^{SWT}, yellow) and Weddell Sea Bottom Water SWT (WSBW^{SWT}, blue); the same colours are used in figure 2.10. The numbers inside the rectangles correspond to the water column thickness in meters, and the ones to the left are the contributions of each SWT in percentage . The abscissa represents latitude and the ordinate distance from the bottom of each cast. The corresponding station numbers are on top of the figure.

to represent LABW and LCW (Table 3), indicating that this level was well represented in the OMP analysis.

The R$_X$ gradually increases towards the interface with the WDW layer, reflecting the higher variability of the lighter waters involved in the production of DWγ^n. The selection of the salinity maximum to characterize WDW^{SWT} was essential for a good representation of the incoming WSDW, but shallower (warmer and fresher) or modified (colder and fresher) portions of this water mass may also interact with the shelf waters to produce the upper parts of the WSDW layer observed on the slope. To represent all variations of the WDW additional SWTs would be needed, but, due to the limitations of the method, only one SWT can be used to represent WDW.

The consistency of the OMP results was also checked against the tracer gases. He and Ne values from the same stations, used for the other parameters (#181, #174, and from ISPOL), were considered for each SWT, taking the data from the nearest bottle. In general, the noble gas values obtained by the OMP analysis agree with the observed characteristics within the water column and the R$_X$ are within the accuracy of the measurements.

Several tests were performed using different values for the SWT properties and weight. These tests were performed to account for the variability in the water mass characteristics, specially concerning the LCW^{SWT}. The use of data from a different year is not ideal so the analysis was also performed using values obtained from a cast made in 1992 (Gordon, 1998).

As mentioned before, a smaller weight was given to oxygen to account for the differences in the oxygen mixing that might be associated with biogeochemical processes. The value

was used because it resulted on the smaller R_X tests with different weights. This approach was used instead of the variance method proposed by Tomczak and Large (1989) because the variability of LABW and LCW could not be estimated due to the lack of knowledge about the source region characteristics.

Due to the large number of possible settings it is difficult to estimate the exact errors, but the general patterns of SWT distribution were kept in all the assessments for which a deeper examination was performed. The results mentioned before and described hereafter are the ones with the smaller R_X.

2.5 Discussion

The OMP results indicate a strong influence of WDW^{SWT} on the upper levels of the dense stratum, and large contributions of WSBW^{SWT} close to the bottom of the deeper stations. On Section 1 (Fig. 2.8, bottom), the LABW^{SWT} dominates the shelf break and is also important on the upper slope (#178), where the dense water observed close to the bottom is represented by a mixture of WSBW^{SWT} and LCW^{SWT}.

At Section 2 (Fig. 2.8, middle), the shelf break characteristics are represented by a mixture of WDW^{SWT} and LABW^{SWT}. On the slope (#168), the mean contribution of LABW^{SWT} is 28%, and it varies between 10% and 45% if the water column is divided in 1-m intervals (not shown); the influence of this SWT is high where the fresh intrusions (thin layers) were observed. At this station (#168), WSBW^{SWT} is the major source water between 1760 and 1820 m depth. Near the ocean floor (from 1820 m until 1860 m depth), it is mixed with LCW^{SWT} and LABW^{SWT} to produce the densest water observed.

Further to the north (Section 3, Fig. 2.8, top), no dense water (DWγ^n) is observed at the shelf break (Fig. 2.4). Next to it (#154), the DWγ^n layer goes from 650 m depth down to the bottom (840 m) and consists of a mixture of WDW^{SWT} and LABW^{SWT}, with small contributions of WSBW^{SWT} in the lower 50 m. Around 1850 m (#153), LABW^{SWT} is more widespread in the water column than on Section 2, WSBW^{SWT} is attached to the bottom, and LCW^{SWT} is more abundant between 1700 and 1800 m.

The increase of dense layer thickness along the 1800-m isobath is caused by an increased amount of all SWTs (Fig. 2.9). The presence of LABW^{SWT} on Section 1 can be explained by the injection of this water mass at the southern margin of the Robertson Trough. The total amount of this SWT in the water column increases by 31 m from the southern to the northern section. Its direct impact is not very strong, but it plays a major role in the conversion of WDW to WSDW; the amount of WDW^{SWT} in the water column shows an increase of 72 m. Nevertheless, mixing between the waters requires time which means that LABW becomes more influential as the rim current flows to the north.

Still following the 1800-m isobath, the contribution of WSBW^{SWT} to the water column thickness expands from 19 m to 72 m between Sections 1 and 2 (Fig. 2.9). This addition of WSBW^{SWT} might come from waters carried down the slope together with LCW. During this process part of the LCW mixes and spreads over the water column while its densest (lower) components continue to flow downslope until they reach the equilibrium depth.

The OMP results indicate that the dense waters originating from Larsen C reach at least the bottom layer of #152 and #169, located at 2400-m depth. Comparing these stations with #176, the Larsen waters seem to influence a layer 1000-m thick, since the southern cast shows higher temperature and salinity, and lower oxygen below 1500m than the two stations to the north (see '−−[' on Fig. 2.5).

The increase of the dense layer thickness observed along the 1800-m isobath and the modifications along the 2400-m isobath are related to the formation of WSDW. This water mass is carried in the northern branch of the Weddell Gyre and might cross the South Scotia Ridge (Gordon et al., 2001) to form AABW (Fig. 2.10). The portion influenced by LABW is lighter and can leave the WS through Philip Passage (Palmer et al., 2012), while the densest waters produced with LCW contributions can only cross one of the deeper gaps east of the South Orkney Plateau (Figs. 2.1 and 2.10).

2.6   Chapter Summary

The production of WSDW and WSBW in the Larsen region has been suggested by several authors (e.g. Fahrbach et al., 1995; Schröder et al., 2002; Absy et al., 2008; Huhn et al., 2008). The scheme proposed here (Fig. 2.10) can explain the fresh, dense water observed at intermediate depths in the northwestern WS (Fahrbach et al., 1995) as well as the cold and saltier lenses observed on the continental slope in front of Larsen C (Absy et al., 2008). Huhn et al. (2008) calculated a production rate of 1.1 ± 0.5 Sv (1 Sv = 10^6 m^3 s^{-1}) of WSBW in the western WS, corresponding to 22% of the total production of this water mass (3.9 ± 1.2 Sv are produced off Filchner-Ronne Ice Shelf) (Huhn et al., 2008) . In this study, no volume estimates are presented, but it is shown that the thickness of the dense layer increases by 70% in a short distance of 200 km (Fig. 2.6, and 2.9).

The contributions of the Larsen region to WSDW and WSBW formation can be noticed by changes in the properties of these water masses passing successive transects perpendicular to the continental slope. Other studies where the importance of the northwestern WS for dense water production was recognized also used sections at different latitudes (Fahrbach et al., 1995; Gordon, 1998; Absy et al., 2008). If only one section is analyzed, it is unlikely that the contributions of LCW and/or the LABW are noticed, especially if it is a section to the north where these water masses are well distributed in the entire water column.

Jullion et al. (2013) suggested that the freshening of AABW in Drake Passage is related to the increased glacial loss from the Antarctic Peninsula after the breakup of Larsen A and B. No time variability was assessed in the present work, but it is clearly shown that in 2013 the waters from Robertson Trough reduced the salinity of WSDW, forming a fresher version of this water mass on Sections 2 and 3 in comparison to the WSDW coming from the south, i.e., Section 1.

Our results also show that less diluted LCW influences layers deeper than 1800 m, with traces reaching at least 2400 m depth, accounting for the densest water that can cross the South Scotia Ridge (Fig. 2.10). This is in agreement with the hypothesis of Schröder et al.
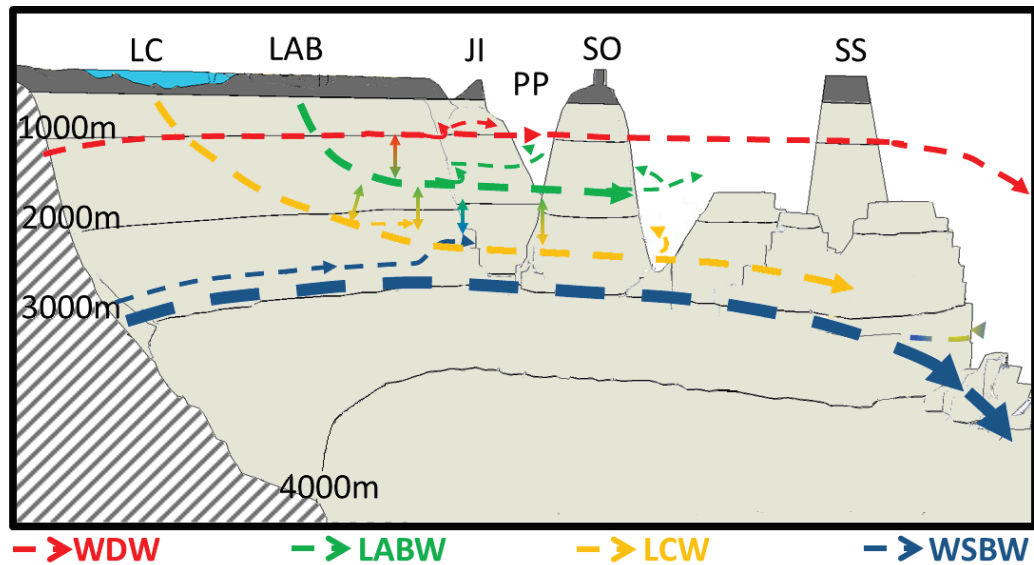
FIGURE 2.10: Proposed mixing scheme for the formation of Antarctic Bottom Water (AABW). The flow of the Warm Deep Water (WDW, red line), Weddell Sea Bottom Water (WSBW, blue line), Larsen C Water (LCW, yellow line) and Larsen A and B Water (LABW, green line) are shown together with the main outflow paths. Abreviations are: Joinville Island (JI), Larsen A and B (LAB), Larsen C (LC), Philip Passage (PP), South Orkney Island (SO), South Sandwich Islands (SS).

(2002) that pulses of dense water coming from a source nearby could cause the variability observed at a mooring at 2500-m depth in the northwestern WS (Schröder et al., 2002; Gyldenfeldt et al., 2002).

To fully understand the production and spreading of AABW and its precursors the importance of the different sources must be understood. The evidence presented so far, together with previous indications strongly suggests that the continental shelf in front of LIS is important for WSDW formation. The Finite Element Sea ice Ocean Model (FESOM) is used to test this hypothesis. In the following chapters, the model is described and the results of three model experiments are presented.

Chapter 3

The Model

3.1 Finite Element Sea-ice Ocean Model (FESOM)

The Finite Element Sea-ice Ocean Model (FESOM) was developed at Alfred Wegener Institute (Timmermann et al., 2009; Wang et al., 2014), as an enhancement of the Finite Element Ocean Model (FEOM) (Danilov et al., 2004). FESOM is a fully-coupled combination of a finite element ocean circulation model which includes the ice shelf cavities and a dynamic-thermodynamic sea-ice component, and has been proved as a good tool for studies of the Southern Ocean (e.g. Wang et al., 2008; Hellmer et al., 2012; Timmermann et al., 2012; Nakayama et al., 2014).

The Ocean component solves the hydrostatic primitive equations and was extensively described in Danilov et al. (,e.g., 2004), Timmermann et al. (2009), and Wang et al. (2014). The ocean-ice shelf interaction is included, based on the three equation approach proposed by Hellmer and Olbers (1989), the cavity has a constant geometry, and the model accounts for the ocean heat loss and represents the Glacial Melt Water (GMW) by changes in the salinity.

The sea-ice is represented by a two-layer model, one layer of snow and one layer of ice with the internal heat capacity of ice neglected (Parkinson and Washington, 1979), and was presented by Timmermann et al. (2009). Ice and snow volume are advected using the velocities obtained from the elastic-viscous-plastic solver described by Danilov et al. (2015).

Ice and ocean components are solved using an unstructured surface triangular grid that was carefully prepared for this study. Globally it includes the Arctic, Pacific, Atlantic and Indian Ocean and the number of surface nodes per unit area is increased in the Southern Ocean, and an additional focus in the southern and western Weddell Sea (WS). The grid length scale (resolution) varies between 4 km and 73 km in the WS (Fig. 3.1). The resolution is increased in all ice shelf cavities, especially under Filchner-Ronne Ice Shelf (FRIS) and Larsen Ice Shelf (LIS). In the central Pacific the resolution decreases to 323 km.

In the vertical, the model uses a hybrid grid with 25 terrain-following (sigma) layers extending from the Antarctic continent down to the 3000-m isobath, and 36 horizontal (z) layers in all other regions (Fig. 3.2). Wang et al. (2008) showed that simulations on purely terrain-following grids or the combination of horizontal and terrain-following grids resolve the overflow processes best in terms of downslope plume propagation, plume thickness and dilution, and they also have the least resolution dependence. Nevertheless, Nakayama
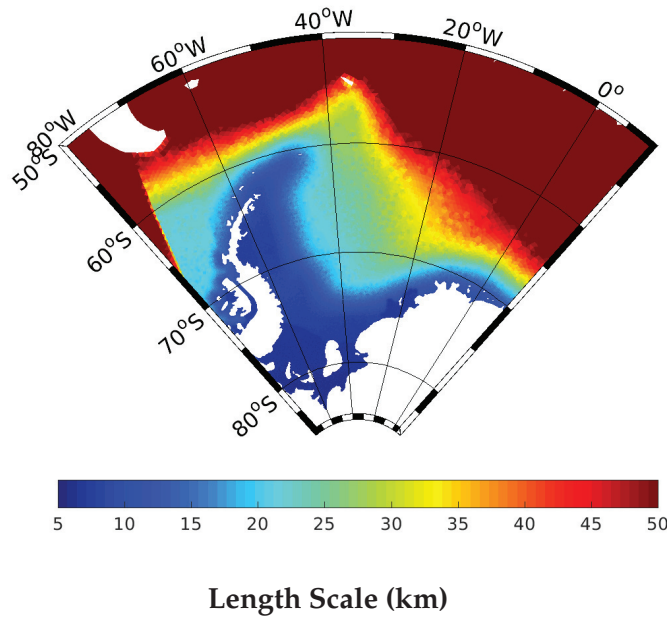
Length Scale (km)

FIGURE 3.1: Grid length scale in the Weddell Sea.

et al. (2014) revealed some difficulties to represent CDW intrusions onto the continental shelf using terrain-following coordinate below the shelf break depth.

Initial tests were performed using shallow and deep limits for the sigma layers, with transition at the shelf break (500-m isobath) and down at the 3500-m isobath. As expected, the dense water plumes flowing down the continental slope were hardly seen with shallow transition, whereas with the deep-sigma transition, i.e. sigma levels extending down to the 3500-m isobath, the WDW signal over the continental slope was partly eroded. With this restrictions in mind, the maximum depth of the sigma layers was chosen to be 3000m. Sigma layers are used only around Antarctica but, even outside the sigma region, the bottom node elements can deviate from z-levels to approximate bathymetry in a smooth way (Timmermann et al., 2009).

Bathymetry and ice shelf geometry have been prepared with an update version of RTopo-1 (Timmermann et al., 2010) that includes data from the more recent International Bathymetric Chart of the Southern Ocean (IBCSO) (Arndt et al., 2013). A comparison between sounding data (Brisbourne et al., 2014) and the bathymetric charts indicates that deep troughs under LIS-C are better represented in RTopo-1 than in IBCSO. Therefore, the deepening near the grounding line suggested in RTopo-1 was kept under all ice shelves.

Neither RTopo nor IBCSO contain information about LIS-B ice thickness, but the best way to evaluate the role this ice shelf played for the ocean circulation is to perform simulations including this ice shelf. In order to fulfill this goal, the LIS-B draft was obtained from E-Topo 1 (Amante and Eakins, 2009) and a second mesh was prepared (Fig. 3.3). The simulation using this mesh is named Experiment LIS-B (EXLB). A third mesh with LIS-C completely removed was used to perform Experiment LIS-C (EXLC). Both experiments are compared with the simulation performed using the original mesh, which serves as the reference simulation.
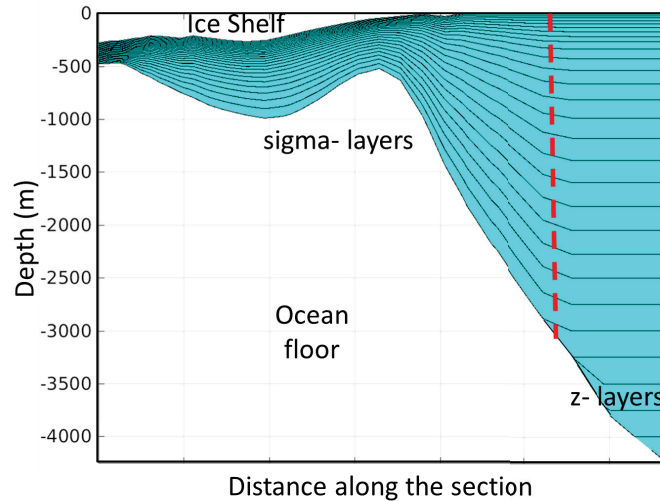
FIGURE 3.2: Distribution of the vertical layers. On the left side of the figure 25 sigma-layers can be seen under the ice shelf. They follow the bathymetry until the 3000-m isobath where they are connected to z-layers, the transition is marked by a red dashed line.

The initial conditions for the temperature and salinity were derived from the World Ocean Atlas 2013 (Locarnini et al., 2013; Zweng et al., 2013). Initial conditions for sea ice, based on sea surface temperature, i.e., wherever the water is colder than -1°C sea ice concentration was set to 0.9 and sea ice thickness to 1 m. All simulations started in 1979 and were integrated for 32 years, until 2010, using 6-hourly fields from the National Centers for Environmental Prediction Climate Forecast System Reanalysis (NCEP-CFSR, Saha et al., 2010). The atmospheric forcing parameters are: air temperature, longwave and shortwave radiation, zonal and meridional wind, humidity, precipitation, and evaporation.

The model results were stored as monthly means. This study focused on ocean potential temperature, salinity, and horizontal velocities. For validation purposes, sea ice concentration and thickness are also analyzed.

3.2 How to obtain a transect/section

To obtain a section of, e.g., temperature or salinity from the irregular mesh used to perform the simulations requires three dimensional interpolation. The first step is to define a section and find the points at which this line intersects the surface triangle sides (Fig. 3.4). For each intersection point a value is given based on the distance from each node involved. This also applies for depth values of points in the sigma layer. This process is repeated for every layer and then triangles are formed in the vertical, which connect two points at the same layer with a third in the layer immediately below or above (Fig. 3.4).

To compute transports, the velocity vector is decomposed to the components parallel and perpendicular to the section. The area of each triangle is multiplied by the mean velocity perpendicular to the plane to calculate the transport through the section. The use of triangles instead of quadrilaterals to compute the transports allows for a better estimate of the near-bottom flow. When the transport is calculated for different water masses, only the
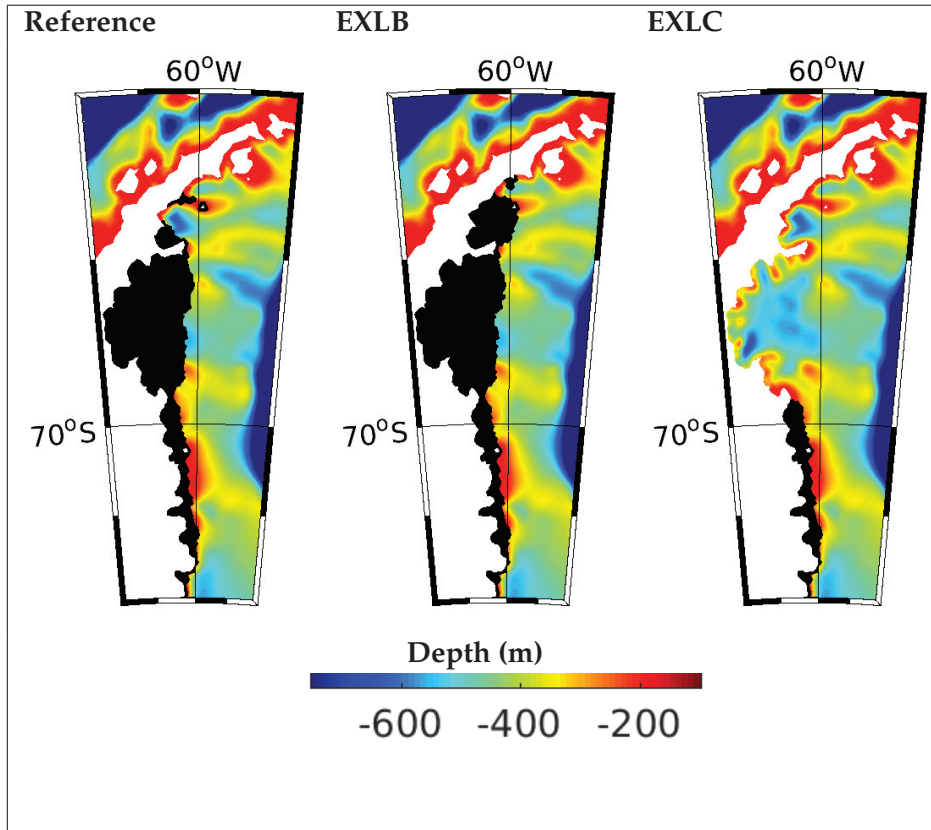
FIGURE 3.3: Larsen Ice Shelf configuration in the mesh used for the reference run (left), EXLB (middle), and EXLC (right). Ice shelves are shown in black and colors represent the bathymetry.

corresponding area of the triangle is considered. However, the transport estimates are subjected to errors due to the interpolation of the original velocity components to the section.

3.3 Validation

The results obtained after 10 years of simulation are evaluated to demonstrate that the model output is a good representation of the real ocean. Model deficiencies are also stated and should be kept in mind during the interpretation of the results.

3.3.1 Sea ice

Monthly means of sea ice concentration derived from satellite data are used to evaluate the model ability to reproduce the sea ice cycle in the WS. The NOAA[1]/NSIDC[2]Climate Data Record of Passive Microwave Sea Ice Concentration, Version 2 (Cavalieri et al., 1997) data was interpolated to the model grid and compared with the reference run.

The averaged sea ice concentration between 1989 and 2010 shows that the WS is fully covered by ice during the winter months (Fig. 3.5A). The melting is strong from December until February, and in March the sea ice cover starts to increase again. In the model

---

[1]American National Oceanic and Atmospheric Administration
[2]American National Snow and Ice Data Center
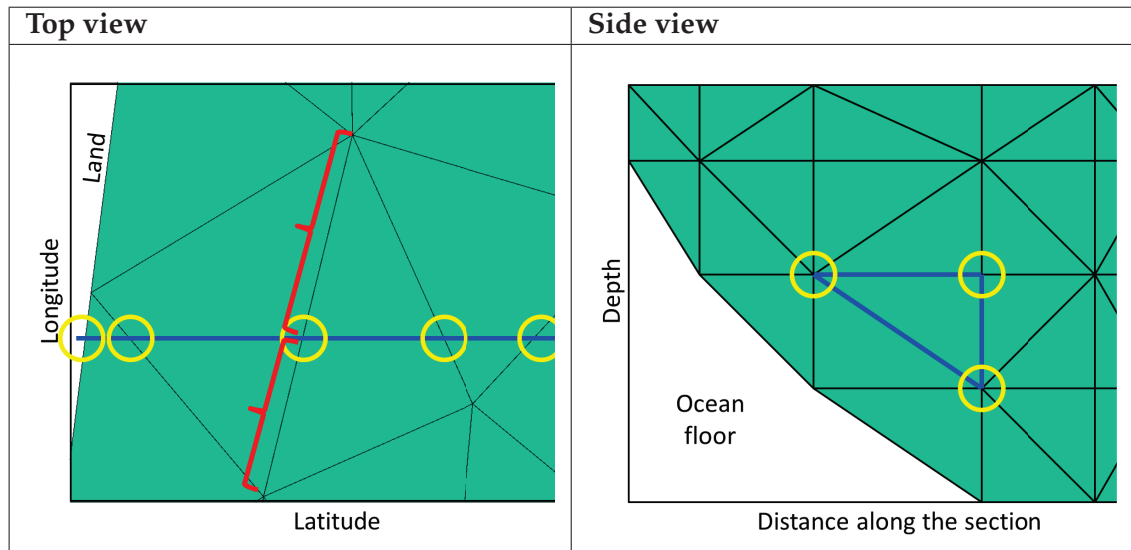
FIGURE 3.4: Surface triangles from a mesh (left), with an section example (blue line), showing the points used on the sections (yellow circles), and the distance to nodes used on the interpolation (red '}'). Lateral view of the triangles formed in a section (right) with an example of points (yellow circles) used to calculate the transport across the corresponding triangle (blue line).

(Fig. 3.5B), the summer sea ice has a higher concentration, and occupies a larger area than observed, while the winter sea ice cover is almost identical to the satellite data.

The temporal variability of the sea ice extent[3]was computed for four subregions of the WS: Northeast (NE), Southeast (SE), Southwest(SW), and Northwest (NW) (Fig. 3.6). The results show that a strong seasonal cycle is present during the whole period, but in several years the minimum sea ice extent is overestimated in the model (Fig. 3.7). This is in contrast to previous model results (Timmermann et al., 2009) which underestimate the summer sea ice extent. The discrepancy between model results can be related to the distinct atmospheric forcing (NCEP/CFSR x NCEP/NCAR) or different closing lead parameter (h_0 = 0.1 x h_0 = 1.0) used to perform the simulations. Besides of the overestimation of summer sea ice extent, the interannual variability is well represented in the model and, in general, when the summer sea ice extent is larger in the observations it is also larger in the model.

To check the model's ability to represent sea ice thickness[4](h_i), upper looking sonar (ULS) data prepared by Behrendt et al. (2013), was used; the mooring positions are shown in Fig. 3.6. Due to the very local nature of the measurements, the comparison is done using monthly means. The overall picture is that the model underestimates sea ice thickness near the continental slope and performs better in the open ocean (Fig. 3.8). For the NE region (moorings 227 and 229), the ULS data shows that the thickening of the ice begins in May while in the model it starts in June (Fig. 3.8 A). In SE and NW, (Figs. 3.8 B and C), the model fails to reproduce the thicker ice near the continent (moorings 206, 207, 210, 212, 217, 233, and 232). Thinner ice in winter is one of the reasons for the absence of ice during summer on moorings 206, 207, 212, and 233.

---

[3]summation of the area corresponding to nodes with an ice concentration greater than 15%

[4]The model output 'ice thickness' (h_i) corresponds to the mean sea ice thickness over the node area
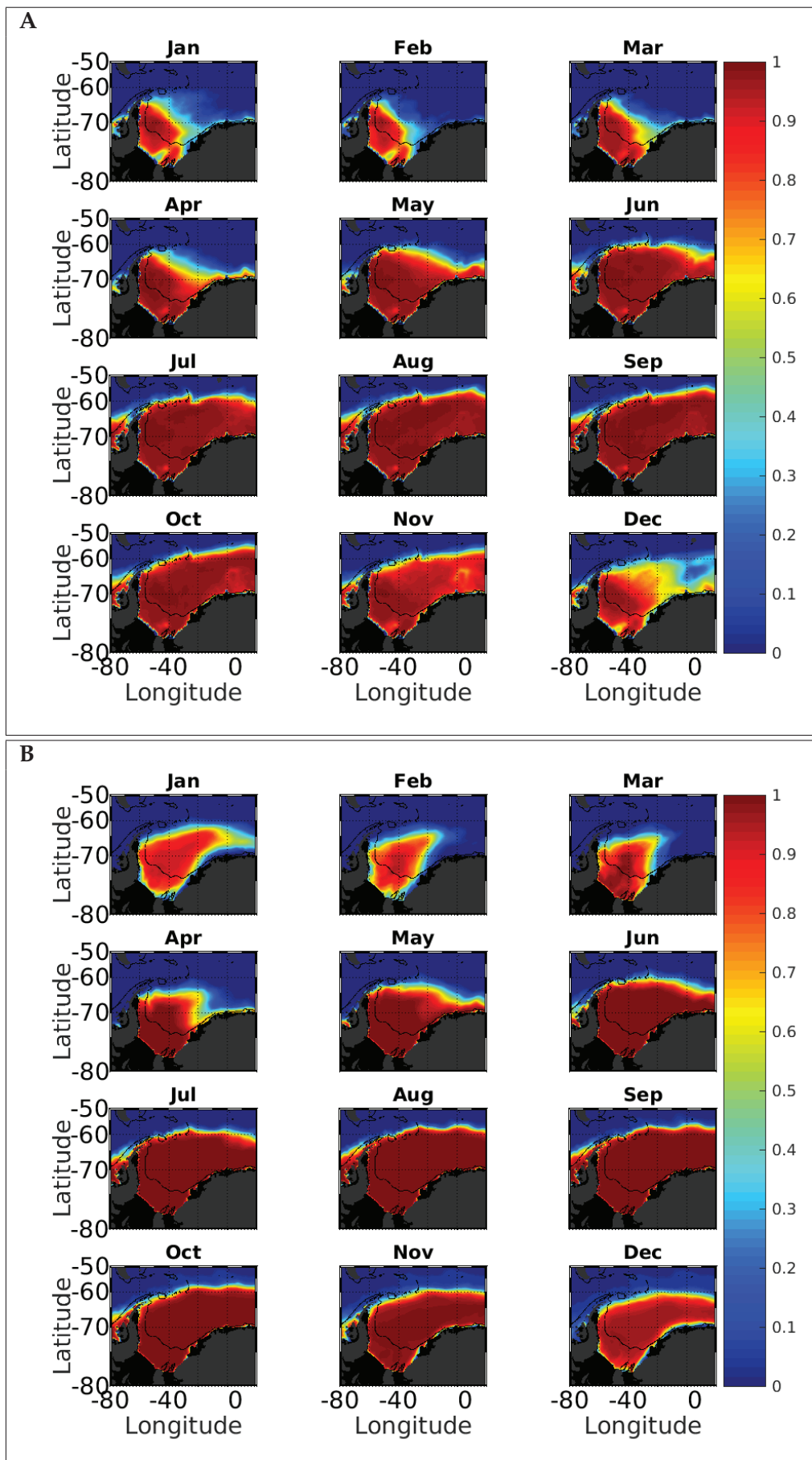
FIGURE 3.5: Satellite (A) and model (B) sea ice concentration in the Weddell Sea
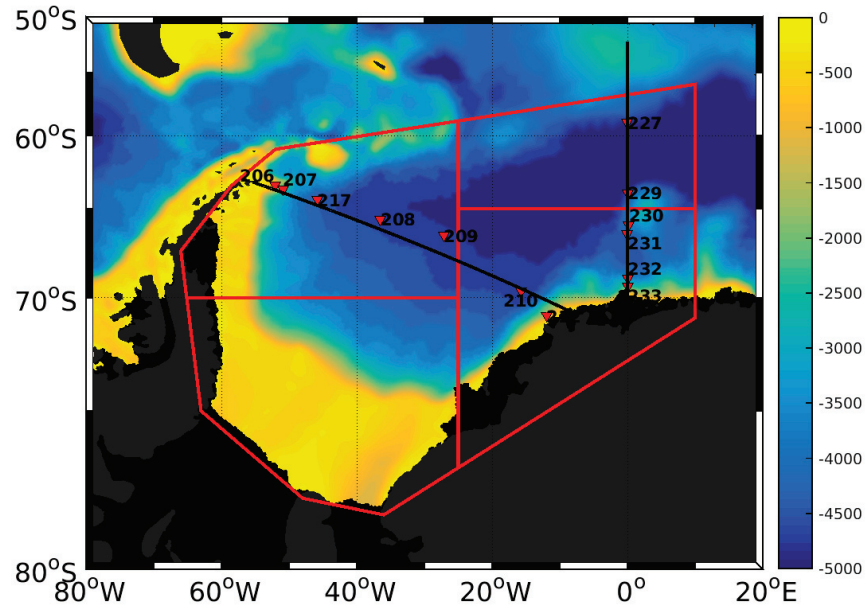
FIGURE 3.6: Weddell Sea regional map. The colors represent batimetry. The black lines are Prime meridian and SR04 sections. The red boxes show the four subregions discussed in the text, i.e. northeast, northwest, southwest, and southeast. The numbered triangles show the ULS moorings position.
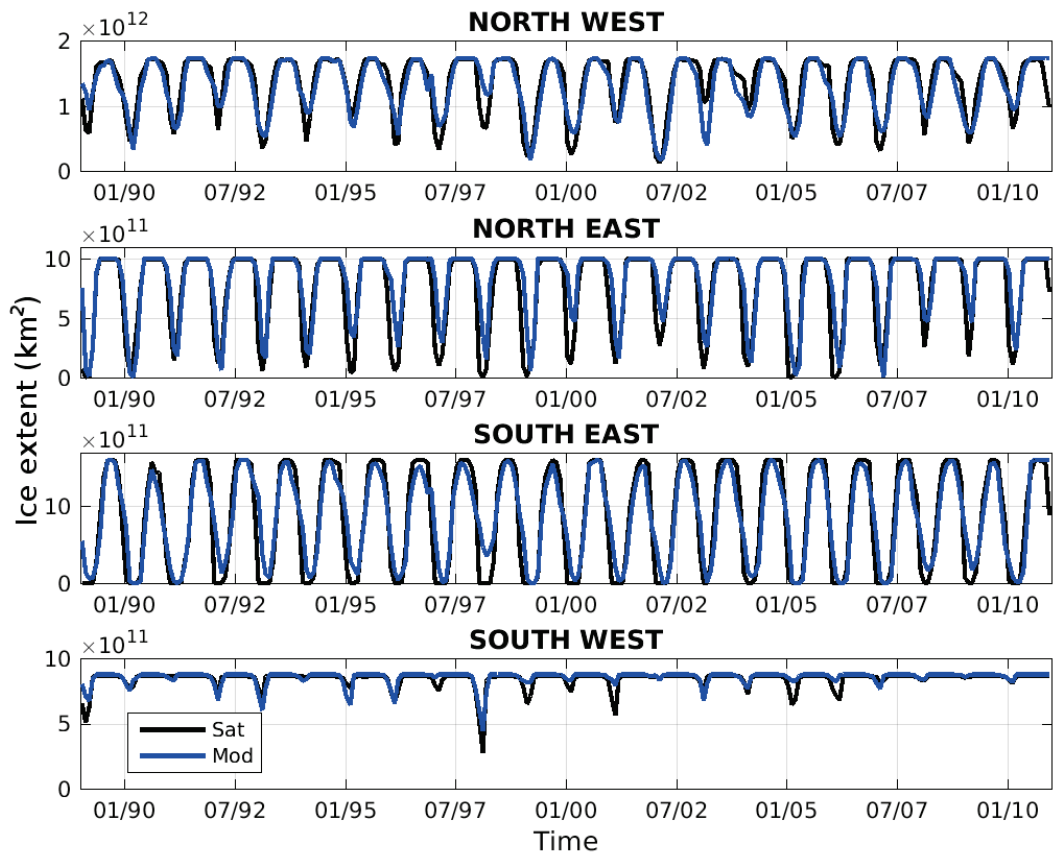
FIGURE 3.7: Sea ice extent time series in the four Weddell Sea subregions, i.e. northeast, northwest, southwest, and southeast. The black line is the ice extent from satellite data (S) and the blue line corresponds to FESOM sea ice extent (Mod).
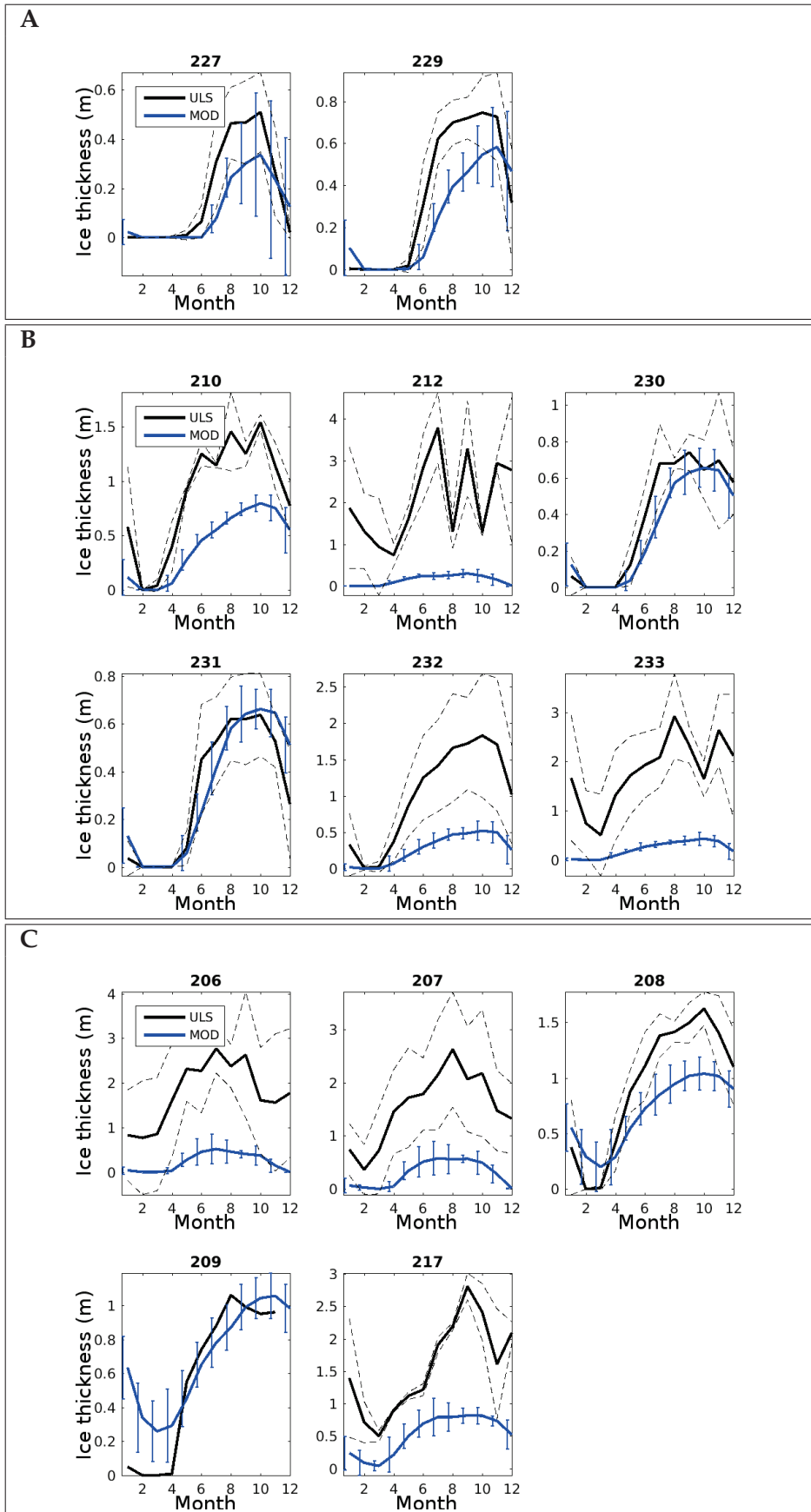
FIGURE 3.8: Monthly mean sea ice thickness in the northeastern (A), southeastern (B), and northwestern (C) subregions, on different moorings positions. The mooring number is shown on the top of each graph. The black line is the ice thickness from the ULS data and the blue line is ice thickness (h_i) from FESOM closest node. Dashed lines and blue bars are standard deviation from ULS and model, respectively.

In a previous work using the Bremerhaven Regional Ice–Ocean Simulations (BRIOS) model, Timmermann et al. (2002) state that the relevant spatial scales for the ice thickening near the coast are much smaller than the grid size, so that the variability of the ULS point measurement can hardly be reproduced by the model. The underestimation of ice volume at the westernmost position (207) is attributed to the overestimation of melting in that region, which prevents the survival of multiyear ice. Despite the finer resolution used in FESOM, i.e. 10 km or higher, the same problems in representing near-coast sea-ice thickness still exist.

Attempts to improve the sea ice representation were made by changing (a) the lead closing parameter (h_0), (b) the drag coefficient between ocean and ice Cd_{oi}, and (c) the drag coefficient between air and ice Cd_{ai}.

When water freezes it can increase either sea ice concentration or actual sea ice thickness[5], the balance between the two is defined by h_0. With a larger h_0 the ice concentration increase is slower, so that a larger fraction of open water remains and the ice grows thicker. The reference simulation uses an $h_0 = 0.1$, for higher h_0s ($h_0 = 0.5$ or 1.0) the ice becomes thicker during winter, but the ice extent increase is much slower in NE, and it decreases faster and excessively in the SE which would increase the discrepancies to the observations.

Drag coefficients used in reference run are $Cd_{oi} = 1.5 \cdot 10^{-3}$ and $Cd_{ai} = 5 \cdot 10^{-3}$. A higher Cd_{oi} solves the overestimation of ice extent in the NE but causes an ice deficiency in the southern regions. An increase in Cd_{ai} ends up with an ice loss everywhere during summer, and if this parameter is reduced the ice expansion in autumn is too slow.

3.3.2 Ice shelf melting

The total area occupied by Antarctic ice shelves in the mesh used is 1,521,272 km^2 and the mean circumpolar basal melting between 1989 and 2010 is 1125.3 Gt year^{-1}. This result corresponds to the lower end of the melt rate range of 1325 ± 235 Gt year^{-1}, calculated by Rignot et al. (2013) for a surveyed area of 1,553,978 km^2.

For a grid with smaller ice shelf area (1510×10^3 km^2), Timmermann et al. (2012) obtained a circumpolar basal melting of 1600 Gt year^{-1}. Their estimate for FRIS is also larger, 138 Gt year^{-1} versus 129 Gt year^{-1}, but for LIS-C melting is slightly lower, 48 Gt year^{-1} versus 52 Gt year^{-1}. Other model estimates of the melting underneath FRIS vary between 49 and 141 Gt year^{-1} (Gerdes et al., 1999; Hellmer, 2004; Makinson et al., 2011; Timmermann et al., 2012), while assessments derived from *in situ* and/or remote sensing observations range between 83 and 156 Gt year^{-1} (Schlosser et al., 1990; Foldvik et al., 2001; Joughin and Padman, 2003; Nicholls et al., 2003; Rignot et al., 2013). For LIS-C, models show a basal melting ranging from 15 to 70 Gt year^{-1} (Hellmer, 2004; Holland et al., 2009; Timmermann et al., 2012) and data estimates span from 20.7 ± 67 to 35 ± 19 Gt year^{-1} (Huhn et al., 2008; Rignot et al., 2013).

FESOM results for ice shelf basal melt rates are thus well within the range of previous studies.

---

[5]The actual sea ice is equal to h_i divided by the ice concentration, the thermodynamic part of the sea ice model is computed using actual sea ice thickness

TABLE 3.1: Comparison of Larsen C basal melting from different sources

Reference	Type	Area (10^3 km^2)	Melt rate (Gt year^{-1})	Melt rate (m year^{-1})
Hellmer, 2004	model	66	38	0.6
Holland et al., 2009	model		15-70	0.27-1.26
Timmermann et al., 2012	model	52	48	1.0
This work	model	54.6	52	0.6
Huhn et al., 2008	OMP		35±19	0.35± 0.19
Rignot et al., 2013	remote sens.	46.4	20.7±67	0.4±1

3.3.3 Ocean

The model results as a mean from 1989 to 2010 are compared with the temperature and salinity data from WOA along the Prime Meridian and the SR04 sections (Fig. 3.6). It is important to note that the Atlas is a product of interpolation of *in situ* data to a regular grid, therefore small features seen on observations might be misrepresented; examples are mentioned in the following paragraphs.

The upwelling of the warmer upper CDW into the central WS is well represented in the model (Fig. 3.9 A), but the two cores in the WG inflow (e.g. Ryan et al., 2016), northern and southern, are joined into one. On both sections, the WDW layer is colder, fresher, and thicker than in WOA and there is no WSBW colder than -0.8 ^{o}C.

Along the Prime Meridian (Fig. 3.9 A), the modeled WSDW and WSBW layers are thinner, and the WDW layer is thicker but colder than seen in WOA. The signature of the ASF can be clearly seen in the model and, although it is not seen in the WOA, its presence was reported in previous works (e.g. Klatt et al., 2005).

The ASF is present at both ends of the SR04 section in the model and in WOA. The WDW found along the slope is cooler in the model and is replaced by MWDW near Kap Norvegia and by WSDW near the AP, flowing along the continental slope. A thin WSDW layer has already been described from observations (e.g. Huhn et al., 2008) and is also present on the data from Cruise ANT XXIX/3 (Figs. 2.3, 2.4, 2.2; Caspel et al., 2015a). The MWDW tongue extending towards the continental shelf seen in the model was also observed before (Gordon, 1998).

Despite the fact that model and Atlas data differ in several details, the good representation of water mass characteristics and distribution and the presence of a dynamical feature like the ASF are indicators that the model is able to simulate the WG in a realistic way. To further address the ability of the model to reproduce the WS circulation, the volume transport was calculated across two section segments: the southern part of the Prime Meridian between 170 and 1100 km away from the coast, and the SR04 between 40 and 750 km away from Joinville Island. The mean transport from 1989 until 2010 is 34.54 Sv westward in the southern Prime Meridian section and 39.85 Sv across the western SR04. These values are
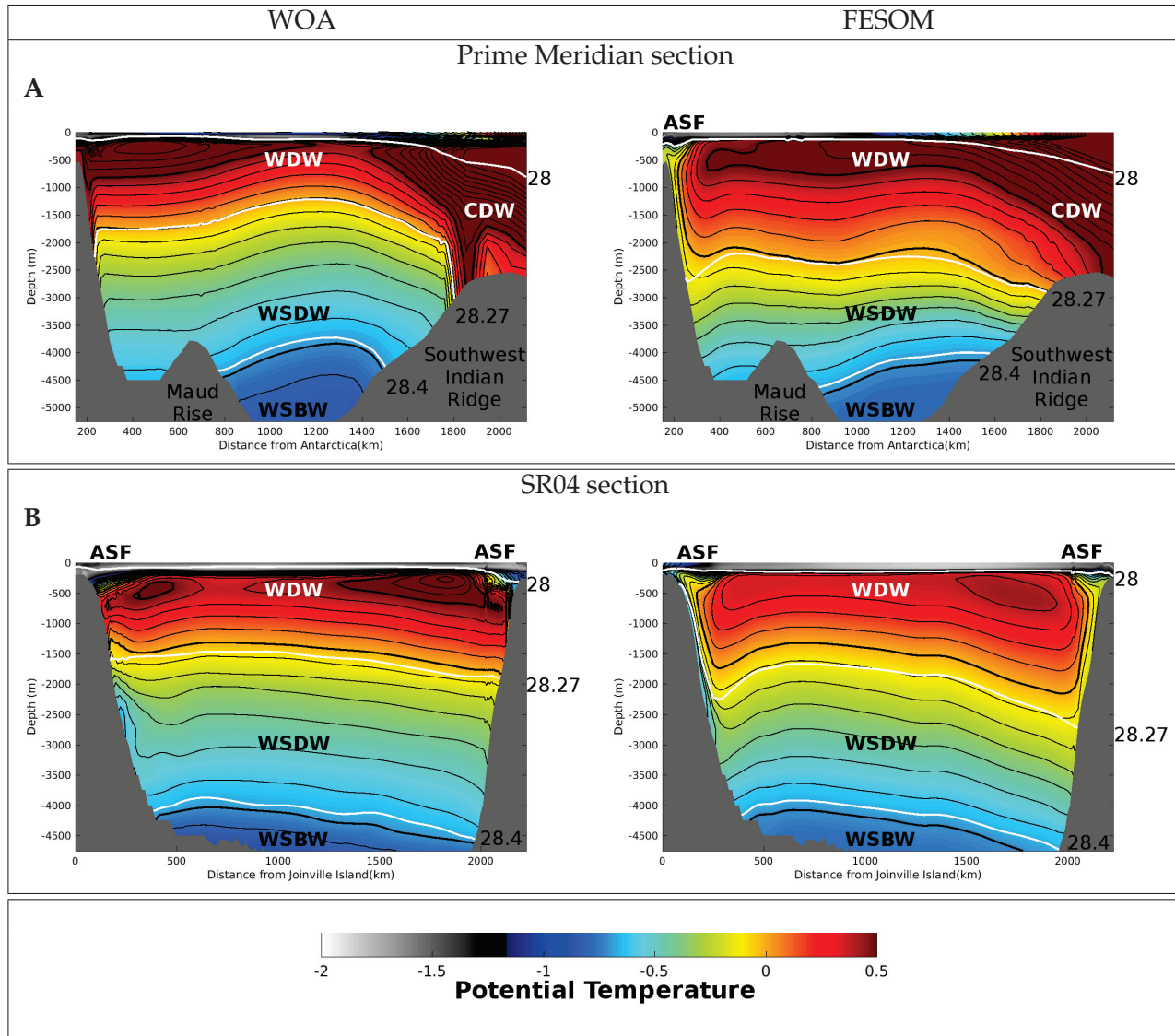
FIGURE 3.9: Mean potential temperature along the two sections shown in Figure 3.6: from the continental slope until the Southwest Indian Ridge along the prime meridian (A), and from Joinvile Island to Kap Norvegia (B - SR04). Contour lines in black every 0.1 ^{o}C; the 0.5, 0.0, and -0.7 ^{o}C are thicker. The white lines are the 28.0, 28.27, and 28.4 kg m^{-3} neutral density contours (γ^n). World Ocean Atlas 2001 (WOA, left), and FESOM reference run mean values from 1989 until 2010 (right). Abbreviations are, Antarctic Slope Front (ASF), Warm Deep Water (WDW), Weddell Sea Bottom Water (WSBW), and Weddell Sea Deep Water (WSDW).

well within the WG transport estimates derived from observations (,e.g., Thompson and Heywood, 2008; Fahrbach et al., 1991; Klatt et al., 2005).

Strong interannual and seasonal transport variability is observed in both sections (Figs. 3.10). Stronger transports occur during winter and it decreases towards summer, the transition time isn't smooth and smaller peaks on the transport happen during spring and autumn. In 1995, the southern branch of the WG changes to a weaker transport regime than the simulated for previous years (Figs. 3.10 A). From 1979 until 1992 most of the monthly mean transport is higher than the mean of the last 22 years and the averaged transport is -48.71 Sv, between 1992 and 1995 it weakens and the mean transport during this period is -38.6 Sv, after 1995 it fluctuates around the mean of the last 22 years but with mean transport of only -30.7 Sv. Near the tip of Antarctica Peninsula a WG weakening is not observed.

Long term transport time series derived from observations are not available for comparison, and given the sparse spatial and temporal resolution of the measurements it is unlikely that they could derived for the whole period simulated with FESOM. Nevertheless, fluctuations of the WG strength have been described before and are mainly related to changes in the wind field (e.g. Wang et al., 2012; Fahrbach et al., 2004; Fahrbach et al., 2011). Thus, the WG variability can be related to atmospheric patterns like the Southern Annular Mode, El Niño/Southern Oscillation, or the Antarctic Circumpolar Wave (Fahrbach et al., 2004; Meredith et al., 2008b; Fahrbach et al., 2011). Changes in the wind also affect the dense water production in the southwestern WS (Wang et al., 2012) and control the export of WSDW across the SSR (Meredith et al., 2008a; Jullion et al., 2010; Fahrbach et al., 2011).

3.3.4   Validation closure

After comparing the output of the reference run outputs with different types of observational data and information found in the literature, I conclude that the circulation, water mass characteristics and distribution, sea ice conditions, and ice shelf melting in the WS are well represented by the model setup. The good representation of circulation and hydrography along the Prime Meridian and SR04 in the model indicate that FESOM is an appropriate tool to study water mass modification in the western WS.
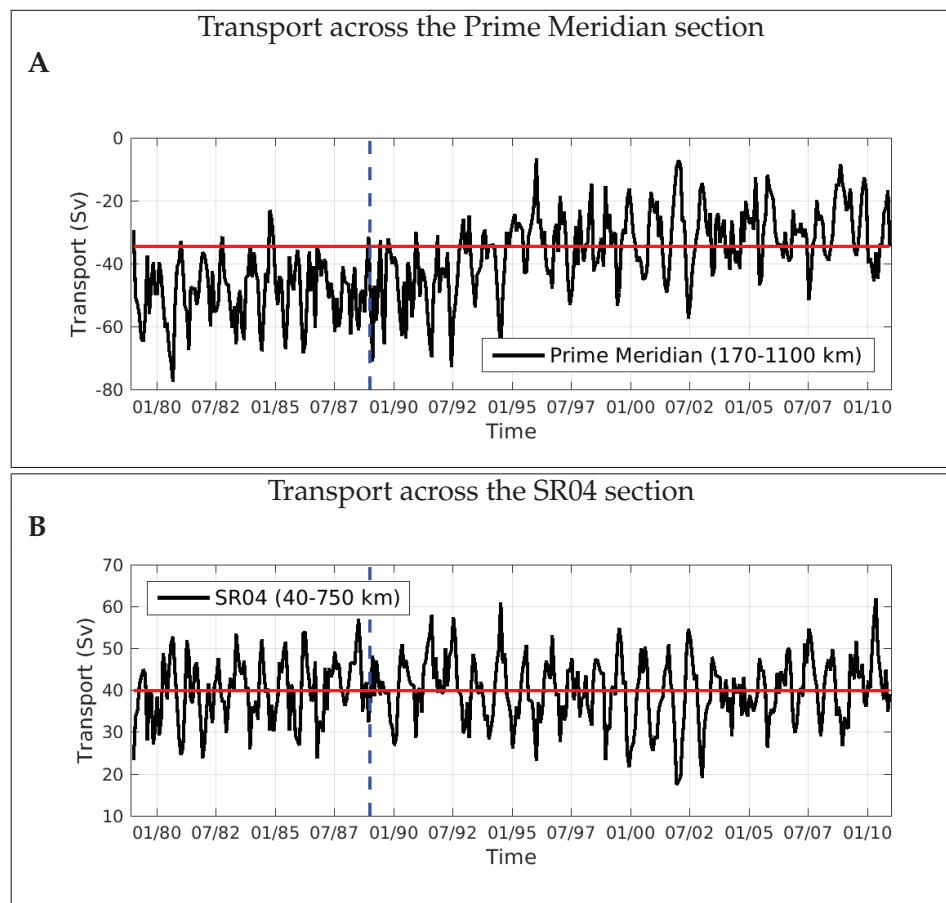
FIGURE 3.10: Time series of volume transport across the souther part of the Pime Meridian section (A), and the western part of the SR04 section (B).

Chapter 4

Results: Dense water formation in the western Weddell Sea

In this Chapter the hypotheses that the western Weddell Sea (WS) is important for WSDW formation is assessed based on the model results. First the dense water production in the reference simulation is evaluated, than the differences in experiments EXLB and EXLC are appraised. In the last part of the Chapter, the impact of changes in Larsen Ice Shelf along the gateways to the fringing basins, Bransfield Strait (BS) and Scotia Sea, are investigated.

As done in Chapter 2, the terms Neutral Deep Water (DWγ^n) to refer to waters in the γ^n-range from 28.27 to 28.4 kg m^{-3}, and Neutral Bottom Water (BWγ^n) for γ^n higher than 28.4 kg m^{-3} are used instead of the more common WSDW and WSBW (Table 2.1).

4.1   Reference simulation

Four zonal and six meridional sections from the FESOM reference run are analyzed to evaluate the formation of dense water in the western WS. The zonal sections extend from the Antarctic Peninsula to the 3500-m isobath (Fig 4.1) and are divided into shelf and slope sections; from south to north the shelf and slope components are named S0, S1, S2, S3, and SL0, SL1, SL2, SL3, respectively. The meridional sections connect the offshore end of the zonal sub-sections and run along either the shelf break or the 3500-m isobath. Mean values mentioned in the text refer to the period between 1989 and 2010 unless stated otherwise.

The mean temperature fields show that WDW is present along the continental slope at all latitudes (Fig. 4.2, left column). Temperatures higher than 0°C are found between 500 and 1750 m depth near the 3500-m isobath, the lower limit follows the bottom geometry towards the coast and converges with the upper 0°C-isotherm near the shelf break. The thickness of the intermediate water (IW) layer is increased by MWDW, and ranges from 100 to 2500 m depth offshore. On the slope, the lower boundary of MWDW (28.27 γ^n isoline) follows more or less parallel to the WDW limit. MWDW intrudes the continental shelf in all but the southern most sections where it is constrained offshore by dense waters observed in the shallow areas of the continental shelf. The mean temperature of IW found on the slope increases from -0.09^{o}C in SL0 to -0.02^{o}C in SL3 (Table A.1); the temperature increase is stronger along the 3500-m isobath and rises from 0°C in SL01 to 0.1^{o}C in SL23 (Table A.2). The salinity (Fig. 4.2, middle column) of the IW is lower close to the surface and in the upper
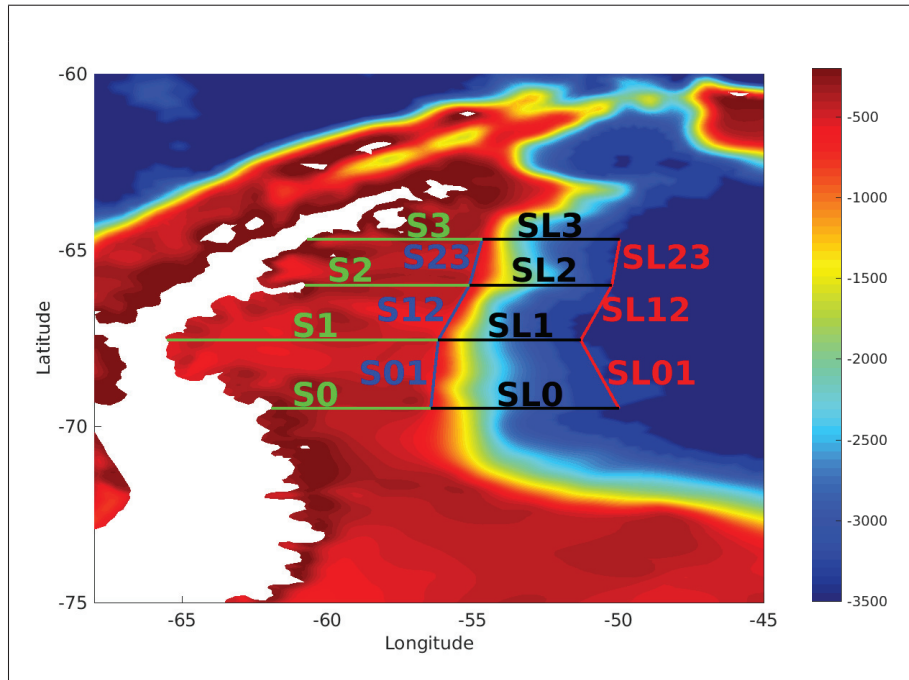
FIGURE 4.1: Northwestern Weddell Sea regional map with the sections used for the analysis of the model results. The zonal sections are divided in continental shelf (green lines) and slope segments (black lines), they are connected by sections along the shelf break (blue lines) and along the 3500-m isobath (red lines). The names used for each part in the text are shown. Background colors represent the bathymetry.

part of the continental slope, near the 3500-m isobath the salinity of the IW increases from south to north (Tables A.1 and A.2).

DWγ^n appears below the IW along the slope and over the outer part of the continental shelf. It is warmer and saltier near the offshore boundary of the sections and colder along the steeper portions of the continental slope (Fig. 4.2, left and middle columns). Therefore the mean temperature and salinity are higher along the 3500-m isobath (SL01, SL12, and SL23) than on the continental slope (SL0, SL1, SL2, and SL3 - Tables A.1 and A.2).

On the southern section (S0 and SL0), a plume of BWγ^n is found on the shelf and the upper part of the continental slope (Fig. 4.2, last row) with mean temperature and salinity of -0.9^{o}C and 34.661 in S0 and -0.73^{o}C and 34.664 in SL0 (Table A.1), respectively. This cold Salty Shelf Water (SSW) exists along the bottom of the shelf break until the middle of LIS-C (S01 in Fig. 4.3; S2/SL2 in Fig. 4.2) and is connected to the cold DWγ^n observed on the continental slope. SSW is formed to the south of the study area and, as it is carried northward by the circulation, its signature disappears due to mixing with the overlaying waters. Although absent in the mean-field figures, small amounts of BWγ^n sporadicly reach SL3 but with higher mean temperature (-0.62^{o}C) and salinity (34.667) than to the south.

The simulated mean meridional velocities (Fig. 4.2, right column) show a strong northward current along the slope that is intensified towards the bottom as described in the literature (e.g. Fahrbach et al., 1994; Fahrbach et al., 2001). The core of the northward flow is in the DWγ^n layer with velocities higher than 0.1 m/s and a maximum of 0.18 m/s in SL3. The quasi-zonal velocities across the three meridional sections, that cross the 'canyons' that

connect the continental shelf with the slope, show an onshore flow in the southern part and offshore flow in the northern part of the 'canyons' (Fig. 4.3). The presence of currents with opposite directions results in small mean net transports across all shelf break sections (Fig. 4.4, Total). Only 0.06 Sv leave the continental shelf through S01, 0.08 Sv cross the shelf break in front of the northern portion of LIS-C (S12), but in the vicinity of Robertson Trough (S23) the mean transport is 0.14 Sv onshore. The WG transport between the shelf break and the 3500-m isobath increases from 8.78 Sv in the south (SL0) to 17.21 Sv in the northern section (SL3). The water volume balance is closed by offshore waters that are carried in the direction of the slope across the 3500-m isobath: 3.07 Sv are carried towards the AP through SL01, the transport reduces to 2.83 Sv and 2.45 Sv across SL12 and SL23, respectively.

To investigate the transport of dense water and how they interact with lighter waters, the total transport through each section was divided based on the neutral densities of the 'water masses' (Fig. 4.4): surface waters (SW) lighter than $\gamma^n = 28$ kg m^{-3}, WDW and MWDW as the intermediate waters (IW) with $28 < \gamma^n < 28.27$ kg m^{-3}, and DWγ^n and BWγ^n.

Along the continental slope, the transport of DWγ^n increases downstream, namely from 3.77 Sv in SL0 to 6.29 Sv in SL3 (Fig. 4.4). 0.04 Sv of DWγ^n leave the continental shelf in front of the northern part of LIS-C (S12) while at the other latitudes the mean transport is from the continental slope to the continental shelf. DWγ^n contributions from offshore are higher than from the continental shelf and raise from 0.27 Sv in the south (SL01) to 0.47 Sv in the north (SL23), nevertheless they are to small to explain in total the increase of the along-slope transport. The DWγ^n budget is closed due to the transformation of BWγ^n and IW to DWγ^n.

0.8 Sv of BWγ^n enter the study region through SL0 and only 0.68 Sv cross SL1. Adding up the small contribution coming from the continental shelf gives a loss of 0.14 Sv of BWγ^n that is converted to DWγ^n due to vertical mixing in the southeastern subregion (SL0-SL01-SL1-S01). Between SL1 and SL2, 0.41 Sv of BWγ^n are transformed in DWγ^n, and 0.09 Sv in the northern slope subregion. After the transformation along the continental slope, only 0.18 Sv of BWγ^n are carried northward through SL3.

Part of the IW mixes with DWγ^n increasing the volume of DWγ^n. In the southeastern region 0.33 Sv of IW become denser, in the middle slope (SL1-SL12-SL2-S12) 0.32 Sv, and between SL2 and SL3 0.1 Sv are converted to DWγ^n, but this value is equal to the error in the total transport estimate in the northeast subregion. IW also mixes with overlaying waters, and small amounts are transformed to SW along the continental slope. Besides of the transformations to lighter and denser waters, the volume of IW transported along the slope increases from 4.17 Sv in the south (SL0) to 10.13 Sv in the north (SL3). The increase occurs because the volume of IW entering the study area across the 3500-m isobath is higher than the volume transformed to SW and DWγ^n combined.

Along the continental shelf the total transport is one order of magnitude smaller than along the continental slope and varies between 0.22 and 0.36 Sv (Fig. 4.4). The transport of DWγ^n and BWγ^n decreases from south to north while the volume advection of SW and IW rises. Since these changes cannot be explained by fluxes across the shelf break, the dense waters entering the study region through S0 must become lighter (colder and fresher, Fig. 4.2) due to the mixing with GMW as they flow northward on the continental shelf.

TABLE 4.1: Correlation between $DW\gamma^n$ and $BW\gamma^n$ transport time series in consecutive sections on the slope.

SEC-SEC	$BW\gamma^n$ x $BW\gamma^n$		$DW\gamma^n$ x $DW\gamma^n$	
	normal	lagged by one month	normal	lagged by one month
SL2 SL3	**0.8672**	0.7613	**0.9513**	0.7072
SL1 SL2	**0.8516**	0.7874	**0.9191**	0.6913
SL0 SL1	0.7878	**0.9160**	**0.8354**	0.7667

The mean transport does not show any evidence of dense waters crossing the shelf break to form WSDW or WSBW. Pulses of dense water coming from the continental shelf as proposed by Schröder et al. (2002) are also not seen in the time series of the monthly mean transport of $DW\gamma^n$ and $BW\gamma^n$ (Fig. 4.5 and 4.6) across the shelf break. There is, however, strong temporal variability of the transport along the continental slope that could be responsible for the variability of the bottom waters observed in the northwestern WS (Schröder et al., 2002). The model results are also inconsistent with the expectations created by the data analysis performed in Chapter 2) and indicate that changes in WSDW properties and volume are caused by processes occurring upstream.

Most of the variability of $DW\gamma^n$ and $BW\gamma^n$ transport in one cross-slope section can be explained by the fluctuations observed on the section immediately south (Table 4.1). Table 4.1 shows that the $BW\gamma^n$ transport through SL1 has a correlation of 0.916 with the $BW\gamma^n$ crossing SL0 the month before. Between the other section pairs (SL1-SL2 and SL2-SL3) and for all $DW\gamma^n$ pairs the normal correlation is higher than the lagged relation with values higher than 0.80. The time lag is probably due to the indentations observed near the shelf break, where the $BW\gamma^n$ is seen.

The high correlations between the dense water transport in consecutive slope subsections and the small transports across the shelf break indicate that, in the model, the waters on the continental shelf off LIS have negligible contribution to WSDW and WSBW flowing along the continental slope. This means that variability of dense waters in the northwestern Weddell Sea (e.g. Schröder et al., 2002) could be triggered by fluctuations of the WG strength (e.g. Fahrbach et al., 2011), events of dense water spill in the southwestern WS (e.g. Wang et al., 2012), or variations of the inflow from the Indian sector (Jullion et al., 2014). The assumption that LIS has a minor influence on the WSDW and WSBW formation is supported by the results from the sensitivity experiments presented in the next sub-chapter.
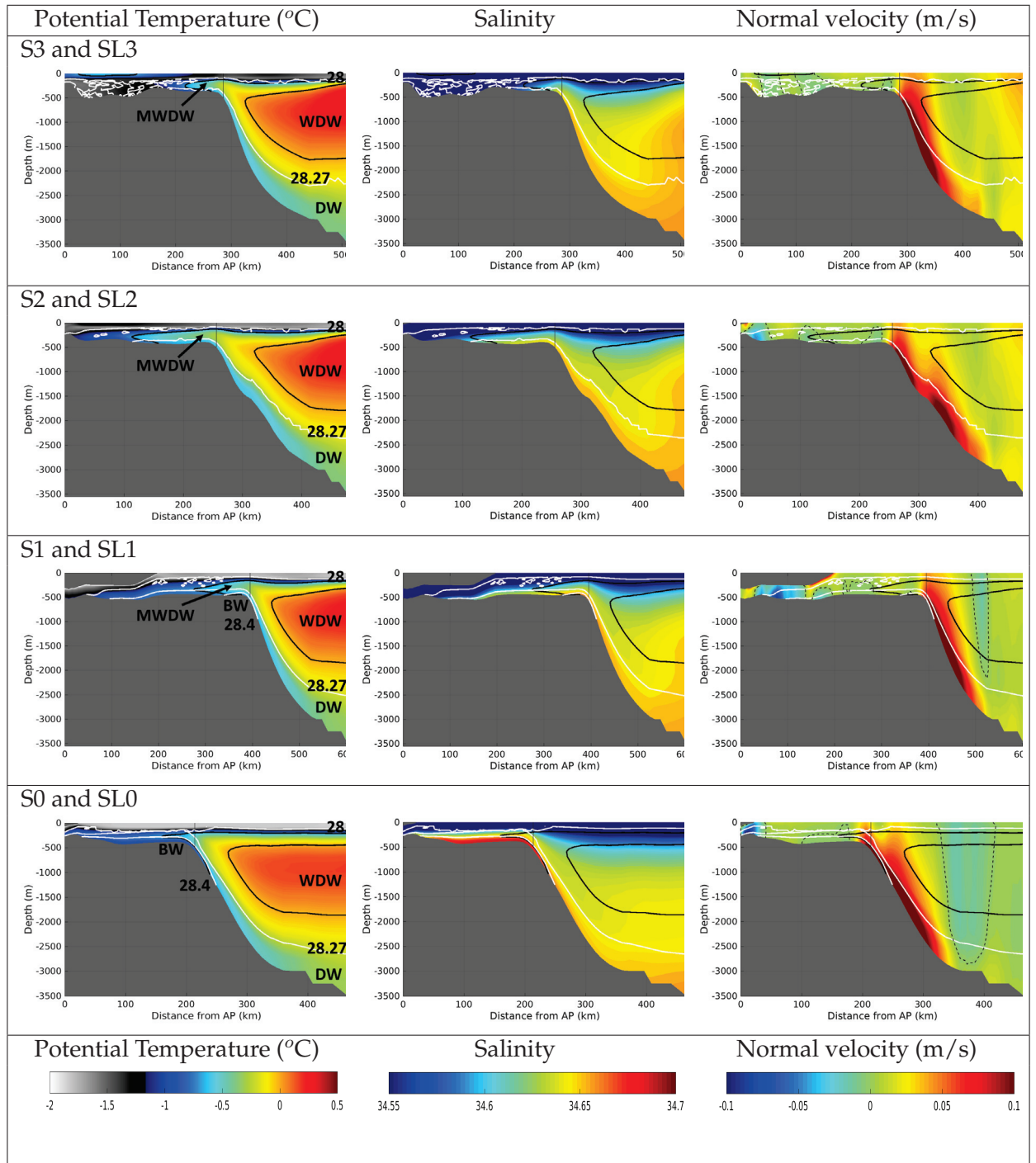
FIGURE 4.2: Mean values (1989-2010) of simulated potential temperature (left), salinity (middle), and normal (meridional) velocity (right) along the 4 zonal sections in the reference run. The shelf (S) and slope (SL) are shown together from south (bottom) to north (top), a black line on the shelf break indicates the division between them. In all figures, the white contours are neutral density (γ^n) isolines of 28, 28.27 and 28.4 kg m^{-3}, the black bold lines are the 0 and -0.7^{o}C isotherms; the neutral density contours are labeled on the potential temperature figures (left). In the velocity figures (right), the dashed lines are 0 m/s contours.
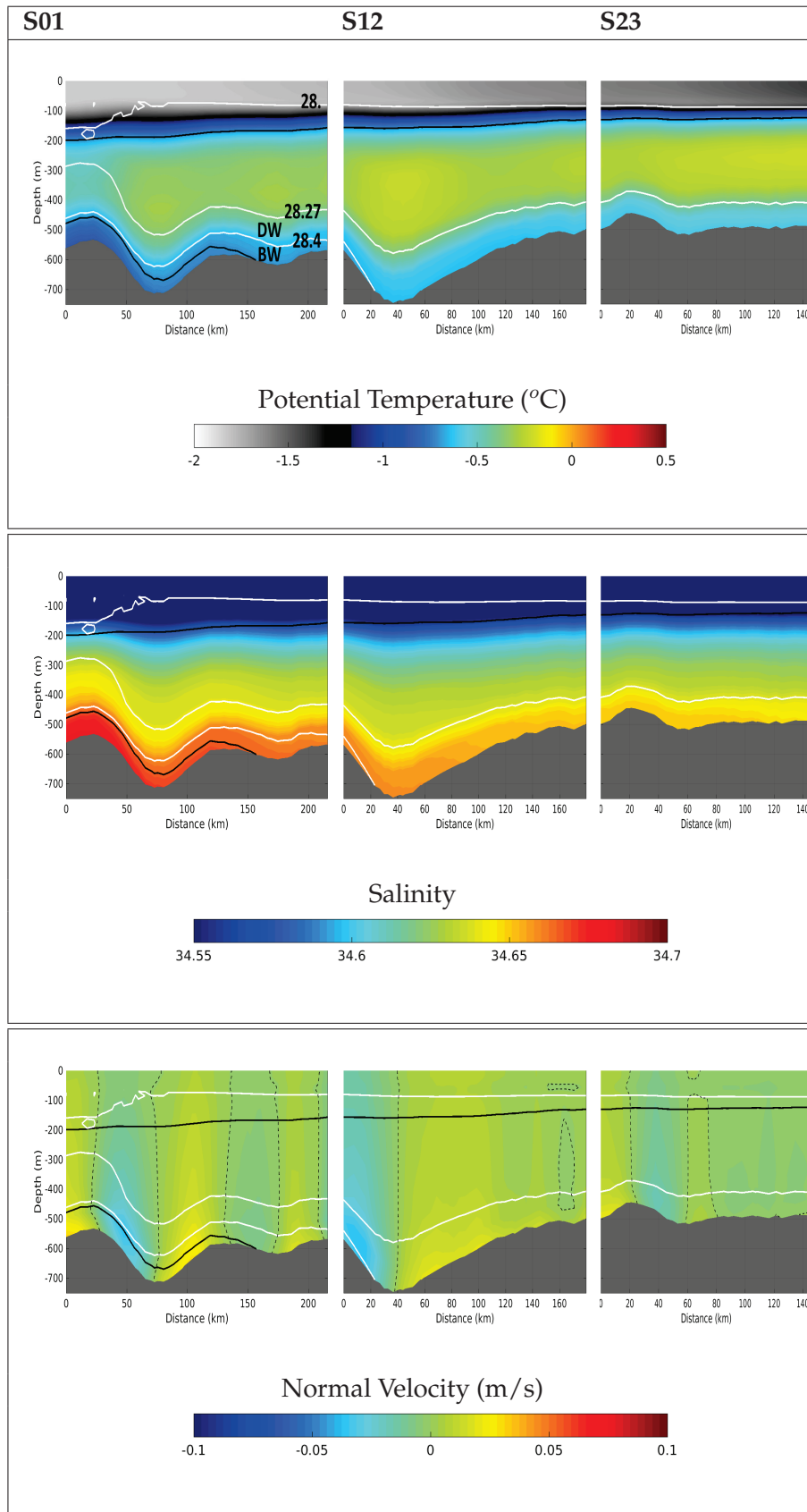
FIGURE 4.3: Mean values (1989-2010) of simulated potential temperature (top), salinity (middle), and normal (on/offshore) velocity (bottom) along the shelf break sections in the reference run. The sections are shown from south (left) to north (right). In all figures, the white contours are neutral density (γ^n) isolines of 28, 28.27 and 28.4 kg m^{-3}, the black bold lines are the -0.7^{o}C isotherms; the neutral density contours are labeled on the top left figure. In the velocity figures (right), the dashed lines are 0 m/s contours.
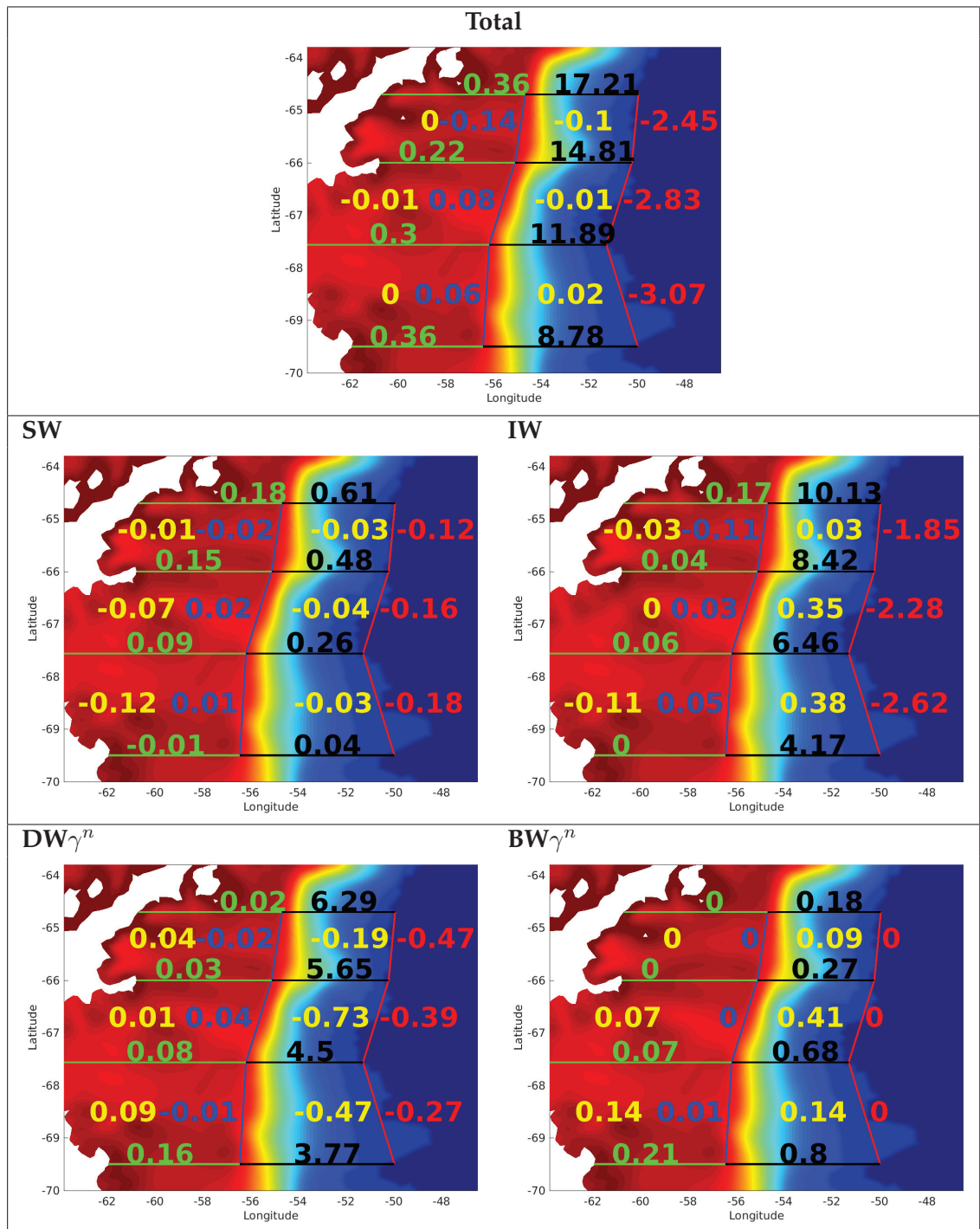
FIGURE 4.4: Simulated mean transport (1989-2010) through all sections for the reference run. The total transport is shown on top. The numbers correspond to the sections with matching colors and the yellow numbers are the net errors. Second row shows the transport of Surface Waters (SW, left) and Intermediate Waters (IW, right), and the third row Neutral Deep Water (DWγ^n, left), and Neutral Bottom Water (BWγ^n, right); positive (negative) yellow numbers indicate that water within the density range was consumed (formed) in the box. Transports are positive to the north or to the east
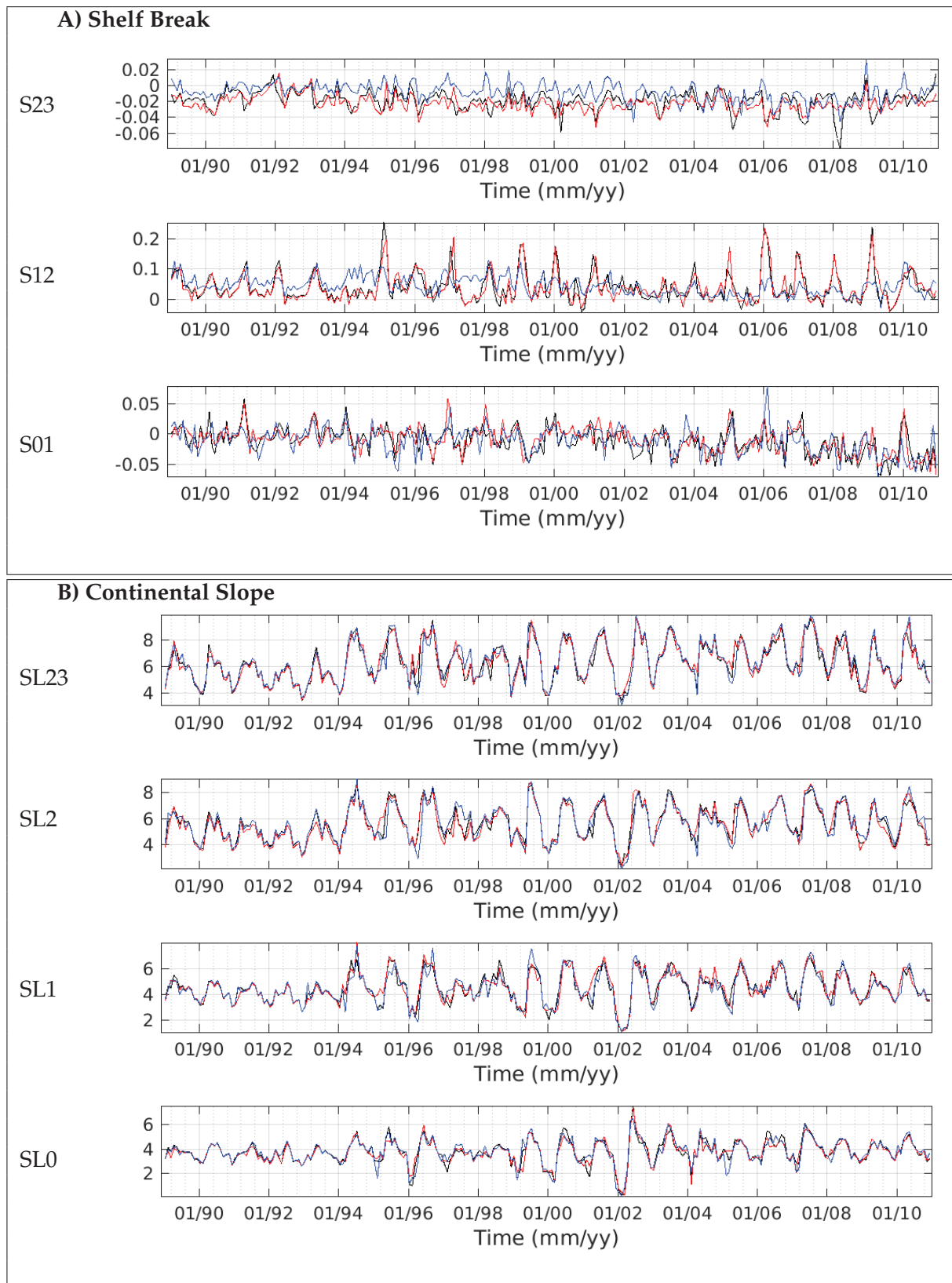
FIGURE 4.5: Neutral Deep Water (DWγ^n) transport time series across the shelf break (A) and along the continental slope (B) in the reference run (black line), EXLB (red line), and EXLC (blue line). Section names are shown to the left of each graph, starting from south (bottom) to north (top). Attention to the variable ordinate axis.
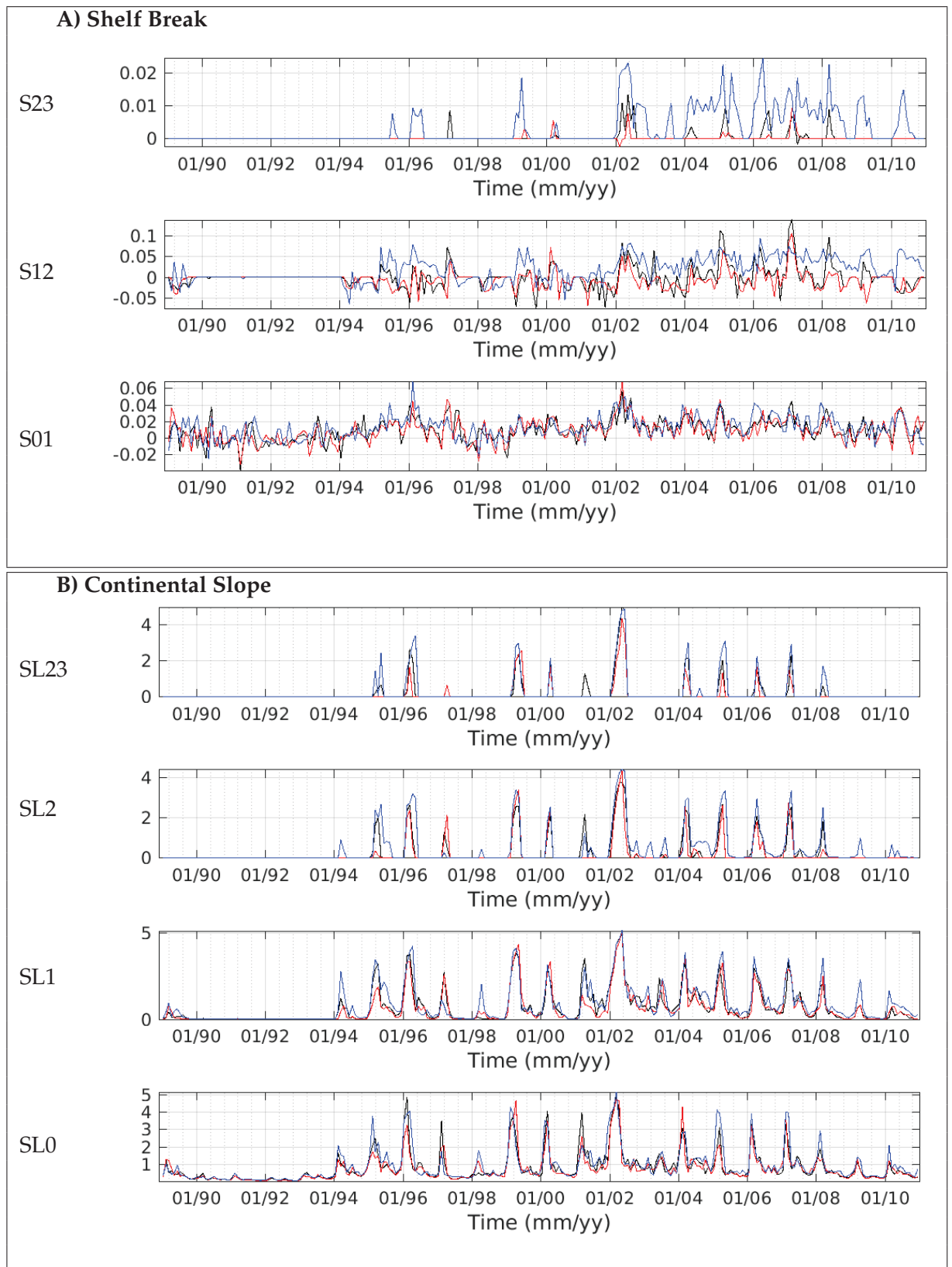
FIGURE 4.6: Neutral Bottom Water (BWγ^n) transport time series across the shelf break (A) and along the continental slope (B) in the reference run (black line), EXLB (red line), and EXLC (blue line). Section names are shown to the left of each graph, starting from south (bottom) to north (top). Attention to the variable ordinate axis.

4.2   Sensitivity experiments

In EXLB, which restores LIS-B to the situation prior to the breakup, the extra GMW coming from the increased ice shelf area causes a freshening of the adjacent continental shelf (S3 in Fig. 4.7). The lighter melt water with a higher buoyancy upwells along the ice shelf border and pulls the bottom waters from the outer continental shelf into the LIS-B cavity as part of the so-called 'ice-pump' (Lewis and Perkin, 1986). As a result, the lower layers become warmer and the surface cools because of the GMW. Part of the warmer waters is carried southward near the coast causing a warming signal at the southern section (S0, Fig. 4.7). Along the slope the temperature and salinity differences between EXLB and the reference run are very small, i.e., the influence of LIS-B on the water thermohaline properties is mainly restricted to the continental shelf.

In EXLC, with LIS-C totally removed, the surface waters on S3 become colder and fresher while the remaining of the continental shelf experience a temperature and salinity increase (Fig. 4.7). The warming and salinification on most of the continental shelf are caused by the reduction of GMW input. The subsurface salinification[1]increases the water column stability leading to the accumulation of fresh water from precipitation and sea ice melt at the surface. In addition, the input of fresh water due to precipitation in the region where LIS-C was removed is carried northward and contributes to the stability of the water column on the northern section. As a consequence, vertical mixing is reduced and sea ice melt water accumulates near the surface dropping the mean temperatures.

On the southern continental shelf (section S0) salinity increases at the surface and intermediate layers. A warming signal is present at mid depth but does not reach the bottom layer (Fig. 4.7). The warming caused by the removal of LIS-C is smaller in the south than in the north because of the mean flow, which, in the reference run, carries the GMW northward. Near the bottom, the SSW contains only small amounts of GMW and does not change its characteristics when GMW from LIS-C is missing. The salinity increase of the already salty intermediate layer leads to an accumulation of the salt from sea ice formation near the surface. Freezing of the saltier surface water during intense sea ice production periods injects more brine into the ocean making the bottom water at S0 slightly saltier and colder in EXLC. Changes seen on the continental shelf affect the surface layer along the slope but cannot influence the deeper layers in the western WS.

The differences in temperature and salinity cause small changes in the offshore transport of DWγ^n and BWγ^n (Fig. 4.6 and 4.5), namely a slight increase in EXLC and a decrease in EXLB. However, these changes have little impact on the transport of dense waters along the continental slope.

The analysis performed indicates that the presence of LIS-B (EXLB) or the absence of LIS-C (EXLC) do not have major impacts on the formation of WSDW and WSBW in the western WS. While, the ice shelves seem to play a larger role for the waters flowing northward on the continental shelf, which allows for the changes to be carried into Bransfield Strait (BS), they have a minor impact on the outflow across South Scotia Ridge (SSR) as disclosed next.

---

[1]Salinity plays a dominant role for the density of cold waters under low pressure.

4.3 Outflow

Two sections, one between Joinville Island and Elephant Island (JOEL) and the other starting at Elephant Island, passing the South Orkney Plateau, continuing along the SSR and ending east of the South Sandwich Trench (SST) (Fig. 4.8), are analyzed to verify whether the changes seen in the sensitivity experiments are carried into BS or the Scotia Sea.

In the reference run, cold and fresh water is advected on the continental shelf from the WS to BS (Fig. 4.9), although this water is warmer than in S3 (Fig. 4.7). The bottom of the southern and northern slope of BS is occupied by saltier and slightly warmer waters than the continental shelf. The center of the depression is filled with a warm water of intermediate salinity originating from the Scotia Sea, probably CDW carried by the ACC.

The cyclonic circulation of BS is marked by a strong westward current at the southern slope opposed by an eastward flow in the middle of the depression that extends from the surface down to the deeper part of the northern slope. The warm water intrusions seen on the northern part of the section are associated to a flow to the west near Elephant Island.

In EXLB, the continental shelf becomes colder and fresher than in the reference run, and the same signal is observed in the surface layer of the entire section. These modifications are caused by the GMW coming from LIS-B; the warm water carried onshore by the 'ice pump', created by the presence of LIS-B, hinders the cooling near the bottom. The current to the west (negative) is stronger on the shelf and in the deeper part of the southern slope and is weaker around the shelf break (Fig. 4.9). The northern part of the cyclonic gyre is stronger and the westward flow coming from Scotia Sea is weaker in EXLB.

In EXLC, the warming of the western WS continental shelf, associated to a freshening near the surface and salinity increase at the bottom (S3 in Fig. 4.7), is transfered to BS (Fig. 4.9). Compared to the reference simulation, the flow from WS into BS is weaker on the continental shelf but stronger near the shelf break. Accordingly, the northern branch of the cyclonic gyre and the westward current related to the warm water inflow are also intensified.

The total mean transport through JOEL in the reference run is -1.5 Sv (westwards), from which half of is attributed to the warm waters (SW and IW) seen on the northern slope (Fig. 4.9, Table A.3). Only 0.17 Sv are carried into BS across the southern continental shelf, mainly SW and IW. On the southern slope, 0.49 Sv of IW and 0.34 Sv of DWγ^n are transported westward as part of the southern branch of the BS cyclonic gyre. The eastward part of the gyre carries 0.19 Sv of SW over the southern slope and 0.13 Sv of DWγ^n transported near the bottom of the northern slope. In EXLB, the volume of DWγ^n transported westward on the southern slope drops to 0.27 Sv, reducing the volume recirculated on the northern slope to 0.1 Sv. In EXLC, the DWγ^n transport increases to 0.43 Sv westward and 0.16 Sv eastward on the southern and northern slopes, respectively. This documents the importance of LIS-C on the ventilation of BS.

On the section along the SSR (Fig. 4.10), between Elephant Island and the South Orkney Plateau waters are, in general, colder and fresher than for the rest of the SSR. The warmest core seen to the east of the plateau indicates the proximity of Upper Circumpolar Deep Water (UCDW), while the salinity maximum can be associated with Lower Circumpolar

Deep Water (LCDW). The warm water seen to the west of the plateau is stronger influenced by WDW, since the Powell Basin cyclonic gyre brings this water mass closer to the section.

DWγ^n is found along the whole section with low salinities in Philip Passage, the Orkney Passage (immediately east of South Orkney Plateau), and the South Sandwich Trench. This fresher version of DWγ^n corresponds to WSDW that escapes the WS to contribute to AABW and, therefore, has similar characteristics as the WSDW seen in S3 (Fig. 4.7). The strongest northward velocities occur in the WSDW outflow areas resulting in a DWγ^n export of 1.88 Sv through Philip Passage, 3.16 Sv through the gaps in SSR, and 8.07 Sv via the South Sandwich Trench (Table A.4). BWγ^n exists only in the South Sandwich Trench and is transported northward at a rate of 0.166 Sv.

The export of DWγ^n through Philip Passage is higher than the WSDW export rates given by Naveira Garabato et al. (2002), 0.7 $\pm$ 0.4 Sv and -0.1 $\pm$ 0.3 Sv derived from LADCP-referenced geostrophic estimates and an inverse box model, respectively, but are smaller than the mean annual values from the simulation performed by Schodlok et al. (2002), 2.2 Sv. The total transport of DWγ^n across the SSR, including Philip Passage, i.e. 6.04 Sv, agrees well with the model (6.4 Sv - Schodlok et al. (2002)) and the geostrophic estimates (6.7 $\pm$ 1.7 Sv - Naveira Garabato et al. (2002)), but are higher than the results from the inverse box model (4.7 $\pm$ 0.7 Sv - Naveira Garabato et al. (2002)). East of the South Sandwich Islands, the export of WSDW in the inverse box model is of 5.07 $\pm$ 4.3 Sv (Naveira Garabato et al., 2002), besides of the large error bar this estimate does not include the contribution of dense waters entering the WS from the east which are included in the global simulation performed with FESOM. This brief juxtaposition of the outflow rates obtained from FESOM results with the literature demonstrates that this import feature for the global circulation is well represented by FESOM.

The comparison of reference simulation with the two experiments along the gateways to BS and Scotia Sea shows that LIS has a direct influence over the BS deep waters and circulation but is of negligible importance for the WS contributions to AABW. Because of relation between BS deep waters and the primary production (e.g. Gonçalves-Araujo et al., 2015), changes in LIS configuration can trigger modifications in the delicate biological cycle of the Southern Ocean.
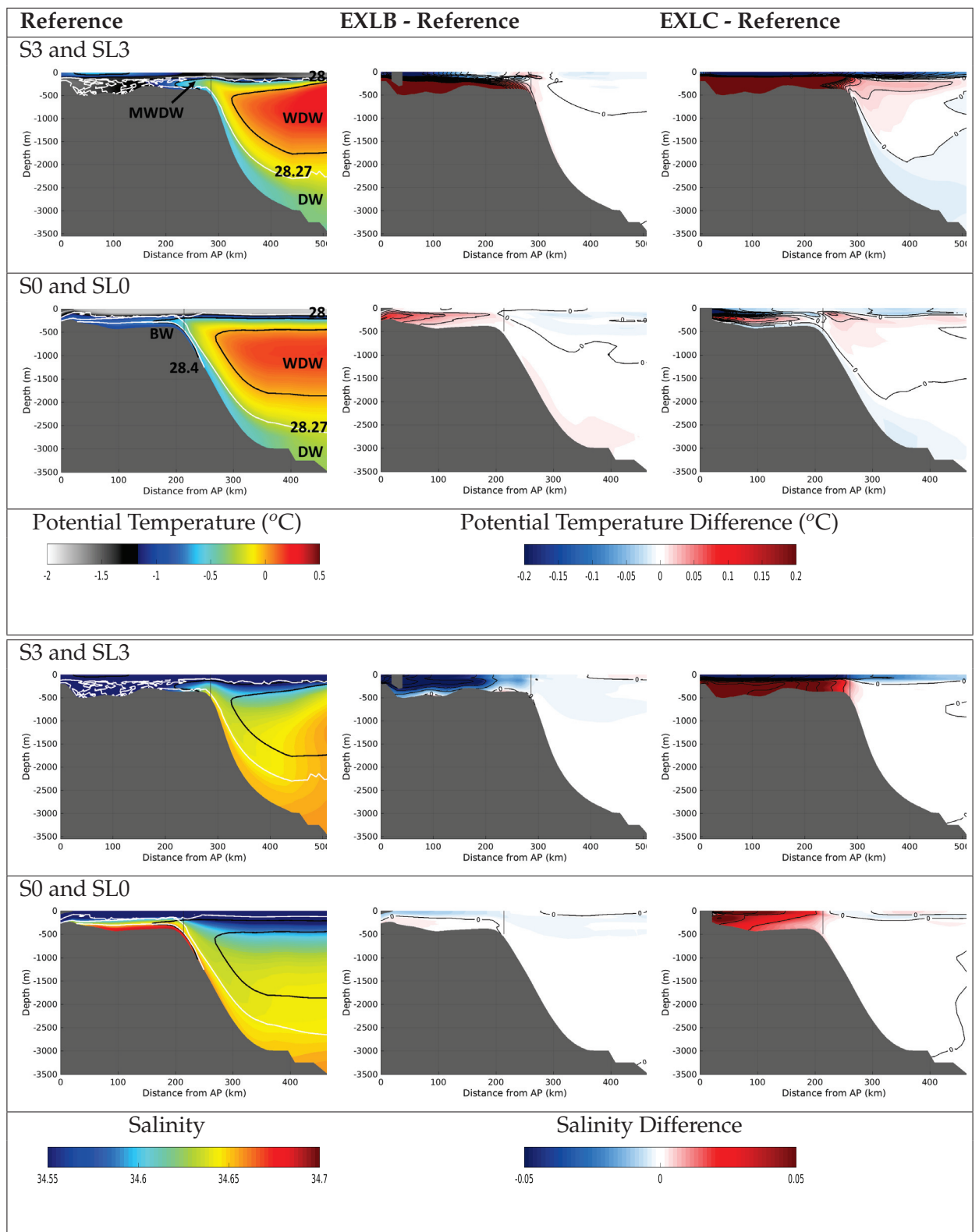
FIGURE 4.7: Mean (1989-2010) simulated potential temperature and salinity along the southern and northern zonal sections in the reference run (left), the difference between EXLB and reference (middle), and EXLC minus reference (right). The white contours on the reference run figures are neutral density (γ^n) isolines of 28, 28.27 and 28.4 kg m^{-3}, and the black bold lines are the 0 and -0.7^{o}C isotherms; the neutral density contours are labeled on the potential temperature figures (left). Black contour lines on the difference figures are shown at 0.02^{o}C and 0.02 intervals.
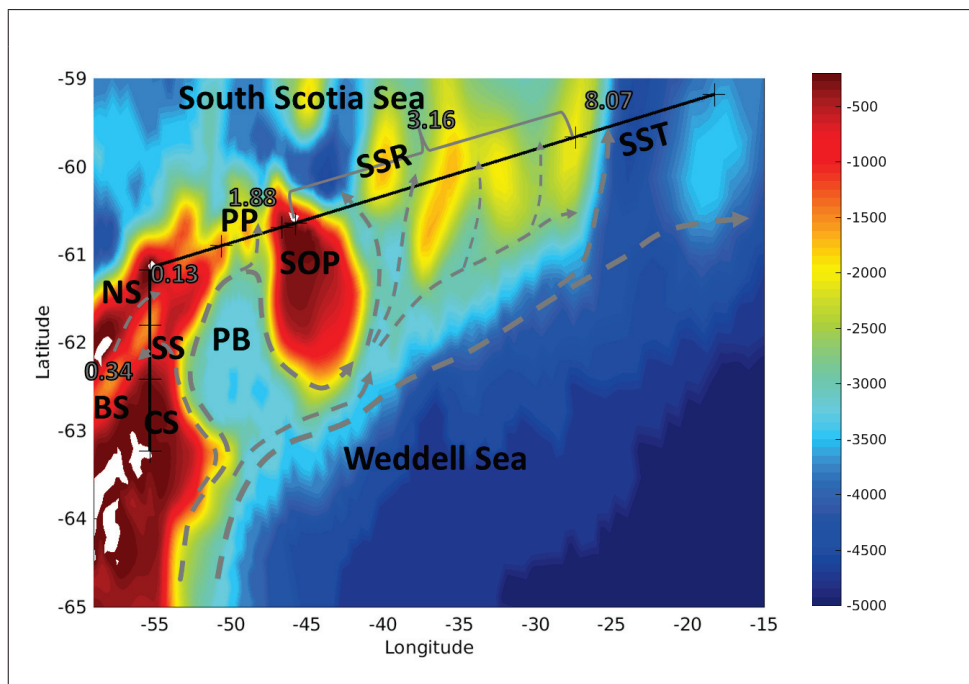
FIGURE 4.8: Northwestern Weddell Sea regional map with the sections used for the outflow analysis (black lines). The gray dashed lines and the gray numbers represent the flow of DWγ^n and the transport in Sv across the subsections, respectively. Abbreviations are listed clockwise: continental shelf subsection (CS), Bransfield Strait (BS), southern slope subsection (SS), northern slope subsection (NS), Elephant Island (EI), Powell Basin (PB), Philip Passage (PP), South Orkney Plateau (SOP), South Scotia Ridge (SSR), South Sandwich Trench (SST). Background colors represent the bathymetry.
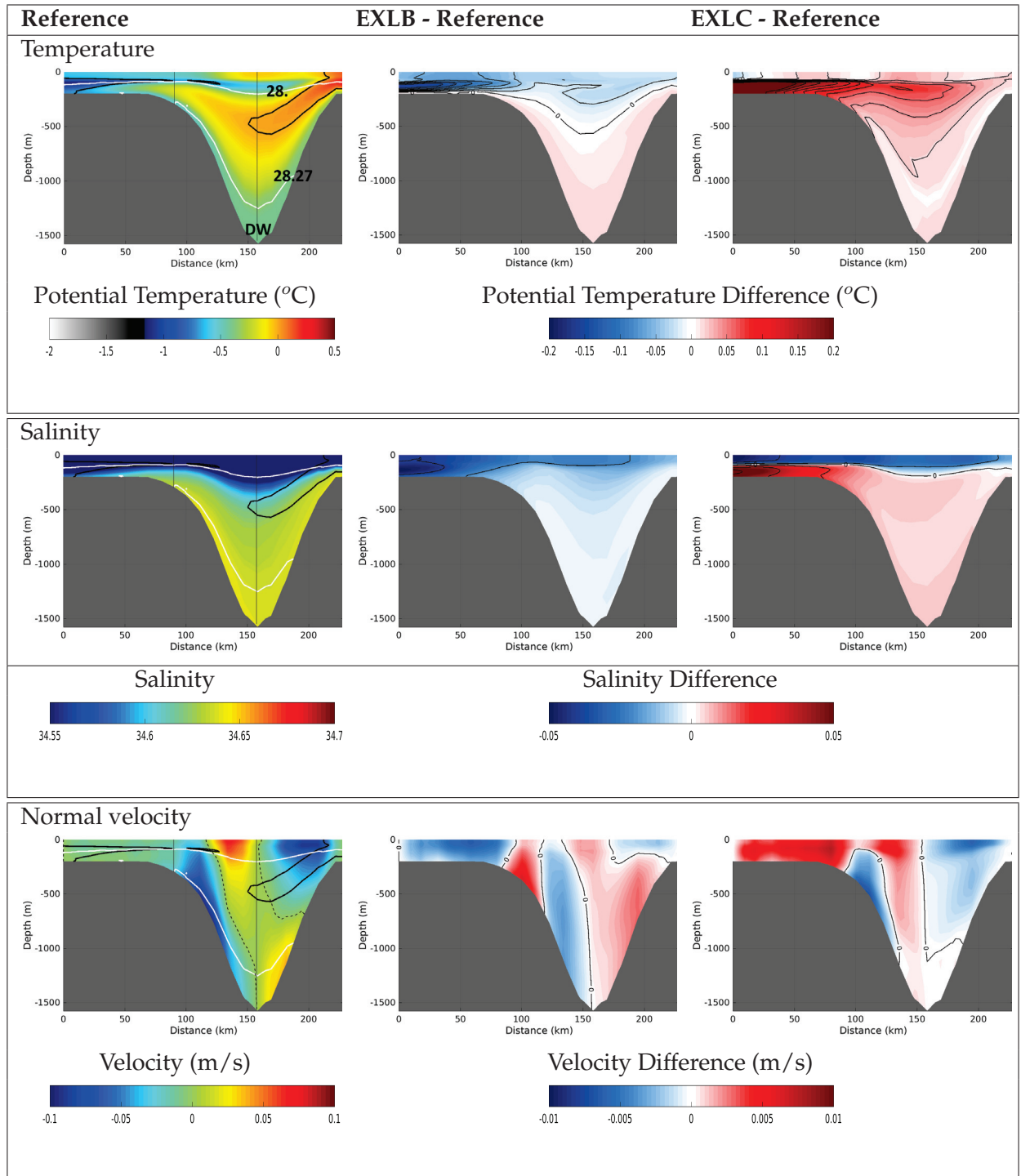
FIGURE 4.9: Mean (1989-2010) simulated values of potential temperature, salinity, and normal velocity along the Joinville-Elephant section in the reference run (left column), the difference between EXLB and reference (middle), and EXLC minus reference (right). The continental shelf (CS), southern slope (SS), and northern slope (NS) divisions are shown as black lines. The white contours in the reference run figures are neutral density (γ^n) isolines of 28, and 28.27 kg m^{-3}, the black bold lines are 0 and -0.7^{o}C isotherms; neutral density contours are labeled on the top left figure. The dashed lines in the velocity figure (bottom left) are 0 m/s contours. Black contour lines on the difference figures are shown at 0.02 intervals.
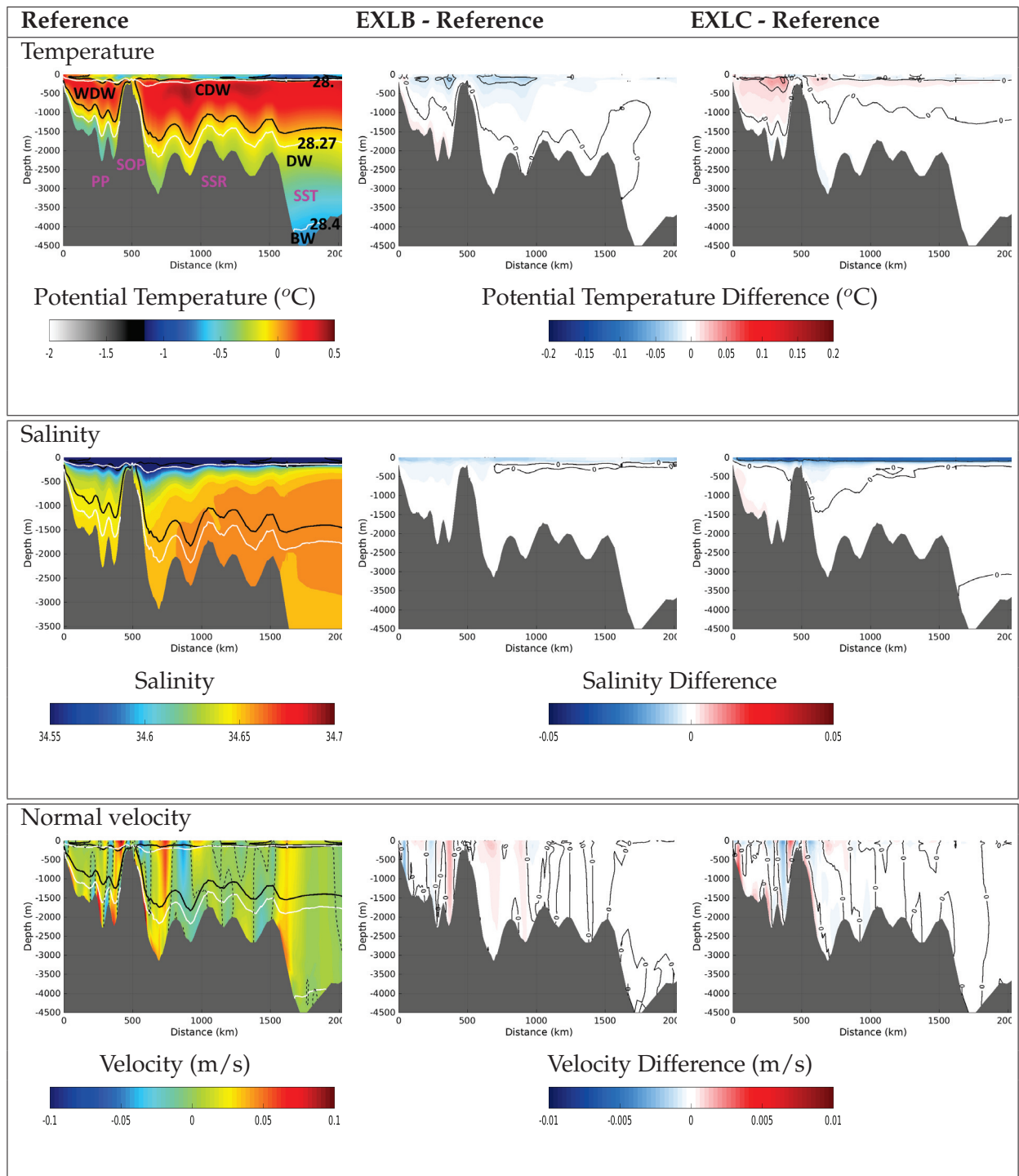
FIGURE 4.10:   Mean (1989-2010) simulated potential temperature, salinity, and normal (in/outflow) velocity along the northern Weddell Sea section in the reference run (left column), the difference between EXLB and reference (middle), and EXLC minus reference (right). The white contours on the reference run figures are neutral density (γ^n) isolines of 28, 28.27 and 28.4 kg m^{-3}, and the black bold lines are 0 and -0.7^{o}C isotherms; the neutral density contours are labeled on the top left figure. The dashed lines in the velocity figure (bottom left) are 0 m/s contours. Black contour lines on the difference figures are shown at 0.02 intervals. Abbreviations in magenta are: Phillip Passage (PP), South Orkney Pateau (SOP), South Scotia Ridge (SSR), and South Sandwich Trench (SST).

Chapter 5

Summary and Outlook

5.1 Summary

Studies based on observations hypothesized that the western Weddell Sea (WS) is a source of WSDW (e.g. Fahrbach et al., 1995; Huhn et al., 2008), an important contributor to AABW. In this study this hypothesis is tested based on observations and model experiments.

The analysis of the hydrographic sections obtained during cruise ANT XXIX-3 shows the thickening of the WSDW (DWγ^n) layer from south to north and the ongoing mixture of dense waters. Supported by the findings of previous studies (e.g Schröder et al., 2002; Absy et al., 2008), a mixing scheme for the production of WSDW is proposed with two local sources of dense waters: (1) the continental shelf in font of Larsen-A Ice shelf (LIS-A) and Larsen-B Ice Shelf, and (2) the continetal shelf in front of Larsen-C Ice Shelf (LIS-C) (Fig. 5.1 a).

The increase of the DWγ^n layer thickness from south to north is also obvious from the modelled sections in front of LIS-C and LIS-B. However, the model results suggest that there is little dense water flowing out from the continental shelf, thus, this region does not have the expected importance for WSDW and WSBW production in the model. This result is supported by the small modifications along the continental slope and the northern margin of the WS, which occurred after a significant environmental change was implemented in the model, namely the removal of LIS-C (EXLC).

Although this seems to contradict the findings based on *in situ* measurements, it is possible to explain most of the observations based on the model results. The dense water observed near the shelf break in front of LIS-C and in the Robertson Through has been assumed to be locally produced, but in the model it is steered towards the AP from the upper part of the continental slope by the local bathymetry. The cold, salty lense described by Absy et al. (2008) may originate from the Salty Shelf Waters (SSW) entering the study region from the south, seen in the model near the shelf break in front of the southern part of LIS-C. Additionally, noble gas measurements (Huhn et al., 2008) indicate that the lense is mainly influenced by HSSW and thus cannot originate only from waters formed in front of Larsen Ice Shelf (LIS), where estimates based on satellite and reanalysis data show that the sea ice production is low (Tamura et al., 2008).

Based on the model results, a new mixing scheme is proposed: SSW formed further upstream is carried into the study region, along its path to the north it mixes with MWDW or WDW to produce a different type of WSDW (Fig. 5.1 b). The mixture process is probably

enhanced when the flow crosses an abrupt bathymetric feature, like the canyons in front of LIS-C, living the impression that the resulting 'new' dense water is originating from a local source.

The previous arguments suggest that the circulation scheme for the western WS, proposed from observations, has flaws that cannot be proved right or wrong without new hydrographic and bathymetric data from the western WS continental shelf. Most of the observational studies are based on data collected northward from LIS, or on the continental slope in front of LIS-C with few measurements near the shelf break or on the continetal shelf. Therefore, the studies can only speculate about the sources of the observed WSDW (e.g. Schröder et al., 2002; Absy et al., 2008; Caspel et al., 2015a).

On the other hand, it could certainly be argued that the model results are incorrect because of: (a) The model is forced by a reanalysis product (CFSR) that may still contain flaws and uncertainties. This can be exemplified by the differences to other reanalysis products from the same 'generation', e.g., mean summer precipitation around Antarctica is higher in CFSR than in ERA Interim (Dee et al., 2011) (Fig. A.2). (b) The ocean floor seems to be unrealistically smooth in front of LIS-C when compared to the features observed in the southern WS or near the tip of AP. It might be that this representation is correct, but even the recent international effort to compile a bathymetric chart of the Southern Ocean (IBCSO; Arndt et al., 2013) had to rely on products derived from remote sensing data due to the lack of in situ measurements in this region. Depth estimates based on grounded icebergs (Luckman et al., 2010) indicate discrepancies of more than 200 m to the General Bathymetric Chart of the Oceans (GEBCO; Hall, 2006), and some heli-CTD casts performed during ISPOL (Hellmer et al., 2008) showed differences of more than 100 m in comparison to the expected depth. Topographic steering by submarine ridges could direct the dense water away from the continental shelf/shelf break, triggering the mixture of waters or mesoscale variability (e.g. Wåhlin, 2002; Darelius et al., 2009).

Concerning the simulations used for this work, it could be argued that the intense melting of sea ice during summer around the AP leads to a stabilization of the water column that hinders deep convection during sea ice formation, avoiding the densification of the shelf waters. Another reason for questioning the model results is the lower salinity of WDW and MWDW, simulated already along the Prime Meridian, which leads to a lack of salt on the continental shelf with the aforementioned consequences. The presence of lighter waters on the continental shelf could affect the volume of dense waters on the slope. However the volumes of DWγ^n and BWγ^n carried along the slope, together with the thickness and position of the dense layer agree with the observations. In addition, the Weddell Gyre strength and the WSDW export across the South Scotia Ridge simulated with FESOM are in good agreement with the estimates from previous studies (e.g. Naveira Garabato et al., 2002; Klatt et al., 2005). Note, the reference simulation was validated for the sea-ice cycle, ice shelf melting, and ocean thermohaline properties prior to the focused study of the western WS.

On the one hand, the data analysis performed in Chapter 2, supporting the results presented in previous studies (e.g. Fahrbach et al., 1995), depicts the western WS as a WSDW source region (Fig. 5.1 a). On the other hand, the model results show that there is no dense

water spill from the continental shelf off LIS. Instead, the variability and thickening of the WSDW layer in the northwestern WS are caused by (a) intensive mixing of Intermediate Water (IW) with $DW\gamma^n$, (b) dense waters formed further upstream in the southwestern WS, and (c) fluctuations of the whole WG.

More *in situ* data are needed to determine whether the western Weddell Sea is a region where dense water is formed or whether it only serves as a conduit for dense waters formed upstream, which interact in the western WS before reaching their equilibrium. Given the importance of that deep water for the local and global circulation, it would be timely to learn more about its path and history before it becomes AABW.

5.2   Outlook

There is plenty of evidence for the time variability of WSDW properties (e.g. Azaneu et al., 2013; Fahrbach et al., 2011; Huhn et al., 2013), and many ideas about the causes have been proposed: (a) changes in the thermohaline properties or volume of the CDW entering the WS, (b) variations of the sea ice cycle, (c) modifications in the wind field, (d) variability in the dense water entering the WS from the east, or (e) differences in the outflow rate. All these mechanisms interact, and their decoupling is a task where model studies can be of great help. However, in order to be useful the models need to be quite realistic and for that it is important to validate their results against observations.

Here, the importance of the continental shelf in the western WS was investigated using FESOM. Contradicting previous ideas (e.g. Gordon et al., 1993; Schröder et al., 2002; Huhn et al., 2008; Jullion et al., 2013), the model shows that this region plays only a minor role in WSDW formation. The model was calibrated against two well-sampled hydrographic sections before the area of interest was analyzed; it would be certainly possible to tune (calibrate) the model to produce dense water off LIS, but that would be a biased procedure based on what is expected.

As discussed before, this issue can only be settled by additional in-situ data. Sampling hydrographic sections in front of LIS-C across the continental shelf and along the shelf break, crossing the channels connecting the continental shelf and the continental slope is desperately needed. The more common cross-slope sections are also important but, as mentioned in Chapter 2, consecutive transects can reveal more than a single realization. Data from oceanographic moorings placed along the Prime Meridian Section and SR04 can be used to study the WSDW variability and provide further constrains for model calibration. The later is proposed in the framework of grant SPP 1158/14, 'Sources and Variability of Weddell Sea Deep Water' [1]. An oceanographic cruise to the western WS should also include extensive bathymetric soundings. A better knowledge of the terrain would be essential to plan the oceanographic sampling and prepare more realistic grids for model studies. To date, the western Weddell Sea is one of the least sampled regions of the world ocean.

Meanwhile, there is a constant effort to improve the numerical model. A new sea ice thermodynamic scheme with two layers of ice and one of snow, which also considers heat

---

[1] proposal n° 20151030542910899308
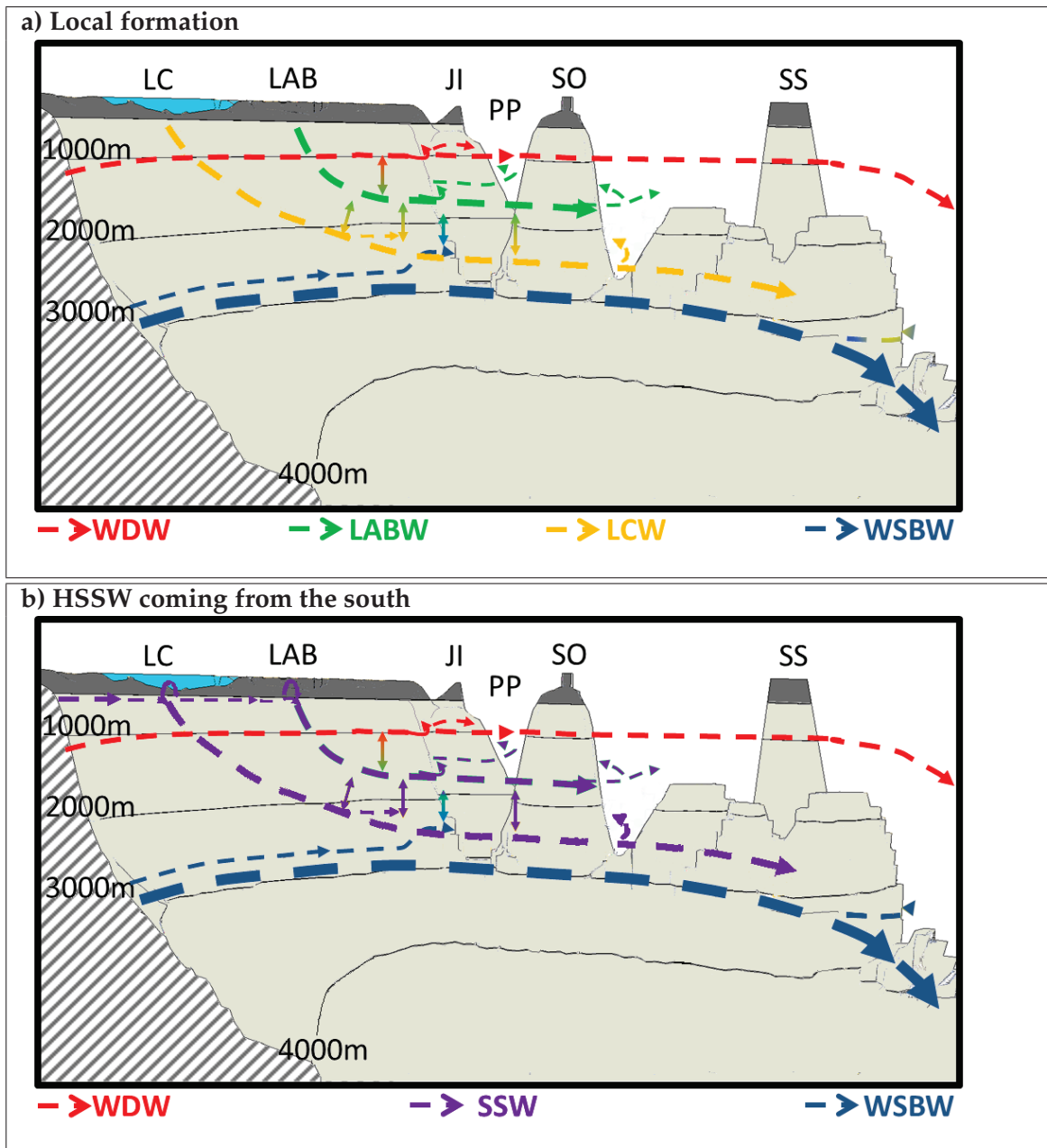
FIGURE 5.1: Proposed mixing scheme for the formation of Antarctic Bottom Water (AABW) in the western Weddell Sea derived from the observations (a - copy of Fig. 2.10), and from the model results (b). The flow of Warm Deep Water (WDW, red line), Weddell Sea Bottom Water (WSBW, blue line), Larsen C Water (LCW, yellow line in a), Larsen A and B Water (LABW, green line in a), and Salty Shelf Water (SSW, purple line in b) are shown together with the main outflow paths. Abreviations are: Joinville Island (JI), Larsen A and B (LAB), Larsen C (LC), Philip Passage (PP), South Orkney Islands (SO), South Sandwich Islands (SS).

storage related to sea ice temperature changes (Winton, 2000), is close to being operational; variable drag coefficients between sea ice and atmosphere will also be tested. In addition, a new mesh for WS studies is designed with higher resolution in the WG recirculation area, where the inflow of CDW occurs. The increased computational cost would be compensated by a reduced number of experiments, since a single evaluation of the model can be used for different studies, like inflow of CDW in the WS, intrusion of warm waters underneath FRIS, HSSW production in the Ronne polynya, and outflow of WSDW to the fringing basins. With a better comprehension of the WS, the variability of AABW found in the abyssal plain of all oceans and, thus, the changes in the global meridional overturning circulation can be better understood and possibly predicted.

Appendix A

Complementary figures and tables

Figures and tables that are not necessary for the understanding of the ideas presented on the main text but might be of interest of a curious reader are shown here.

TABLE A.1: Mean transport, temperature, and salinity of the four 'water masses' across the zonal sections

SEC	WM	Ref			EXLB			EXLC		
		Tr(Sv)	θ (°C)	Sal	Tr(Sv)	θ (°C)	Sal	Tr(Sv)	θ (°C)	Sal
S0	SW	-0.013	-1.7	34.374	-0.001	-1.58	32.387	-0.01	-1.81	34.44
	IW	-0.002	-1.32	34.53	0.008	-1.28	34.53	0.009	-1.56	34.52
	DWγ^n	0.155	-0.79	34.626	0.128	-0.76	34.628	0.155	-0.77	34.63
	BWγ^n	0.215	-0.9	34.661	0.238	-0.88	34.664	0.217	-0.99	34.655
S1	SW	0.09	-1.69	34.236	0.01	-0.95	21.703	0.097	-1.67	34.28
	IW	0.061	-0.99	34.546	0.13	-0.92	34.549	0.061	-0.93	34.565
	DWγ^n	0.078	-0.7	34.63	0.073	-0.65	34.635	0.085	-0.66	34.637
	BWγ^n	0.066	-0.72	34.657	0.098	-0.7	34.66	0.064	-0.76	34.662
S2	SW	0.147	-1.39	34.319	0.03	-1.36	34.103	0.159	-1.5	34.25
	IW	0.036	-0.87	34.553	0.087	-0.74	34.558	0.064	-0.65	34.585
	DWγ^n	0.034	-0.65	34.631	0.057	-0.58	34.636	0.031	-0.57	34.645
	BWγ^n	0.001	-0.82	34.642	0.014	-0.89	34.634	0.001	-0.65	34.662
S3	SW	0.175	-1.02	34.344	0.068	-1.08	34.279	0.326	-1.17	34.261
	IW	0.172	-1.18	34.514	0.108	-0.76	34.525	0.086	-0.66	34.577
	DWγ^n	0.018	-1.05	34.564	0.09	-0.57	34.62	0.005	-0.58	34.635
	BWγ^n	-0.002	-1.83	34.559	0.001	-1.88	34.54	-0.001	-0.95	34.632
SL0	SW	0.035	-1.77	34.376	0.032	-1.77	34.375	0.038	-1.79	34.379
	IW	4.173	-0.09	34.618	4.084	-0.09	34.617	4.262	-0.09	34.618
	DWγ^n	3.772	-0.38	34.65	3.781	-0.37	34.65	3.734	-0.38	34.65
	BWγ^n	0.802	-0.73	34.664	0.911	-0.73	34.664	0.741	-0.73	34.665
SL1	SW	0.261	-1.7	34.327	0.269	-1.7	34.328	0.275	-1.74	34.329
	IW	6.455	-0.07	34.622	6.394	-0.07	34.622	6.602	-0.06	34.623
	DWγ^n	4.496	-0.38	34.651	4.463	-0.38	34.651	4.501	-0.39	34.652
	BWγ^n	0.675	-0.64	34.665	0.842	-0.63	34.665	0.6	-0.64	34.666
SL2	SW	0.477	-1.61	34.316	0.499	-1.61	34.319	0.493	-1.68	34.313
	IW	8.418	-0.06	34.623	8.362	-0.06	34.623	8.669	-0.05	34.624
	DWγ^n	5.652	-0.4	34.652	5.642	-0.4	34.652	5.577	-0.41	34.652
	BWγ^n	0.265	-0.62	34.667	0.41	-0.61	34.667	0.204	-0.61	34.667
SL3	SW	0.613	-1.45	34.293	0.649	-1.45	34.295	0.633	-1.55	34.282
	IW	10.131	-0.02	34.628	10.062	-0.02	34.628	10.279	-0.01	34.629
	DWγ^n	6.294	-0.38	34.652	6.394	-0.38	34.652	6.324	-0.39	34.653
	BWγ^n	0.176	-0.62	34.667	0.244	-0.61	34.668	0.122	-0.61	34.669

TABLE A.2: Mean transport, temperature, and salinity of the four 'water masses' across the meridional sections

SEC	WM	Ref			EXLB			EXLC		
		Tr(Sv)	θ (°C)	Sal	Tr(Sv)	θ (°C)	Sal	Tr(Sv)	θ (°C)	Sal
SL01	SW	-0.181	-1.78	34.33	-0.184	-1.77	34.332	-0.193	-1.79	34.331
	IW	-2.618	0	34.628	-2.66	0	34.628	-2.698	0	34.629
	DWγ^n	-0.268	-0.29	34.654	-0.268	-0.28	34.654	-0.268	-0.29	34.654
	BWγ^n	0	NaN	NaN	0	NaN	NaN	0	NaN	NaN
SL12	SW	-0.162	-1.75	34.293	-0.161	-1.74	34.294	-0.166	-1.78	34.294
	IW	-2.283	0.06	34.638	-2.269	0.06	34.637	-2.336	0.06	34.638
	DWγ^n	-0.391	-0.3	34.656	-0.385	-0.3	34.656	-0.391	-0.31	34.656
	BWγ^n	0	NaN	NaN	0	NaN	NaN	0	NaN	NaN
SL23	SW	-0.124	-1.66	34.238	-0.123	-1.66	34.241	-0.127	-1.71	34.234
	IW	-1.853	0.1	34.645	-1.814	0.1	34.645	-1.881	0.1	34.645
	DWγ^n	-0.472	-0.31	34.657	-0.475	-0.31	34.657	-0.471	-0.31	34.657
	BWγ^n	0	NaN	NaN	0	NaN	NaN	0	NaN	NaN
S01	SW	0.012	-1.76	34.373	0.013	-1.75	34.37	0.012	-1.78	34.389
	IW	0.049	-0.72	34.585	0.05	-0.71	34.585	0.052	-0.71	34.586
	DWγ^n	-0.013	-0.5	34.646	-0.013	-0.5	34.647	-0.011	-0.5	34.646
	BWγ^n	0.01	-0.73	34.668	0.012	-0.72	34.667	0.009	-0.73	34.67
S12	SW	0.016	-1.62	34.327	0.024	-1.61	34.326	0.014	-1.72	34.329
	IW	0.03	-0.53	34.593	0.042	-0.51	34.593	0.022	-0.46	34.6
	DWγ^n	0.038	-0.54	34.649	0.042	-0.54	34.65	0.038	-0.5	34.651
	BWγ^n	-0.001	-0.64	34.664	0.018	-0.63	34.665	-0.007	-0.63	34.666
S23	SW	-0.019	-1.44	34.313	-0.007	-1.43	34.313	-0.018	-1.59	34.303
	IW	-0.105	-0.47	34.594	-0.059	-0.44	34.595	-0.118	-0.39	34.604
	DWγ^n	-0.019	-0.55	34.647	-0.009	-0.53	34.648	-0.023	-0.53	34.652
	BWγ^n	0	-0.63	34.664	0.003	-0.61	34.665	0	-0.6	34.667

TABLE A.3: Mean transport, temperature, and salinity of the four 'water masses' across the section between Joinville Island and Elephant Island

SEC	WM	Ref			EXLB			EXLC		
		Tr(Sv)	θ (°C)	Sal	Tr(Sv)	θ (°C)	Sal	Tr(Sv)	θ (°C)	Sal
CS	SW	-0.083	-0.58	34.341	-0.13	-0.7	34.322	-0.045	-0.58	34.31
	IW	-0.084	-0.59	34.568	-0.102	-0.59	34.553	-0.033	-0.41	34.592
	DW	-0.003	-0.66	34.616	-0.001	-0.7	34.611	-0.005	-0.46	34.639
	BW	0	-1.79	34.541	0			0	-1.55	34.579
SS	SW	0.188	-0.39	34.353	0.197	-0.43	34.34	0.211	-0.37	34.335
	IW	-0.487	-0.19	34.614	-0.595	-0.19	34.612	-0.399	-0.13	34.619
	DW	-0.336	-0.43	34.639	-0.269	-0.43	34.637	-0.428	-0.4	34.645
	BW	0			0			0		
NS	SW	-0.479	-0.23	34.367	-0.497	-0.26	34.356	-0.514	-0.2	34.352
	IW	-0.408	-0.13	34.619	-0.299	-0.13	34.617	-0.467	-0.09	34.623
	DW	0.13	-0.4	34.64	0.095	-0.39	34.639	0.162	-0.38	34.644
	BW	0			0			0		

TABLE A.4: Mean transport, temperature, and salinity of the four 'water masses' across the section along the northern Weddell Sea section

| SEC	WM	Ref			EXLB			EXLC		
		Tr(Sv)	θ (ºC)	Sal	Tr(Sv)	θ (ºC)	Sal	Tr(Sv)	θ (ºC)	Sal
PHP	SW	0.803	-0.26	34.336	0.82	-0.27	34.333	0.818	-0.23	34.324
	IW	3.424	0.05	34.63	3.487	0.04	34.629	3.312	0.06	34.631
	DW	1.881	-0.37	34.65	1.868	-0.37	34.649	1.915	-0.37	34.651
	BW	0	NaN	NaN	0	NaN	NaN	0	NaN	NaN
SSR	SW	0.782	-0.26	34.231	0.804	-0.27	34.225	0.78	-0.25	34.221
	IW	4.604	0.15	34.646	4.794	0.15	34.646	4.471	0.15	34.646
	DW	3.169	-0.21	34.659	3.135	-0.21	34.658	3.228	-0.21	34.659
	BW	0	NaN	NaN	0	NaN	NaN	0	NaN	NaN
SST	SW	0.886	-0.76	33.833	0.886	-0.77	33.826	0.886	-0.77	33.814
	IW	8.632	0.15	34.656	8.694	0.14	34.656	8.528	0.15	34.656
	DW	8.074	-0.39	34.658	8.071	-0.39	34.658	8.119	-0.39	34.658
	BW	0.166	-0.68	34.652	0.169	-0.68	34.652	0.166	-0.68	34.652
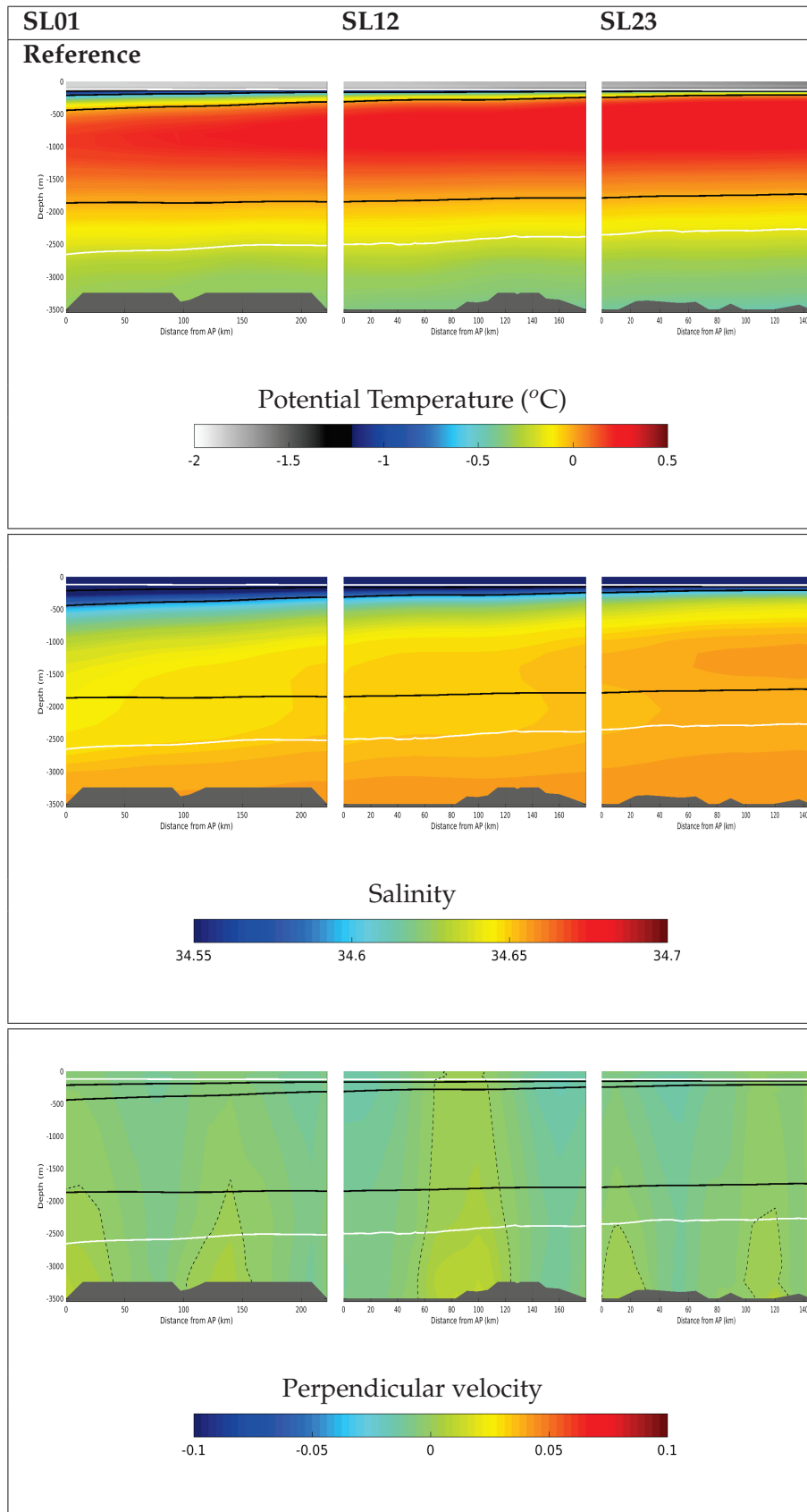
FIGURE A.1: Mean values (1989-2010) of simulated potential temperature (top), salinity (middle), and normal (on/offshore) velocity (bottom) in the sections along 3500m isobath in the reference run. The sections are shown from south (left) to north (right). The white contours are neutral density (γ^n) isolines of 28 and 28.27 kg m^{-3}, the black bold lines are the 0°C isotherms, the dashed lines are 0 m/s velocity contours.
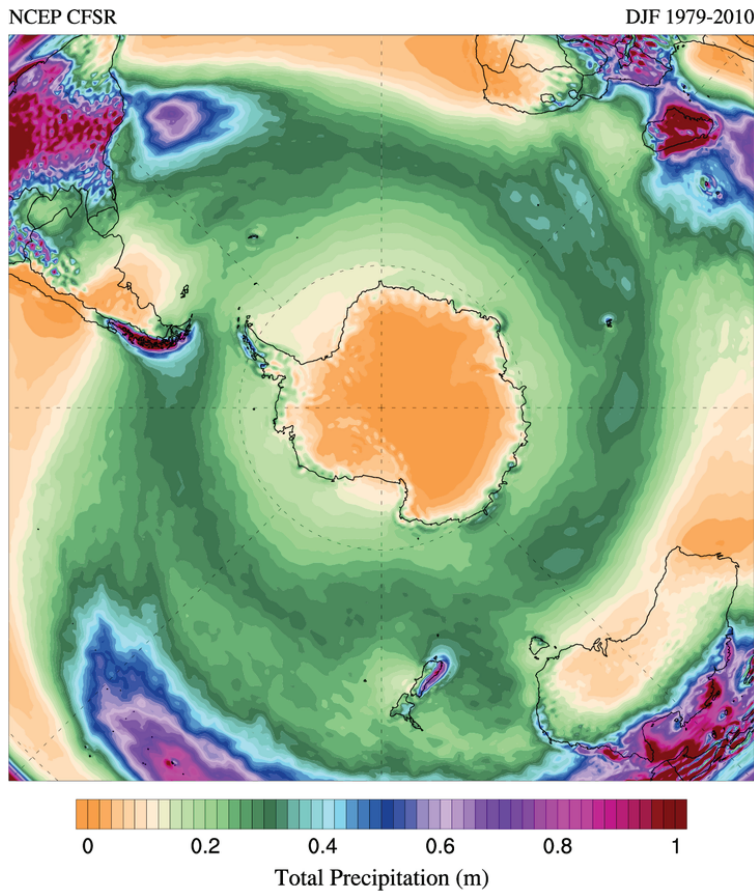
FIGURE A.2: CFSR and ERA Interim summer mean precipitation. The averaged period is from 1979 until 2010. **Image obtained using Climate Reanalyzer (http://cci-reanalyzer.org), Climate Change Institute, University of Maine, USA.**

Bibliography

Absy, J. M., M. Schröder, R. Muench, and H. H. Hellmer (2008). "Early summer thermohaline characteristics and mixing in the western Weddell Sea". In: *Deep Sea Research Part II: Topical Studies in Oceanography* 55.8, pp. 1117–1131.

Amante, Christopher and Barry W Eakins (2009). *ETOPO1 1 arc-minute global relief model: procedures, data sources and analysis*. US Department of Commerce, National Oceanic et al.

Arndt, Jan Erik, Hans Werner Schenke, Martin Jakobsson, Frank O. Nitsche, Gwen Buys, Bruce Goleby, Michele Rebesco, Fernando Bohoyo, Jongkuk Hong, Jenny Black, Rudolf Greku, Gleb Udintsev, Felipe Barrios, Walter Reynoso-Peralta, Morishita Taisei, and Rochelle Wigley (2013). "The International Bathymetric Chart of the Southern Ocean (IBCSO) Version 1.0—A new bathymetric compilation covering circum-Antarctic waters". In: *Geophysical Research Letters* 40.12, pp. 3111–3117. ISSN: 1944-8007.

Azaneu, Marina, Rodrigo Kerr, Mauricio M Mata, and Carlos AE Garcia (2013). "Trends in the deep Southern Ocean (1958–2010): implications for Antarctic Bottom Water properties and volume export". In: *Journal of Geophysical Research: Oceans* 118.9, pp. 4213–4227.

Behrendt, A, W Dierking, E Fahrbach, and H Witte (2013). "Sea ice draft in the Weddell Sea, measured by upward looking sonars". In: *Earth System Science Data* 5.1, pp. 209–226.

Brisbourne, Alex, Andy Smith, Edward King, Keith Nicholls, Paul Holland, and Keith Makinson (2014). "Seabed topography beneath Larsen C Ice Shelf from seismic soundings". In: *The Cryosphere* 8, pp. 1–13.

Caspel, M van, M Schröder, O Huhn, and HH Hellmer (2015a). "Precursors of Antarctic Bottom Water formed on the continental shelf off Larsen Ice Shelf". In: *Deep Sea Research Part I: Oceanographic Research Papers* 99, pp. 1–9.

Caspel, Mathias Rucker van, João Marcelo Absy, Qiang Wang, Hartmut H Hellmer, and Michael Schröder (2015b). "The Flow of Dense Water Plumes in the Western Weddell Sea Simulated with the Finite Element Ocean Model (FEOM)". In: *Towards an Interdisciplinary Approach in Earth System Science*. Springer, pp. 125–129.

Cavalieri, Donald J, Claire L Parkinson, Per Gloersen, and H Jay Zwally (1997). "Arctic and Antarctic Sea Ice Concentrations from Multichannel Passive- Microwave Satellite Data Sets: User's Guide". In: *NASA* 19980076134.

Danilov, Sergey, Gennady Kivman, and Jens Schröter (2004). "A finite-element ocean model: principles and evaluation". In: *Ocean Modelling* 6.2, pp. 125–150.

Danilov, Sergey, Qiang Wang, Ralph Timmermann, Nikolay Iakovlev, Dmitry Sidorenko, Madlen Kimmritz, Thomas Jung, and Jens Schröter (2015). "Finite-Element Sea Ice Model (FESIM), version 2". In: *Geoscientific Model Development* 8.6, pp. 1747–1761.

Darelius, E, LH Smedsrud, S Østerhus, A Foldvik, and T Gammelsrød (2009). "Structure and variability of the Filchner overflow plume". In: *Tellus A* 61.3, pp. 446–464.

Dee, DP, SM Uppala, AJ Simmons, Paul Berrisford, P Poli, S Kobayashi, U Andrae, MA Balmaseda, G Balsamo, P Bauer, et al. (2011). "The ERA-Interim reanalysis: Configuration and performance of the data assimilation system". In: *Quarterly Journal of the Royal Meteorological Society* 137.656, pp. 553–597.

Evans, Jeffrey, Carol J. Pudsey, Colm ÓCofaigh, Peter Morris, and Eugene Domack (2005). "Late Quaternary glacial history, flow dynamics and sedimentation along the eastern margin of the Antarctic Peninsula Ice Sheet". In: *Quaternary Science Reviews* 24.5-6, pp. 741–774. ISSN: 0277-3791.

Fahrbach, E., M. Hoppema, G. Rohardt, O. Boebel, O. Klatt, and A. Wisotzki (2011). "Warming of deep and abyssal water masses along the Greenwich meridian on decadal time scales: The Weddell gyre as a heat buffer". In: *Deep Sea Research Part II: Topical Studies in Oceanography* 58.25 26, pp. 2509–2523.

Fahrbach, Eberhard, Martin Knoche, and Gerd Rohardt (1991). "An estimate of water mass transformation in the southern Weddell Sea". In: *Marine Chemistry* 35.1, pp. 25–44.

Fahrbach, Eberhard, Gerd Rohardt, Michael Schröder, and Volker Strass (1994). "Transport and structure of the Weddell Gyre". In: *Annales Geophysicae*. Vol. 12. 9. Springer, pp. 840–855.

Fahrbach, Eberhard, Gerd Rohardt, Norbert Scheele, Michael Schröder, Volker Strass, and Andreas Wisotzki (1995). "Formation and discharge of deep and bottom water in the northwestern Weddell Sea". In: *Journal of Marine Research* 53.4, pp. 515–538.

Fahrbach, Eberhard, Sabine Harms, Gerd Rohardt, Michael Schröder, and Rebecca A Woodgate (2001). "Flow of bottom water in the northwestern Weddell Sea". In: *Journal of Geophysical Research: Oceans* 106.C2, pp. 2761–2778.

Fahrbach, Eberhard, Mario Hoppema, Gerd Rohardt, Michael Schröder, and Andreas Wisotzki (2004). "Decadal-scale variations of water mass properties in the deep Weddell Sea". In: *Ocean Dynamics* 54.1, pp. 77–91.

Foldvik, A, T Gammelsrød, E Nygaard, and S Østerhus (2001). "Current measurements near Ronne Ice Shelf: Implications for circulation and melting". In: *Journal of Geophysical Research: Oceans* 106.C3, pp. 4463–4477.

Foldvik, A., T. Gammelsrød, S. Østerhus, E. Fahrbach, G. Rohardt, M. Schröder, K. W. Nicholls, L. Padman, and R. A. Woodgate (2004). "Ice shelf water overflow and bottom water formation in the southern Weddell Sea". In: *J. Geophys. Res.* 109.C2, p. C02015.

Foldvik, Arne and Tor Gammelsrød (1988). "Notes on Southern Ocean hydrography, sea-ice and bottom water formation". In: *Palaeogeography, Palaeoclimatology, Palaeoecology* 67.12, pp. 3–17.

Foster, Theodore D and Eddy C Carmack (1976). "Frontal zone mixing and Antarctic Bottom Water formation in the southern Weddell Sea". In: *Deep Sea Research and Oceanographic Abstracts*. Vol. 23. 4. Elsevier, pp. 301–317.

Franco, Bárbara C, Mauricio M Mata, Alberto R Piola, and Carlos AE Garcia (2007). "Northwestern Weddell Sea deep outflow into the Scotia Sea during the austral summers of 2000 and 2001 estimated by inverse methods". In: *Deep Sea Research Part I: Oceanographic Research Papers* 54.10, pp. 1815–1840.

Frants, Marina, Sarah T. Gille, Christopher D. Hewes, Osmund Holm-Hansen, Mati Kahru, Aaron Lombrozo, Christopher I. Measures, B. Greg Mitchell, Haili Wang, and Meng Zhou (2013). "Optimal multiparameter analysis of source water distributions in the Southern Drake Passage". In: *Deep Sea Research Part II: Topical Studies in Oceanography* 90.0, pp. 31 –42. ISSN: 0967-0645.

Gerdes, Rüdiger, Jürgen Determann, and Klaus Grosfeld (1999). "Ocean circulation beneath Filchner-Ronne Ice Shelf from three-dimensional model results". In: *Journal of Geophysical Research: Oceans* 104.C7, pp. 15827–15842.

Gonçalves-Araujo, Rafael, Márcio Silva de Souza, Virginia Maria Tavano, and Carlos Alberto Eiras Garcia (2015). "Influence of oceanographic features on spatial and interannual variability of phytoplankton in the Bransfield Strait, Antarctica". In: *Journal of Marine Systems* 142, pp. 1–15.

Gordon, Arnold L (1998). "Western Weddell Sea thermohaline stratification". In: *Ocean, ice, and atmosphere: Interactions at the Antarctic continental Margin* 75, pp. 215–240.

Gordon, Arnold L., Bruce A. Huber, Hartmut H. Hellmer, and Amy Ffield (1993). "Deep and Bottom Water of the Weddell Sea's Western Rim". In: *Science* 262.5130, pp. 95–97.

Gordon, Arnold L, Manfred Mensch, Dong Zhaoqian, William M Smethie, and Jose Bettencourt (2000). "Deep and bottom water of the Bransfield Strait eastern and central basins". In: *Journal of Geophysical Research: Oceans* 105.C5, pp. 11337–11346.

Gordon, Arnold L, Martin Visbeck, and Bruce Huber (2001). "Export of Weddell Sea Deep and Bottom Water". In: *Journal of Geophysical Research: Oceans (1978-2012)* 106.C5, pp. 9005–9017.

Graeve, Martin, Harald Bohlmann, Laura Fillinger, Dieter Gerdes, and Rainer Knust (2013). *Physical oceanography during Polarstern cruise ANT-XXVII/3 (PS77, CAMBIO)*. Bremerhaven.

Gutt, Julian, Michael Schröder, and Volker Sieger (2013). "The Expedition of the Research Vessel Polarstern to the Antarctic in 2013 (ANT-XXIX/3)". In: *Reports on Polar and Marine Research* 665, p. 151.

Gyldenfeldt, A.B. von, E. Fahrbach, M.A. García, and M. Schröder (2002). "Flow variability at the tip of the Antarctic Peninsula". In: *Deep Sea Research Part II: Topical Studies in Oceanography* 49.21, pp. 4743–4766.

Hall, John K (2006). "GEBCO Centennial Special Issue–Charting the secret world of the ocean floor: the GEBCO project 1903–2003". In: *Marine Geophysical Researches* 27.1, pp. 1–5.

Hellmer, H., M. Schröder, C. Haas, GS Dieckmann, and M. Spindler (2008). "The ISPOL drift experiment". In: *Deep Sea Research Part II: Topical Studies in Oceanography* 55.8, pp. 913–917.

Hellmer, Hartmut H (2004). "Impact of Antarctic ice shelf basal melting on sea ice and deep ocean properties". In: *Geophysical Research Letters* 31.10.

Hellmer, Hartmut H, Frank Kauker, Ralph Timmermann, Jürgen Determann, and Jamie Rae (2012). "Twenty-first-century warming of a large Antarctic ice-shelf cavity by a redirected coastal current". In: *Nature* 485.7397. 10.1038/nature11064, pp. 225–228.

Hellmer, HH and DJ Olbers (1989). "A two-dimensional model for the thermohaline circulation under an ice shelf". In: *Antarctic Science* 1.04, pp. 325–336.

Holland, Paul R, Hugh FJ Corr, David G Vaughan, Adrian Jenkins, and Pedro Skvarca (2009). "Marine ice in Larsen ice shelf". In: *Geophysical Research Letters* 36.11.

Holland, Paul R, Hugh FJ Corr, Hamish D Pritchard, David G Vaughan, Robert J Arthern, Adrian Jenkins, and Marco Tedesco (2011). "The air content of Larsen ice shelf". In: *Geophysical Research Letters* 38.10.

Huhn, Oliver, Hartmut H. Hellmer, Monika Rhein, Christian Rodehacke, Wolfgang Roether, Michael P. Schodlok, and Michael Schröder (2008). "Evidence of deep- and bottom-water formation in the western Weddell Sea". In: *Deep Sea Research Part II: Topical Studies in Oceanography* 55.8 9, pp. 1098–1116.

Huhn, Oliver, Monika Rhein, Mario Hoppema, and Steven van Heuven (2013). "Decline of deep and bottom water ventilation and slowing down of anthropogenic carbon storage in the Weddell Sea, 1984–2011". In: *Deep Sea Research Part I: Oceanographic Research Papers* 76, pp. 66–84.

Jackett, David R and Trevor J McDougall (1997). "A neutral density variable for the world's oceans". In: *Journal of Physical Oceanography* 27.2, pp. 237–263.

Joughin, Ian and Laurence Padman (2003). "Melting and freezing beneath Filchner-Ronne Ice Shelf, Antarctica". In: *Geophysical Research Letters* 30.9.

Jullion, Loïc, SC Jones, AC Naveira Garabato, and Michael P Meredith (2010). "Wind-controlled export of Antarctic Bottom Water from the Weddell Sea". In: *Geophysical Research Letters* 37.9.

Jullion, Loïc, Alberto C Naveira Garabato, Michael P Meredith, Paul R Holland, Peggy Courtois, and Brian A King (2013). "Decadal freshening of the Antarctic Bottom Water exported from the Weddell Sea". In: *Journal of Climate* 26, pp. 8111 –8125.

Jullion, Loïc, Alberto C Naveira Garabato, Sheldon Bacon, Michael P Meredith, Pete J Brown, Sinhue Torres-Valdés, Kevin G Speer, Paul R Holland, Jun Dong, Dorothée Bakker, et al. (2014). "The contribution of the Weddell Gyre to the lower limb of the Global Overturning Circulation". In: *Journal of Geophysical Research: Oceans* 119.6, pp. 3357–3377.

Karstensen, Johannes and Matthias Tomczak (1995). "OMP Analysis Package for MATLAB Version 2.0". In: *http://omp.ifm-geomar.de/* downloaded in 2013.

Klatt, Olaf, Eberhard Fahrbach, Mario Hoppema, and Gerd Rohardt (2005). "The transport of the Weddell Gyre across the Prime Meridian". In: *Deep Sea Research Part II: Topical Studies in Oceanography* 52.3, pp. 513–528.

Knust, Rainer (2012). "Expeditionsprogramm Nr. 90, FS Polarstern, ANT-XXIX/1, ANT-XXIX/2, ANT-XXIX/3". In: *Expeditionsprogramm Polarstern*.

Kusahara, Kazuya and Hiroyasu Hasumi (2014). "Pathways of basal meltwater from Antarctic ice shelves: A model study". In: *Journal of Geophysical Research: Oceans* 119.9, pp. 5690–5704.

Lemke, Peter (2009). "The expedition of the research vessel "Polarstern" to the Antarctic in 2006 (ANT-XXIII/7)". In: *Reports on Polar and Marine Research* 586.

Lewis, EL and RG Perkin (1986). "Ice pumps and their rates". In: *Journal of Geophysical Research: Oceans* 91.C10, pp. 11756–11762.

Locarnini, RA, AV Mishonov, JI Antonov, TP Boyer, HE Garcia, OK Baranova, MM Zweng, CR Paver, JR Reagan, DR Johnson, et al. (2013). "World ocean atlas 2013, volume 1: temperature". In: *NOAA Atlas NESDIS* 73, p. 40.

Luckman, Adrian, Laurie Padman, and Daniela Jansen (2010). "Persistent iceberg groundings in the western Weddell Sea, Antarctica". In: *Remote Sensing of Environment* 114.2, pp. 385–391.

Mackas, David L., Kenneth L. Denman, and Andrew F. Bennett (1987). "Least squares multiple tracer analysis of water mass composition". In: *Journal of Geophysical Research: Oceans* 92.C3, pp. 2907–2918. ISSN: 2156-2202.

Makinson, Keith, Paul R Holland, Adrian Jenkins, Keith W Nicholls, and David M Holland (2011). "Influence of tides on melting and freezing beneath Filchner-Ronne Ice Shelf, Antarctica". In: *Geophysical Research Letters* 38.6.

Marson, Juliana M, Lawrence A Mysak, Mauricio M Mata, and Ilana Wainer (2015). "Evolution of the deep Atlantic water masses since the last glacial maximum based on a transient run of NCAR-CCSM3". In: *Climate Dynamics*, pp. 1–13.

Meredith, Michael P (2013). "Oceanography: Replenishing the abyss". In: *Nature Geoscience* 6.3, pp. 166–167.

Meredith, Michael P, Alberto C Naveira Garabato, Arnold L Gordon, and Gregory C Johnson (2008a). "Evolution of the Deep and Bottom Waters of the Scotia Sea, Southern Ocean, during 1995-2005*". In: *Journal of Climate* 21.13, pp. 3327–3343.

Meredith, Michael P, Eugene J Murphy, Elizabeth J Hawker, John C King, and Margaret I Wallace (2008b). "On the interannual variability of ocean temperatures around South Georgia, Southern Ocean: Forcing by El Niño/Southern Oscillation and the southern annular mode". In: *Deep Sea Research Part II: Topical Studies in Oceanography* 55.18, pp. 2007–2022.

Nakayama, Yoshihiro, Ralph Timmermann, Michael Schröder, and HH Hellmer (2014). "On the difficulty of modeling Circumpolar Deep Water intrusions onto the Amundsen Sea continental shelf". In: *Ocean Modelling* 84, pp. 26–34.

Naveira Garabato, Alberto C., Elaine L. McDonagh, David P. Stevens, Karen J. Heywood, and Richard J. Sanders (2002). "On the export of Antarctic Bottom Water from the Weddell Sea". In: *Deep Sea Research Part II: Topical Studies in Oceanography* 49.21, pp. 4715–4742.

Nicholls, Keith W, L Padman, Michael Schröder, RA Woodgate, Adrian Jenkins, and Svein Østerhus (2003). "Water mass modification over the continental shelf north of Ronne Ice Shelf, Antarctica". In: *Journal of Geophysical Research: Oceans* 108.C8.

Nicholls, Keith W, Svein Østerhus, Keith Makinson, Tor Gammelsrød, and Eberhard Fahrbach (2009). "Ice-ocean processes over the continental shelf of the southern Weddell Sea, Antarctica: A review". In: *Reviews of Geophysics* 47.3, RG3003.

Nicholls, KW (1997). "Predicted reduction in basal melt rates of an Antarctic ice shelf in a warmer climate". In: *Nature* 388.6641, pp. 460–462.

Nicholls, KW, CJ Pudsey, and P. Morris (2004). "Summertime water masses off the northern Larsen C Ice Shelf, Antarctica". In: *Geophysical research letters* 31.9, p. L09309.

Orsi, A. H., G. C. Johnson, and J. L. Bullister (1999). "Circulation, mixing, and production of Antarctic Bottom Water". In: *Progress in Oceanography* 43.1, pp. 55–109.

Palmer, Margarita, Damià Gomis, Maria del Mar Flexas, Gabriel Jordà, Loic Jullion, Takamasa Tsubouchi, and Alberto C. Naveira Garabato (2012). "Water mass pathways and transports over the South Scotia Ridge west of 50°W". In: *Deep Sea Research Part I: Oceanographic Research Papers* 59, pp. 8–24.

Parkinson, Claire L and Warren M Washington (1979). "A large-scale numerical model of sea ice". In: *Journal of Geophysical Research: Oceans* 84.C1, pp. 311–337.

Rack, Wolfgang and Helmut Rott (2004). "Pattern of retreat and disintegration of the Larsen B ice shelf, Antarctic Peninsula". In: *Annals of Glaciology* 39.1, pp. 505–510.

Rignot, E, S Jacobs, J Mouginot, and B Scheuchl (2013). "Ice-shelf melting around Antarctica". In: *Science* 341.6143, pp. 266–270.

Rott, Helmut, Pedro Skvarca, and Thomas Nagler (1996). "Rapid collapse of northern Larsen ice shelf, Antarctica". In: *Science* 271.5250, p. 788.

Ryan, S, M Schröder, O Huhn, and R Timmermann (2016). "On the warm inflow at the eastern boundary of the Weddell Gyre". In: *Deep Sea Research Part I: Oceanographic Research Papers* 107, pp. 70–81.

Saha, Suranjana, Shrinivas Moorthi, Hua-Lu Pan, Xingren Wu, Jiande Wang, Sudhir Nadiga, Patrick Tripp, Robert Kistler, John Woollen, David Behringer, et al. (2010). "The NCEP climate forecast system reanalysis". In: *Bulletin of the American Meteorological Society* 91.8, pp. 1015–1057.

Schlosser, Peter, Reinhold Bayer, Arne Foldvik, Tor Gammelsrød, Gerd Rohardt, and Karl Otto Münnich (1990). "Oxygen 18 and helium as tracers of ice shelf water and water/ice interaction in the Weddell Sea". In: *Journal of Geophysical Research: Oceans* 95.C3, pp. 3253–3263.

Schodlok, Michael P, Hartmut H Hellmer, and Aike Beckmann (2002). "On the transport, variability and origin of dense water masses crossing the South Scotia Ridge". In: *Deep Sea Research Part II: Topical Studies in Oceanography* 49.21, pp. 4807–4825.

Schröder, M., H. H. Hellmer, and J. M. Absy (2002). "On the near-bottom variability in the northwestern Weddell Sea". In: *Deep Sea Research Part II: Topical Studies in Oceanography* 49.21, pp. 4767–4790.

Schröder, M., Andreas Wisotzki, and Mathias van Caspel (2013a). *Physical oceanography during POLARSTERN cruise ANT-XXIX/3*. Tech. rep. Alfred Wegener Institute, Helmholtz Center for Polar and Marine Research, Bremerhaven.

— (2013b). *Physical oceanography measured on water bottle samples during POLARSTERN cruise ANT-XXIX/3*. Tech. rep. Alfred Wegener Institute, Helmholtz Center for Polar and Marine Research, Bremerhaven.

Schröder, Michael and Eberhard Fahrbach (1999). "On the structure and the transport of the eastern Weddell Gyre". In: *Deep Sea Research Part II: Topical Studies in Oceanography* 46.1, pp. 501–527.

Shepherd, Andrew, Duncan Wingham, Tony Payne, and Pedro Skvarca (2003). "Larsen ice shelf has progressively thinned". In: *Science* 302.5646, pp. 856–859.

Sültenfuß, Jürgen, Wolfgang Roether, and Monika Rhein (2009). "The Bremen mass spectrometric facility for the measurement of helium isotopes, neon, and tritium in water". In: *Isotopes in Environmental and Health Studies* 45.2, pp. 83–95.

Talley, Lynne D (2013). "Closure of the global overturning circulation through the Indian, Pacific, and Southern Oceans: Schematics and transports". In: *Oceanography* 26.1, pp. 80–97.

Tamura, Takeshi, Kay I Ohshima, and Sohey Nihashi (2008). "Mapping of sea ice production for Antarctic coastal polynyas". In: *Geophysical Research Letters* 35.7.

Thompson, Andrew F and Karen J Heywood (2008). "Frontal structure and transport in the northwestern Weddell Sea". In: *Deep Sea Research Part I: Oceanographic Research Papers* 55.10, pp. 1229–1251.

Timmermann, R., A. Beckmann, and H. H. Hellmer (2002). "Simulations of ice-ocean dynamics in the Weddell Sea 1. Model configuration and validation". In: *Journal of Geophysical Research: Oceans* 107.C3, pp. 10–1–10–11. ISSN: 2156-2202.

Timmermann, Ralph, Sergey Danilov, Jens Schröter, Carmen Böning, Dmitry Sidorenko, and Katja Rollenhagen (2009). "Ocean circulation and sea ice distribution in a finite element global sea ice–ocean model". In: *Ocean Modelling* 27.3, pp. 114–129.

Timmermann, Ralph, A Le Brocq, Tara Deen, E Domack, Pierre Dutrieux, B Galton-Fenzi, Hartmut Hellmer, A Humbert, Daniela Jansen, Adrian Jenkins, et al. (2010). "A consistent data set of Antarctic ice sheet topography, cavity geometry, and global bathymetry". In: *Earth System Science Data* 2.2, pp. 261–273.

Timmermann, Ralph, Qiang Wang, and HH Hellmer (2012). "Ice-shelf basal melting in a global finite-element sea-ice/ice-shelf/ocean model". In: *Annals of Glaciology* 53.60, pp. 303–314.

Tomczak, Matthias (1981). "A multi-parameter extension of temperature/salinity diagram techniques for the analysis of non-isopycnal mixing". In: *Progress in Oceanography* 10.3, pp. 147–171.

Tomczak, Matthias and Daniel GB Large (1989). "Optimum multiparameter analysis of mixing in the thermocline of the eastern Indian Ocean". In: *Journal of Geophysical Research* 94.C11, pp. 16141–16.

Wåhlin, AK (2002). "Topographic steering of dense currents with application to submarine canyons". In: *Deep Sea Research Part I: Oceanographic Research Papers* 49.2, pp. 305–320.

Wang, Q., S. Danilov, D. Sidorenko, R. Timmermann, C. Wekerle, X. Wang, T. Jung, and J. Schröter (2014). "The Finite Element Sea Ice-Ocean Model (FESOM) v.1.4: formulation of an ocean general circulation model". In: *Geoscientific Model Development* 7.2, pp. 663–693.

Wang, Qiang, Sergey Danilov, and Jens Schröter (2008). "Comparison of overflow simulations on different vertical grids using the finite element ocean circulation model". In: *Ocean Modelling* 20.4, pp. 313–335.

Wang, Qiang, Sergey Danilov, Eberhard Fahrbach, Jens Schröter, and Thomas Jung (2012). "On the impact of wind forcing on the seasonal variability of Weddell Sea Bottom Water transport". In: *Geophysical Research Letters* 39.6.

Whitworth, T, AH Orsi, S-J Kim, WD Nowlin, and RA Locarnini (1998). "Water masses and mixing near the Antarctic Slope Front". In: *Ocean, ice, and atmosphere: interactions at the Antarctic continental margin*, pp. 1–27.

Whitworth, TIII, WD Nowlin, AH Orsi, RA Locarnini, and SG Smith (1994). "Weddell Sea shelf water in the Bransfield Strait and Weddell-Scotia confluence". In: *Deep Sea Research Part I: Oceanographic Research Papers* 41.4, pp. 629–641.

Winton, Michael (2000). "A reformulated three-layer sea ice model". In: *Journal of Atmospheric and Oceanic Technology* 17.4, pp. 525–531.

Zweng, MM, JR Reagan, JI Antonov, RA Locarnini, AV Mishonov, TP Boyer, HE Garcia, OK Baranova, DR Johnson, D Seidov, et al. (2013). "World Ocean Atlas 2013, Volume 2: Salinity". In: *NOAA Atlas NESDIS* 74, p. 39.